Functional peptide-based structures for corneal repair

Irene Guzmán Soto

Thesis submitted to the University of Ottawa in partial Fulfillment of the requirements for the

Master of Applied Science in Biomedical Engineering

Ottawa-Carleton Institute of Biomedical Engineering

Faculty of Engineering

University of Ottawa

ABSTRACT

Currently, around 28 million people globally suffer from the consequences of corneal blindness and most of them are part of a long waiting list; availability of donor tissue is highly limited. Furthermore, even those who are treated are in risk of developing post-surgery complications, mainly due to microbial infections. Hence, cell-free biomaterials with enhanced properties to prevent corneal associated infections would provide a safe alternative. We evaluated the efficacy of different peptides for the functionalization of collagen-based hydrogels through the *in situ* synthesis of silver nanoparticles (AgNPs). The produced biomaterials were characterized and evaluated *in vitro* for biocompatibility and potential antimicrobial activity. From the diverse strategies evaluated, the localized formation of AgNPs onto the periphery of cornea-shaped collagen hydrogels may represent a more promising option.

ACKNOWLEDGEMENTS

It is my pleasure to take this opportunity to acknowledge and thank those who have been pivotal for the successful completion of this thesis. First, I would like to thank Dr. Emilio I. Alarcon not only for opening the doors of his lab for me to learn from the best but also for being a supportive and encouraging supervisor who goes beyond formalities and cares for the person, not only the student. Moreover, the interculturality and interdisciplinarity of the BEaTS Lab@UOHI have been, not only enjoyable, but also crucial for the development of this project. In this sense, I would like to thank all the great scientists in our lab who directly or indirectly contributed to this learning experience by sharing their knowledge, skills, and sparing some of their time to share more than SOPs. Thank you Mayté, Çagla, Marcelo, Maxime, Christopher, Înes, Nicole MM, Nicole C, Sandra, and everyone in our team.

I would also like to express my gratitude to the Power Corporation of Canada uOGlobal scholarship partner, Dr. EIA, Dr. MG, MP&MM, and Octavio Narvaez for supporting my studies.

In a personal sense, I would like to thank my parents for being out of the extraordinary during my last 36 years. Thank you for being always by my side, no matter the distance; thanks for doing the impossible. Family and friends have been a key balance, thank you C&V, and Luly for all your help. Finally, I would like to express how proud I am of having a great team at home. Thank you, Randy, for your tirelessly support. Thank you, Rebeca and Alexander for being an inspiration, this is for you.

TABLE OF CONTENTS

ABSTRACT ii

ACKNOWLEDGEMENTS iii

LIST OF ABBREVIATIONS ix

LIST OF FIGURES xii

GENERAL INTRODUCTION 1

CHAPTER 1 | CORNEAL INFECTIONS 4

1.1 INTRODUCTION 4

1.2 RATIONALE 6

1.3 OBJECTIVE 6

1.4 RESULTS | BIOFILM REVIEW 6

A. INTRODUCTION: Fundamental concepts on biofilm development 8

B. *IN VITRO* MODELS FOR BIOFILM ASSESSMENT 14

1. Currently used *in vitro* biofilm models. 14

2. Recently developed *in vitro* biofilm models. 16

C. *IN VIVO* MODELS FOR BIOFILM ASSESSMENT 17

1. Currently used *in vivo* biofilm models. 17

2. Recently developed *in vivo* biofilm models. 18

D. ROADMAP FOR THE SELECTION OF MORE REPRESENTATIVE BIOFILM MODELS 19

E. GENERAL LIMITATIONS OF *IN VIVO* AND *IN VITRO* BIOFILM MODELS 21

CHAPTER 2 | NANOTECHNOLOGY 22

2.1 INTRODUCTION 22

2.1.1 Nanomaterials 22

2.1.2 Silver Nanoparticles (AgNPs)....23
2.1.2.1 Synthesis of AgNPs....24
2.1.2.2 Limitations of AgNPs....27
2.1.3 Need of capping agents for stabilization of AgNPs....28
2.1.4 CLKRS as capping agent....29
2.2 NEXT GENERATION OF CLKRS PEPTIDES....30
2.2.1 HYPOTHESIS....30
2.2.2 OBJECTIVE....30
2.2.3 METHODOLOGY....30
2.2.3.1 Peptide synthesis....31
2.2.3.2 Synthesis of AgNPs....32
2.2.3.2.1 Citrate capped AgNPs (C@AgNPs)....32
2.2.3.2.2 Peptide capped AgNPs....32
2.2.3.3 Characterization of AgNPs by absorption spectroscopy....33
2.2.3.4 Size of AgNPs by Dynamic Light Scattering (DLS)....33
2.2.3.5 AgNPs stability under high ionic strength....34
2.2.4 STATISTICAL ANALYSIS....34
2.2.5 RESULTS AND DISCUSSION....35
2.2.5.1 Effect of capping agent on stability of AgNPs....35
2.2.5.2 Size of peptide capped AgNPs by DLS....38
2.2.5.3 Stability of peptide capped AgNPs under high ionic strength conditions....40
2.2.6 CONCLUSIONS....41
CHAPTER 3 | BIOMATERIALS FOR CORNEAL REPAIR....42

3. 1 INTRODUCTION 42
3.2 RATIONALE 43
3.3 HYPOTHESIS 43
3.4 OBJECTIVE 44
3.5 METHODOLOGY 45
Chemicals and reagents 45
A. COMPRESSED COLLAGEN HYDROGELS 45
A.1 Solutions 46
A.2 Collagen-based hydrogel preparation 46
A.3 Compression of Collagen Hydrogels 47
A.4 Mass loss after compression 48
A.5 Scanning Electron Cryo-Microscopy (Cryo-SEM) of compressed hydrogels 48
A.6 Hydrogel degradation by collagenase 49
A.7 *In situ* functionalization of compressed collagen hydrogels 50
A.7.1 Direct exposure into the AgNPs reagent mix 50
A.7.1.1 Plasmon band of functionalized compressed hydrogels 51
A.7.1.2 Zone of inhibition (ZOI) assay 52
A.7.1.3 Live/dead assay 55
A.7.2 Deposition of peptide capped AgNPs formed in microdroplets 56
A.7.2.1 Cryo-SEM/Energy Dispersive Spectroscopy (EDS) analysis 57
B. CORNEA-SHAPED HYDROGELS 58
B.1 Preparation of solutions 58
B.2 Preparation of cornea-shaped hydrogels 59

B.3 *In situ* functionalization of cornea-shaped collagen hydrogels with peptide capped AgNPs 60

B.3.1 Refractive index (RI) of functionalized corneal implants 61

B.3.2 Inductively Coupled Plasma-Mass Spectrometry (ICP-MS) 61

3.6 P6 PEPTIDE ANALYSIS 62

3.6.1 Proliferation of human corneal epithelial cells (HCEC) 62

3.6.2 Evaluation of antimicrobial activity by turbidimetry 63

3.7 RESULTS AND DISCUSSION 64

3.7.1 COLLAGEN HYDROGEL COMPRESSION 64

3.7.1.1 Microstructure of compressed hydrogels by Cryo-SEM 65

3.7.1.2 Hydrogel degradation by collagenase 67

3.7.2 *IN SITU* FUNCTIONALIZATION OF COMPRESSED HYDROGELS | Exposure into AgNPs reagent mix 69

3.7.2.1 Plasmon absorption of functionalized compressed hydrogels 69

3.7.2.2 ZOI assay 70

3.7.2.3 Cell viability 74

3.7.3 *IN SITU* FUNCTIONALIZATION OF COMPRESSED HYDROGELS | Microdroplets 76

3.7.3.1 Cryo-SEM/EDS analysis 77

3.7.4 COLLAGEN-BASED HYDROGELS | Cornea-shaped hydrogels 78

3.7.4.1 *In situ* functionalization of cornea-shaped collagen hydrogels with peptide capped AgNPs 78

3.7.4.2 RI of functionalized corneal implants 79

3.7.4.3 ICP-MS 80

3.8 P6 PEPTIDE ANALYSIS 81

3.8.1 Proliferation of GFP-HCEC *in vitro* 81

3.8.2 Antimicrobial activity by turbidimetry 83

3.10 CHAPTER CONCLUSIONS 83

4. OUTLOOK AND FUTURE DIRECTIONS 84

5. REFERENCES 85

6. SUPPLEMENTARY MATERIALS 100

LIST OF ABBREVIATIONS

AFM	Atomic force microscopy
Ag	Silver
$AgNO_3$	Silver nitrate
AgNPs	Silver nanoparticles
ATCC	American type culture collection
Au	Gold
BDDGE	1,4-Butanediol diglycidyl ether
BPE	Bovine pituitary extract
C@AgNPs	Citrate capped AgNPs
$CaCl_2$	Calcium chloride
CFU	Colony forming units
Citrate	Sodium citrate tribasic dihydrate
CO_2	Carbon dioxide
COMP	Compressed
Cryo-SEM	Scanning electron cryo-microscopy
DEMEM	Dulbecco's modified eagle's medium
DLS	Dynamic light scattering
EDS	Energy dispersive spectroscopy
FBS	Fetal bovine serum

FCH	Functionalized collagen hydrogel
G-NP	Gel-No peptide
GFP	Green fluorescent protein
GFP-HCEC	HCEC expressing green fluorescent protein
HCEC	Human corneal epithelial cells
HCl	Hidrochloric acid
HEPES	2-[4-(2-Hydroxyethyl)piperazin-1-yl]ethanesulfonic acid
HUVEC	Human umbilical vein endothelial cells
I-2959	Irgacure-2959:2-Hydroxy-4′-(2-hydroxyethoxy)-2-methylpropiophenone
ICP-MS	Inductively coupled plasma-mass spectrometry
k-SFM	Keratinocyte serum free medium
KCl	Potassium chloride
LB	Luria Bertani
LOD	Limit of detection
MHA	Mueller-Hinton agar
Na_2CO_3	Sodium carbonate
NaCl	Sodium chloride
$NaHCO_3$	Sodium bicarbonate
NMs	Nanomaterials
NaOH	Sodium hydroxide
NC	Non-compressed

NG-NP	No gel-No peptide
NG-P5	No gel-peptide 5
NG-P6	No gel-peptide 6
NG-P9	No gel-peptide 9
NIH	National Institutes of Health
NPs	Nanoparticles
OD	Optical density
PBS	Phosphate-buffered saline
rEGF	Human recombinant epithelial growth factor
RI	Refractive index
RP-HLPC	Reversed phase-high performance liquid chromatography
SPB	Surface plasmon band
SPR	Surface plasmon resonance
Tris	Tris (hydroxymethyl) aminomethane
UV	Ultraviolet
UV-Vis	Ultraviolet-visible
ZOI	Zone of inhibition

LIST OF FIGURES

Figure 1. Human cornea anatomy 4

Figure 2. Synthesis of AgNPs by photochemical reduction via ketyl radicals 26

Figure 3. Functions of capping agents on synthesis and properties of AgNPs 28

Figure 4. Semicondensed structures of the second generation of CLKRS peptides 30

Figure 5. Methodology followed for assays part of the Nanotechnology chapter 31

Figure 6. Potential interpretation of most common changes observed on the plasmon band of AgNPs 36

Figure 7. SPB of peptide capped AgNPs at different concentrations 37

Figure 8. Hydrodynamic size of AgNPs produced with different concentrations of P5, P6, and P9 peptides 39

Figure 9. Ionic strength assay of peptide capped AgNPs 40

Figure 10. Schematic representation of the rational and objectives of Chapter 3 44

Figure 11. Methodology for compressed collagen hydrogels 45

Figure 12. Schematic of the functionalization and analysis of processed cornea shaped hydrogels 58

Figure 13. Compression of collagen-based hydrogels 64

Figure 14. Representative cryo-SEM image captures at different magnifications showing the resulting microstructure of compressed hydrogels 66

Figure 15. Compressed collagen hydrogel degradation by collagenase 68

Figure 16. SPB of compressed collagen hydrogels after exposure to photoirradiation into the AgNPs reagent mix containing either P5, P6, or P9 to act as capping agents 69

Figure 17. ZOI test results for functionalized compressed collagen hydrogels in the bacterial strain *S. aureus* ATCC 25293..... 71

Figure 18. *In vitro* biocompatibility of compressed collagen hydrogels functionalized with peptide capped AgNPs in HUVEC culture after 24 h of incubation. 75

Figure 19. Schematic of the setting used for the *in situ* synthesis of peptide capped AgNPs in microdroplets for their deposition onto compressed collagen hydrogels..... 76

Figure 20. Cryo-SEM/EDS results of the *in situ* functionalization of compressed collagen hydrogels after deposition of microdroplets 77

Figure 21. Representative images of localized *in situ* functionalization of corneal implants.... 78

Figure 22. RI values of functionalized corneal implants..... 79

Figure 23. Silver content in functionalized corneal hydrogels..... 80

Figure 24. *In vitro* proliferation of GFP-HCEC after incubation with different concentrations of P6 peptide..... 82

Figure 25. Antimicrobial activity of P6 evaluated by turbidimetry 83

Software used for figure making:

- KaleidaGraph v4.5.2 for data analysis and plotting.
- BioRender for figures and schematics.

GENERAL INTRODUCTION

The human body, a perfectly structured and organized machine, is not only equipped to work in synchrony between all the components and systems that form it, it also has the ability to fix certain problems when things do not go as expected. Our bodies are even able to regenerate themselves to some degree when cells and tissues become damaged. However, this capability is limited, causing operational disfunctions that can be observed in the form of illness or certain medical conditions.

The understanding and constant development of health medicine has allowed an increase in life expectancy throughout the years (Garmany *et al.*, 2021). A couple of years ago, life expectancy in the U.S. and Canada was reported to be 78.8 and 82.1 years, respectively (StatCan, 2021; Xu *et al.*, 2021). Having reduced mortality rates thanks to a greater accessibility to treatments and therapies, has led to increased morbidity rates for a great number of diseases (Garmany *et al.*, 2021). In this sense, the field of Regenerative Medicine has been in continuous development with the goal of providing diverse alternatives, not only for the ageing population, but for all those with disease, trauma, and congenital defects that have suffered from tissue loss and require the repair/replacement of body components and functions (Garmany *et al.*, 2021; Sadtler *et al.*, 2016). One of the main approaches of Regenerative Medicine applications is the design, creation, and application of Biomaterials to reach this goal (Rahmati *et al.*, 2018). It is important to highlight that not any material has the potential for being used as a biomaterial. In order to be successfully used as such, and depending on the final application, a biomaterial must meet certain requirements,

including biocompatibility, biodegradability, and suitable mechanical properties (dos Santos *et al.*, 2017). There is a long list of materials that have been evaluated as potential corneal replacements in patients with diverse corneal impairments, including corneal trauma and dystrophies, dry eye, corneal curvature defects, corneal inflammatory disorders, and corneal microbial infections (Hancox *et al.*, 2020; Mobaraki *et al.*, 2019). From those, collagen-based biomaterials have shown to be a promising alternative (Khatoon *et al.*, 2020; McTiernan *et al.*, 2020; Xeroudaki *et al.*, 2020; Zhao *et al.*, 2016). On the other hand, Nanoscience and Nanotechnology have contributed to the development of a variety of approaches for Biomedical applications, including corneal repair (Weng *et al.*, 2017).

In the present thesis, three different chapters have been included to describe a research study on a combined approach of Nanotechnology and Biomaterials for corneal repair applications. Chapter number one provides a short overview of human corneal structure and highlights the demanding need for the fabrication of corneal replacements. Then, it focusses on chronic microbial infections in the form of biofilms, one of the most common post-operative complications after corneal transplantation, and one of the main limitations for the translation of biomaterials into the clinic. In the second chapter, the use of silver nanoparticles (AgNPs) coated with different peptide structures is proposed as an alternative to improve their potential for biomedical applications. Production of AgNPs and their characterization in terms of stability was done to identify the best peptide candidates and experimental conditions. Finally, chapter 3 describes the proposed use of collagen-based biomaterials functionalized *in*

situ with peptide-capped AgNPs for corneal repair applications. Temporal eye patches and corneal implants were produced and modified, considering the experimental conditions selected from the previous chapter for their functionalization. Also, the antimicrobial activity and biocompatibility of such materials were evaluated and reported in this chapter.

CHAPTER 1 | CORNEAL INFECTIONS

1.1 INTRODUCTION

The cornea is a transparent, dome-shaped structure that is positioned in the anterior surface of the eye (Sridhar, 2018). It serves several functions of particular importance for the eye's physiology. For instance, the cornea acts as a mechanical barrier to protect the inner environment and structures of the eye from physical and chemical insults. Moreover, the cornea functions as an immunological barrier against external agents, where its structure and transparency provide about two thirds of the refractive power of the eye, playing a main role in vision (Jhanji *et al.*, 2021). The human cornea has a relatively simple anatomy which is comprised of five stratified layers (**Figure 1**).

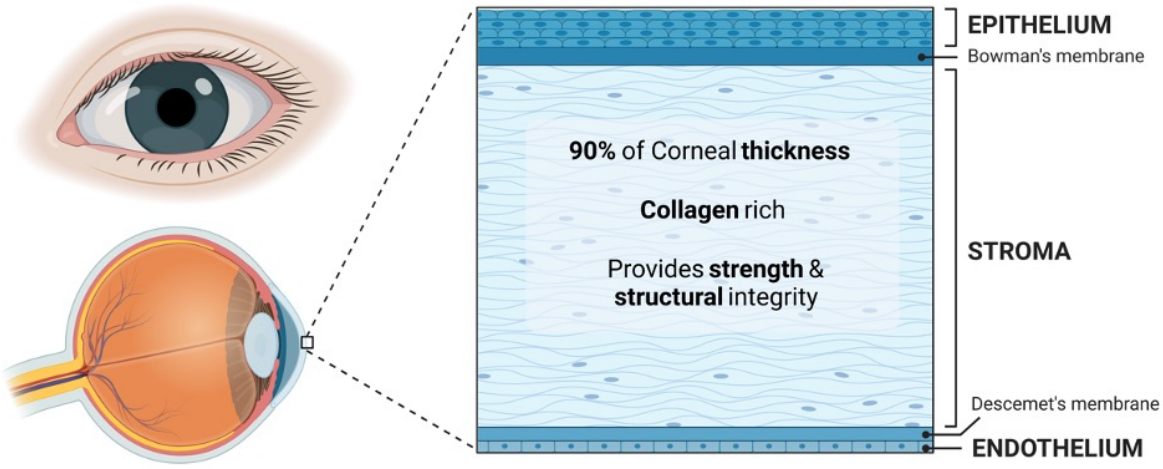

Figure 1. Human cornea anatomy. Structural organization of the five layers that compose human the cornea.

Corneal stroma represents approximately 90% of the corneal thickness, providing strength and structural integrity to it (Meek & Knupp, 2015). One of the main components of this layer is collagen, being its highly organized spacing and alignment an essential

feature for corneal transparency (Matthyssen *et al.*, 2018). Due to its continuous exposure to the external environment, the cornea may become damaged, as in the case of physical trauma, burns, bacterial and viral infections, or due to aging and heritable conditions (Whitcher *et al.*, 2001). Depending on the level of damage, a permanent reduction in corneal transparency may occur and, as consequence, this can result in vision loss (Bocheux *et al.*, 2019).

Reports from almost 10 years ago indicate that corneal blindness affects around 28 million people globally (Oliva *et al.*, 2012), representing a clinical challenge due to a limited access to donor tissue; less than 2% of these patients receive corneal transplantation (Gain *et al.*, 2016). Moreover, even patients who are part of such small percentage are in risk of further complications (Perez *et al.*, 2020). There are some other important considerations that may affect the success of tissue grafting, such as immune rejection of the transplant and post-surgery complications, including neovascularization and chronic microbial infections in the form of biofilms (Anshu *et al.*, 2011; Sharif & Sharif, 2019; Wagoner *et al.*, 2009). It is precisely microbial colonization of implantable devices one of the main limitations that face the diverse technologies that are continuously being developed to cover the need of human tissue donors (Khatoon *et al.*, 2018).

1.2 RATIONALE

To develop fully functional and successful approaches for biomedical applications, a better understanding of the chronic microbial infections commonly associated to them is required.

1.3 OBJECTIVE

To conduct a comprehensive literature review of the fundamental concepts on biofilm formation and main considerations for the design of more representative *in vivo* and *in vitro* models for their study, which would ultimately contribute to the development of successful antibiofilm treatments and therapies.

1.4 RESULTS I BIOFILM REVIEW

A comprehensive commissioned review entitled “Mimicking biofilm formation and development: Recent progress in *in vitro* and *in vivo* biofilm models” was published on iScience (Cell Press). Over 400 references were consulted to gain the required involvement in the field and be able to have a better understanding of the main events occurring during biofilm development. Generally, biofilm studies are carried out by interdisciplinary groups, which enriches the perspective and final outcomes. Hence, this review was structured for welcoming scientists from different fields of expertise to the field of biofilms. Schematics and brief explanations of fundamental concepts were included to help understand abstract concepts and mechanisms. In the first section, we offered the reader an overall picture of biofilm development by presenting a general

overview of the cellular, molecular, mechanical, and physicochemical mechanisms and events involved. One of our goals was to discuss the wide variety of special considerations affecting biofilm formation and development, which are usually underestimated when selecting the experimental models for the study of biofilms and the evaluation of potential antibiofilm strategies. Moreover, we considered that once having a better appreciation of such, the reader would become more critical when evaluating the previous and recently developed *in vitro* and *in vivo* biofilm models. Finally, a brief discussion of the general advantages and limitations of biofilm models/studies was presented, along with a road map that may serve as a guide for the selection or creation of more representative biofilm models.

Here, due to space constraints, only a list of contents, figures, and tables of the review will be included to show the main points addressed. To gain access to the full version of this review, please consult the corresponding reference (Guzmán-Soto *et al.*, 2021). Note that these materials were not included in the list of figures and tables of this document to avoid potential confusions, as labelling matches the original paper.

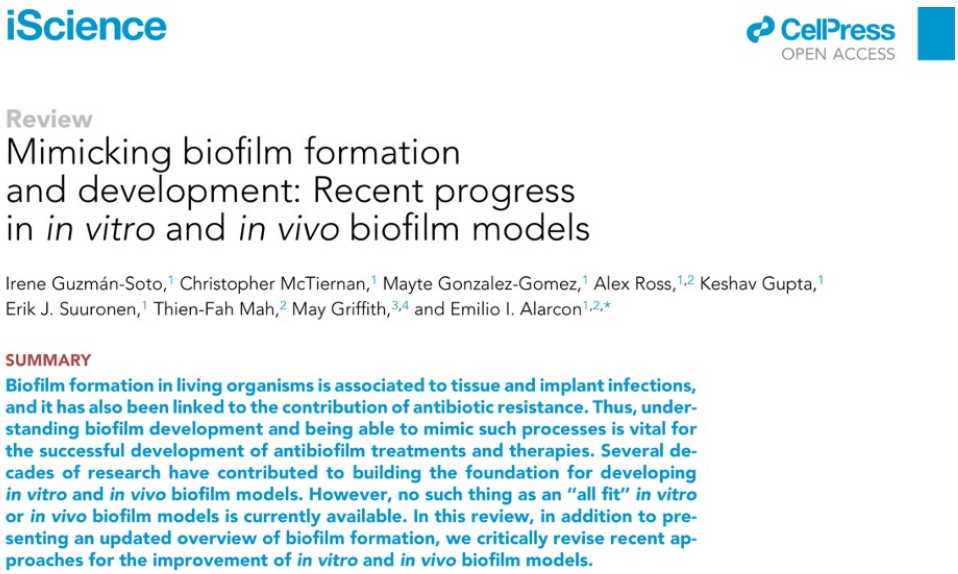

iScience

CellPress
OPEN ACCESS

Review

Mimicking biofilm formation and development: Recent progress in *in vitro* and *in vivo* biofilm models

Irene Guzmán-Soto,[1] Christopher McTiernan,[1] Mayte Gonzalez-Gomez,[1] Alex Ross,[1,2] Keshav Gupta,[1] Erik J. Suuronen,[1] Thien-Fah Mah,[2] May Griffith,[3,4] and Emilio I. Alarcon[1,2,*]

SUMMARY

Biofilm formation in living organisms is associated to tissue and implant infections, and it has also been linked to the contribution of antibiotic resistance. Thus, understanding biofilm development and being able to mimic such processes is vital for the successful development of antibiofilm treatments and therapies. Several decades of research have contributed to building the foundation for developing *in vitro* and *in vivo* biofilm models. However, no such thing as an "all fit" *in vitro* or *in vivo* biofilm models is currently available. In this review, in addition to presenting an updated overview of biofilm formation, we critically revise recent approaches for the improvement of *in vitro* and *in vivo* biofilm models.

A. INTRODUCTION | Fundamental concepts on biofilm development

Biofilm development is a complex and varied process, which may be different depending on the microbial species involved, the host, and microenvironmental conditions. In general, some of the main stages of bacterial biofilm formation (**Figure 1**) may include the following events: (1) adsorption, (2) adhesion, (3) formation of microcolonies, (4) maturation, and (5) dispersal.

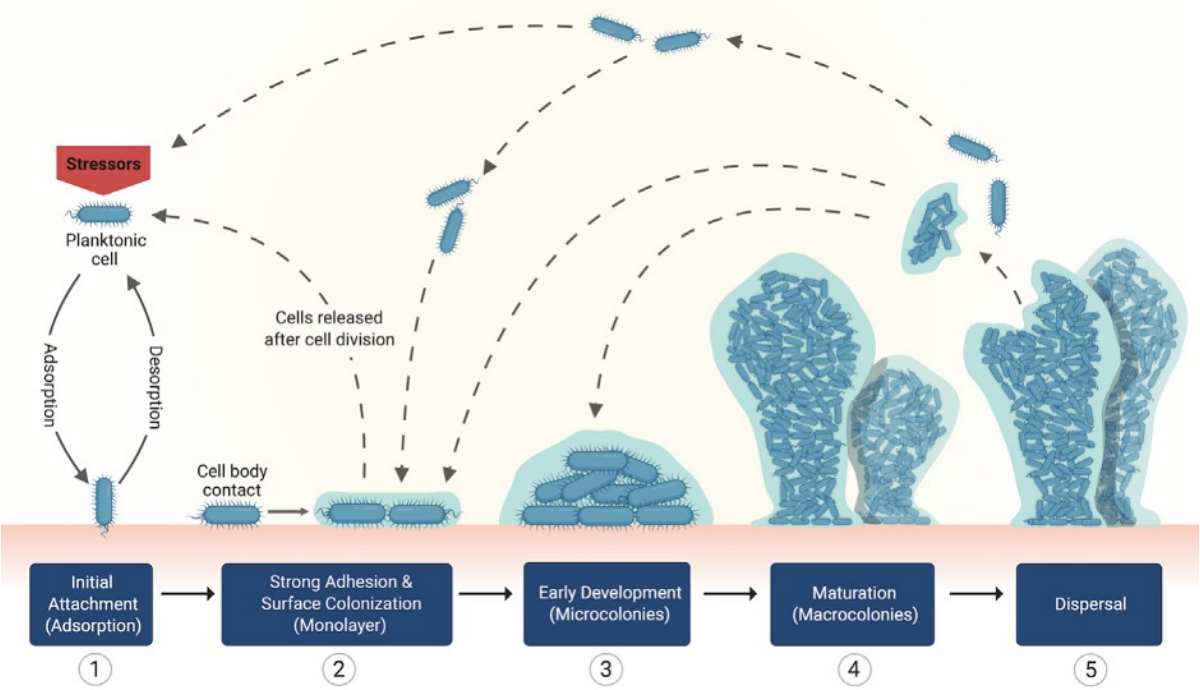

Figure 1. Schematic representation for single bacterial species biofilm formation on a solid surface.

1. **Initial attachment:** Adsorption of bacterial cells to the surface (*reversible* attachment).

Initially, nonspecific attraction-repulsion physicochemical interactions occur between bacteria and the surface. If the repulsive forces are surpassed, an unspecific or specific appendages-mediated temporal attachment occurs (**Figure 2**).

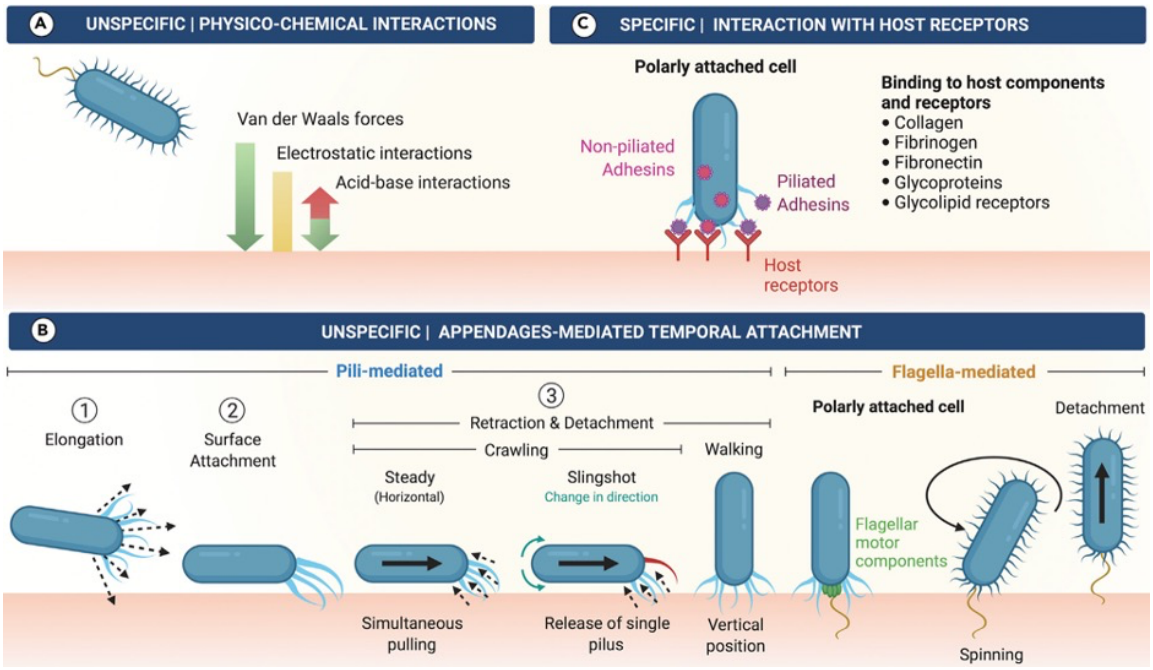

Figure 2. Schematic representation for the main nonspecific and specific interactions between bacteria and surfaces.

2. **Bacterial adhesion to the surface**: Increased adhesion strength.

The attachment strength of the loosely adhered bacterial cells gradually increases due to the molecular alterations that occur at the biochemical level as consequence of the mechanical cues experienced during surface sensing (**Figure 3**).

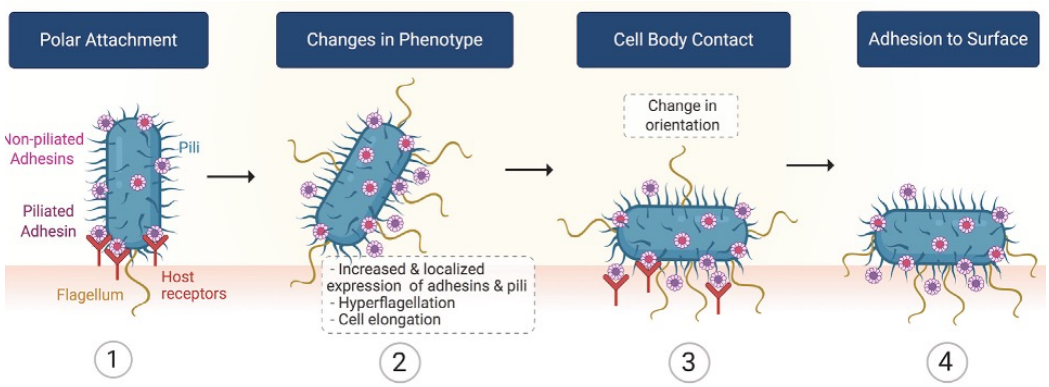

Figure 3. Schematic representation of the functional steps involved in bacteria adhesion to a surface.

3. **Cell growth and division**: Formation of microcolonies, cellular communication, and extracellular polymeric substance (EPS) matrix production.

Once a strong bacteria-to-surface adhesion has been achieved, attached bacteria grow and divide, colonizing the surface. Bacterial cells aggregate, forming bacterial clusters known as microcolonies (**Figure 4**).

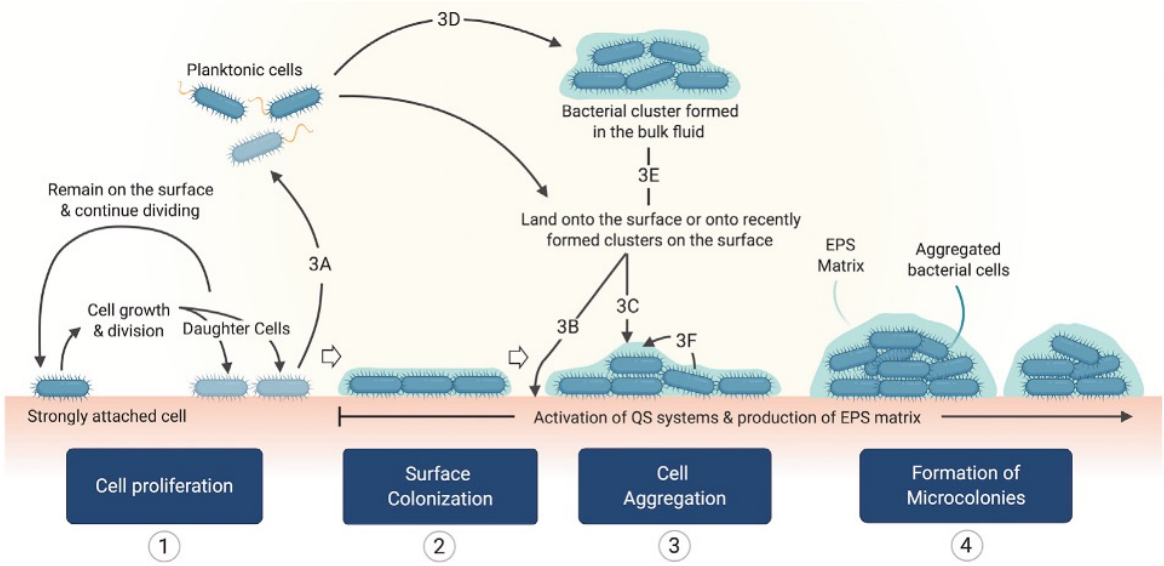

Figure 4. Potential routes for the formation of microcolonies.

As microcolonies are being formed, cell arrangements go from an initial single layer of attached cells to multilayered 3D cell aggregates. To reach this spatial distribution, bacteria must communicate with each other and express particular genes for the secretion of EPS matrix (**Figure 5**), which will serve as a structural support for the stabilization of microcolonies and further biofilm network.

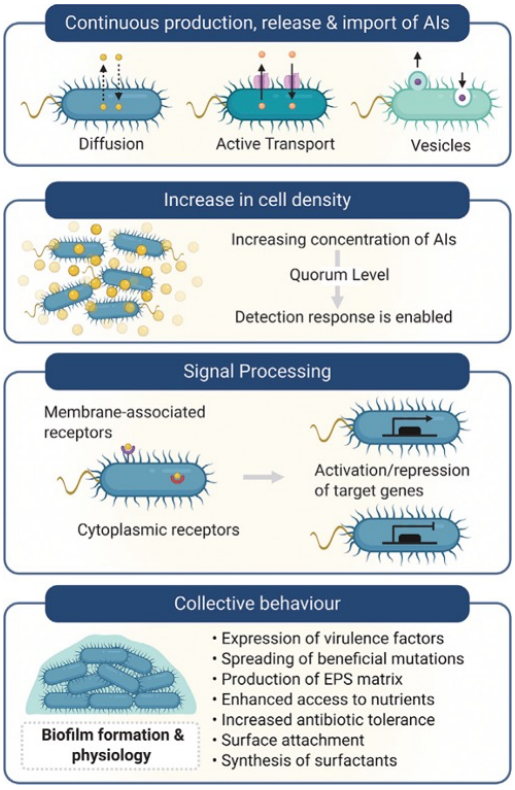

Figure 5. Cellular communication through quorum sensing (QS) influences biofilm formation and physiology.

4. Biofilm maturation.

Bacterial microcolonies spread out forming larger aggregates referred to as ‘‘macrocolonies’’, the mature form of biofilms. These are highly heterogeneous in their 3D structure, morphology, and physiology (Figure 6). As the microenvironment is not the same for bacteria in different regions of the biofilm, the presence of growth rate, metabolic activity, oxygen concentration, and pH gradients is observed. Bacterial cells in the inner biofilm regions show reduced metabolic activity, which provides them with the beneficial property of being resistant to conventional antibiotics. Moreover, genetic diversity is found among biofilm-living bacteria, which is observed by the presence of bacterial subpopulations showing different phenotypes, such as persister cells and small colony variants, which exhibit a high antibiotic tolerance, contributing to infection chronicity and further spread and colonization.

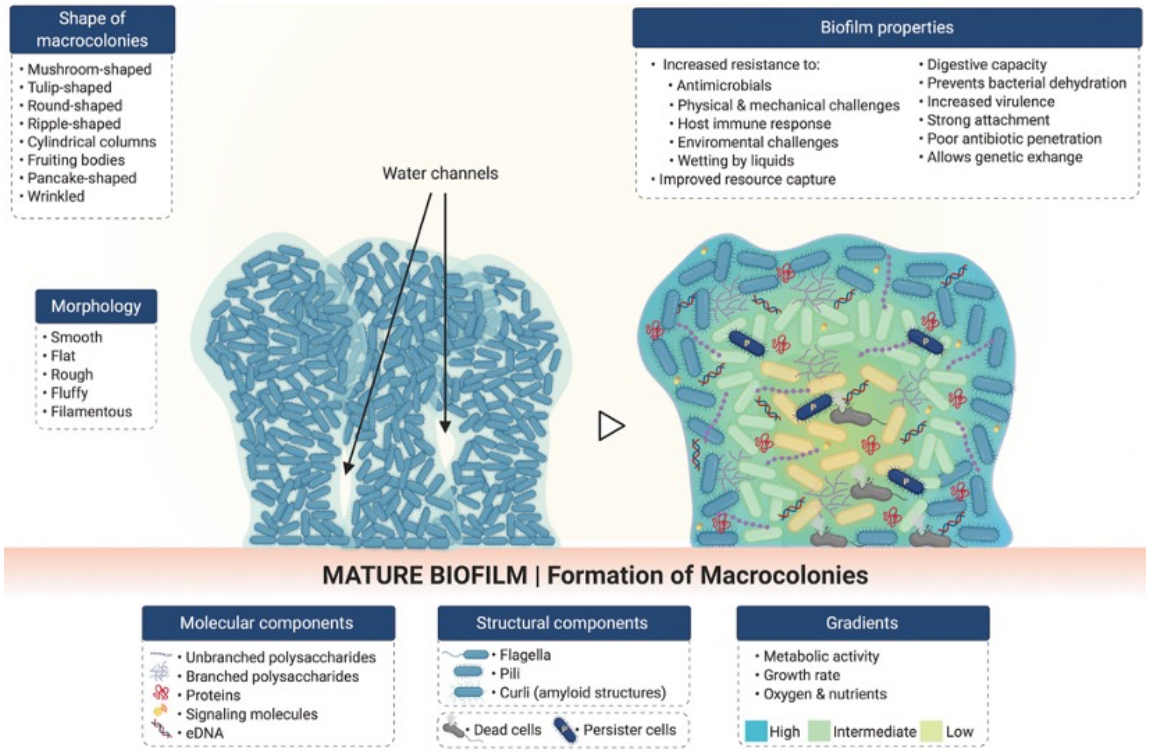

Figure 6. Morphology and architecture of mature biofilms.

As any other element recognized as foreign by the immune system, biofilm formation elicits the activation of different cells and mechanisms intended to clear it from the host. Although immune cells and mediators offer a wide variety of strategies to prevent pathogenic microbial invasion, biofilm-living microorganisms as well as biofilm molecular and structural components have the ability of modulating and evading immune attack. Some of the main mechanisms that contribute to this immune regulation are summarized in Figure 7.

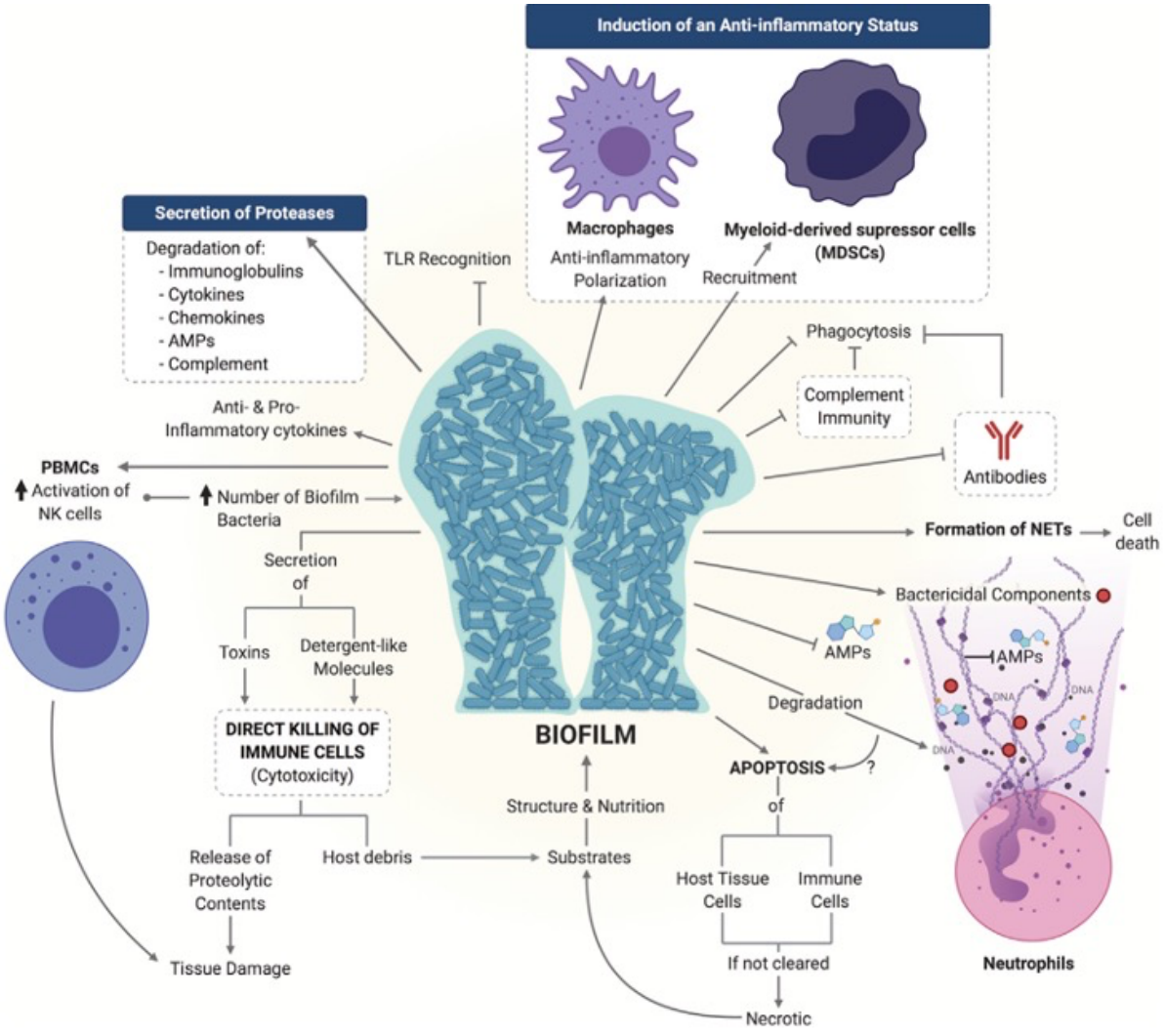

Figure 7. Biofilms modulate and evade immune responses from the host utilizing a variety of mechanisms.

5. Biofilm dispersal.

At some point after reaching maturity, biofilms suffer a partial structural loss that may occur by detachment and/or dispersion (**Figure 8**). Detachment involves four mechanisms that imply the release or loss of biofilm portions as a consequence of mechanical and shear stress (abrasion, erosion, and sloughing) as well as the impact of immune attack from the host (grazing). Dispersion, on the other hand, implies more than being torn away from the biofilm by external stressors; it requires the sensing and processing of particular signals, which culminate in the expression of the corresponding physiological alterations. Biofilm dispersion is a well-regulated process affecting particular cells and regions within the biofilm. Furthermore, the dispersed cells are, at this stage, more virulent than their planktonic counterparts but less than those within the parent biofilm.

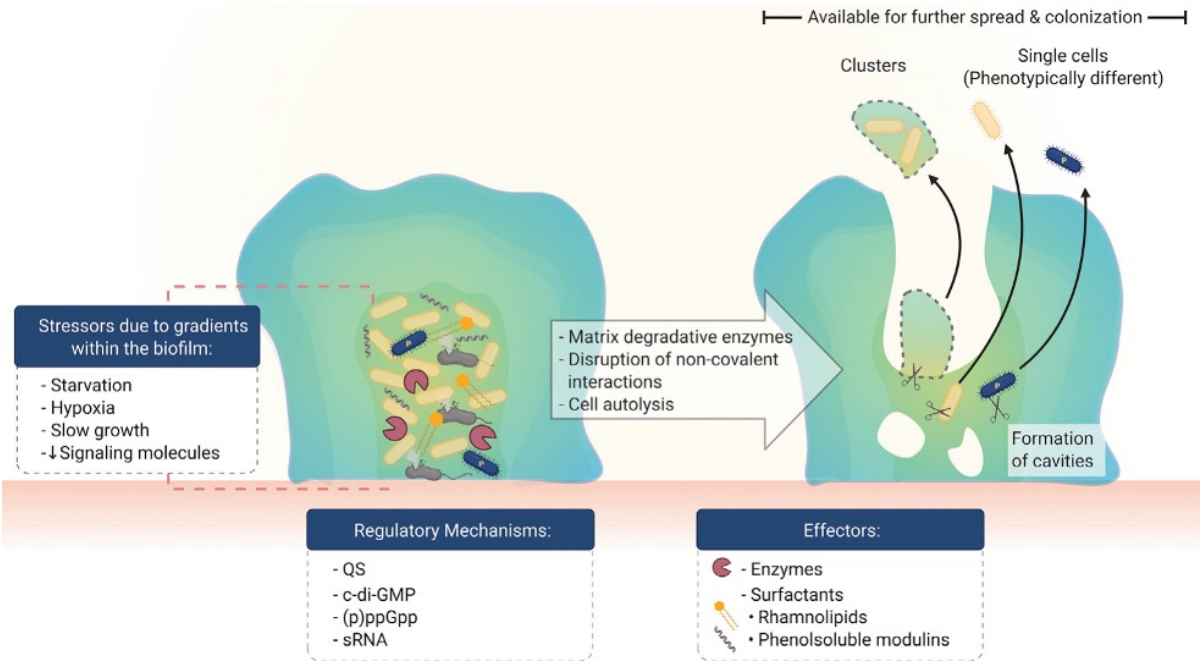

Figure 8. Bacterial cells and clusters are dispersed from the biofilm.

B. *IN VITRO* MODELS FOR BIOFILM ASSESSMENT

1. Currently used *in vitro* biofilm models.

In vitro biofilm models are used as the first step in testing new materials and methods meant to interact with biofilms. The variety of *in vitro* biofilm models can be classified into two main groups (**Table 1**), depending on the availability of nutrients over time.

Table 1. General characteristics of *in vitro* static and dynamic biofilm models.

	Static	Dynamic
		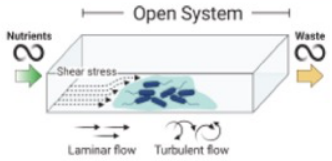
Nutrient supply	Finite (may be replenished periodically)	Continuous
Flow	No	Yes, over the biofilm surface
Shear stress	Null to mild (if shaken)	Adjustable: Different hydrodynamic conditions can be adapted
Waste and planktonic cells	Accumulated	Removed as nutrients are replenished
Length of experiments	Short (days)	Long (from days to weeks)
Throughput screening	High: Different species/strains and conditions can be simultaneously evaluated	Low to medium
Technical complexity	Low	Medium to high
Complexity of setup procedures	None	Considerable, time consuming
Specialized equipment	Little (requires mostly common laboratory equipment)	Required (e.g., reactors or fermenting systems)
Cost per replicate	Low	Medium to high
Particularly useful for	Early stages of biofilm development Genetic screening	Study of mature biofilms

Mimicking native conditions of biofilms of clinical relevance is a challenging task. It requires the incorporation of elements from the host (cellular, molecular, and environmental), the alteration of those as in the health condition of interest, and the particular combination of microbial species and strains involved in biofilm formation. Hence, it is not only required to replicate the disease and all its components, but also the combined conditions of disease-biofilm development. Several biofilm models and devices have been proposed throughout the years and, although each of them offers

different types of improvements for growing and studying biofilms, all of them present inherent disadvantages and limitations. Currently, there is still a need for standardized models, methods, and devices suitable for the evaluation of medical-related biofilms. Figure 9 shows the commonly used strategies for *in vitro* biofilm studies.

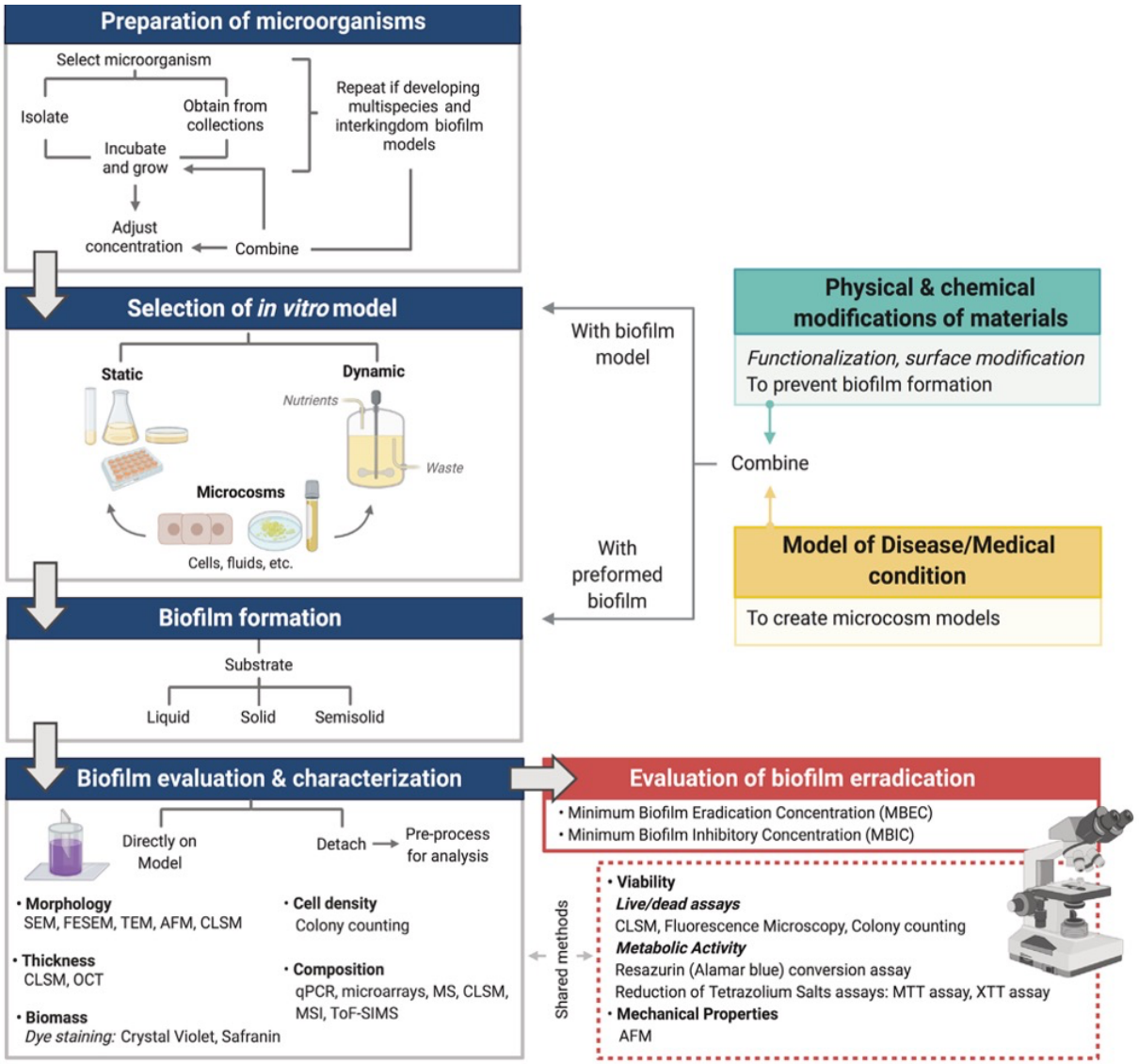

Figure 9. Overall steps of current standard *in vitro* protocols of biofilm formation.

2. Recently developed *in vitro* biofilm models.

In this review, we selected biofilm models published from 2015 to date, which include a unique or an innovative way of biofilm formation and/or offer an improved biofilm monitoring and evaluation strategy.

2.1 Static *in vitro* biofilm models.

The main characteristics of recently developed static *in vitro* biofilm models (**Table 2**) show a tendency to (1) utilize small sized or miniaturized devices; (2) offer a platform for real-time monitoring of biofilm development; (3) evaluate biofilm properties under native conditions (undisrupted); (4) allow the *in situ* evaluation of potential antimicrobial treatments; (5) improve reproducibility by forming biofilms with customized shapes and dimensions; (6) consider the maturation state of the biofilm; and (7) include particular elements to better resemble the microenvironment of biofilm formation for certain medical conditions.

Table 2. Sample table of the representative examples for recent *in vitro* biofilm models selected in this review.

Graphic depiction	Description	Application	Microorganism(s) evaluated	Advantages	Limitations
Recent static *in vitro* biofilm models					
3D bioprinted biofilm construct (Ning et al., 2019)					
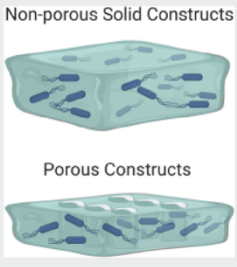	Double crosslinked alginate-based bioink is used to print solid and porous 3D bacterial structures	Formation of mature biofilms for antimicrobial testing	*E. coli* clinical isolate (American Type Culture Collection [ATCC] 25922), methicillin-resistant *S. aureus* (MRSA, clinical isolate, ATCC 700788), methicillin-sensitive *S. aureus* (MSSA, clinical isolate, ATCC 29213) *P. aeruginosa*, PAO1 (wild-type strain, ATCC 47085) Cell density: Initial: OD_{600nm} = 1.0 Final: Visually reported (3D reconstructed CLSM z stack images)	• Customizable predesigned biofilm thickness and dimensions • Construct stability for up to 4 weeks • Adequate cell viability • Suitable for aerobic and anaerobic biofilms • Allows biofilm formation monitoring • Suitable for antimicrobial testing (biofilm penetration and eradication) • Greater antimicrobial resistance than 2D cultures • Cost effective	• Constructs with thickness of 0.5 mm or thinner are structurally unstable • Missing interaction with cellular and molecular components • Decreased cell density as thickness increases • Restricted to biofilms grown in semisolid conditions

2.2 Dynamic *in vitro* biofilm models.

Most of the recently published *in vitro* dynamic models involve slight modifications of previously developed models instead of a completely novel approach for biofilm development and/or evaluation. Although this implies carrying already identified limitations associated to that particular device or model, the adaptation of currently available technologies is also a convenient approach if it provides significant improvements (**Table 2**).

C. *IN VIVO* MODELS FOR BIOFILM ASSESSMENT

1. Currently used *in vivo* biofilm models.

While *in vitro* biofilm models are powerful tools when it comes to reproducibly testing the effects of simple treatments and factors, they fail to account for the dynamic and complex nature of the interactions at play between the host (i.e., immune system) and bacteria that make up the biofilm as well as the potential for interaction with other bacteria. As such, the development of robust *in vivo* models is key in validating *in vitro* results and a necessary step in the testing of new treatments and devices on the path toward clinical translation. The common strategy currently followed for in vivo biofilm studies is represented in **Figure 10**.

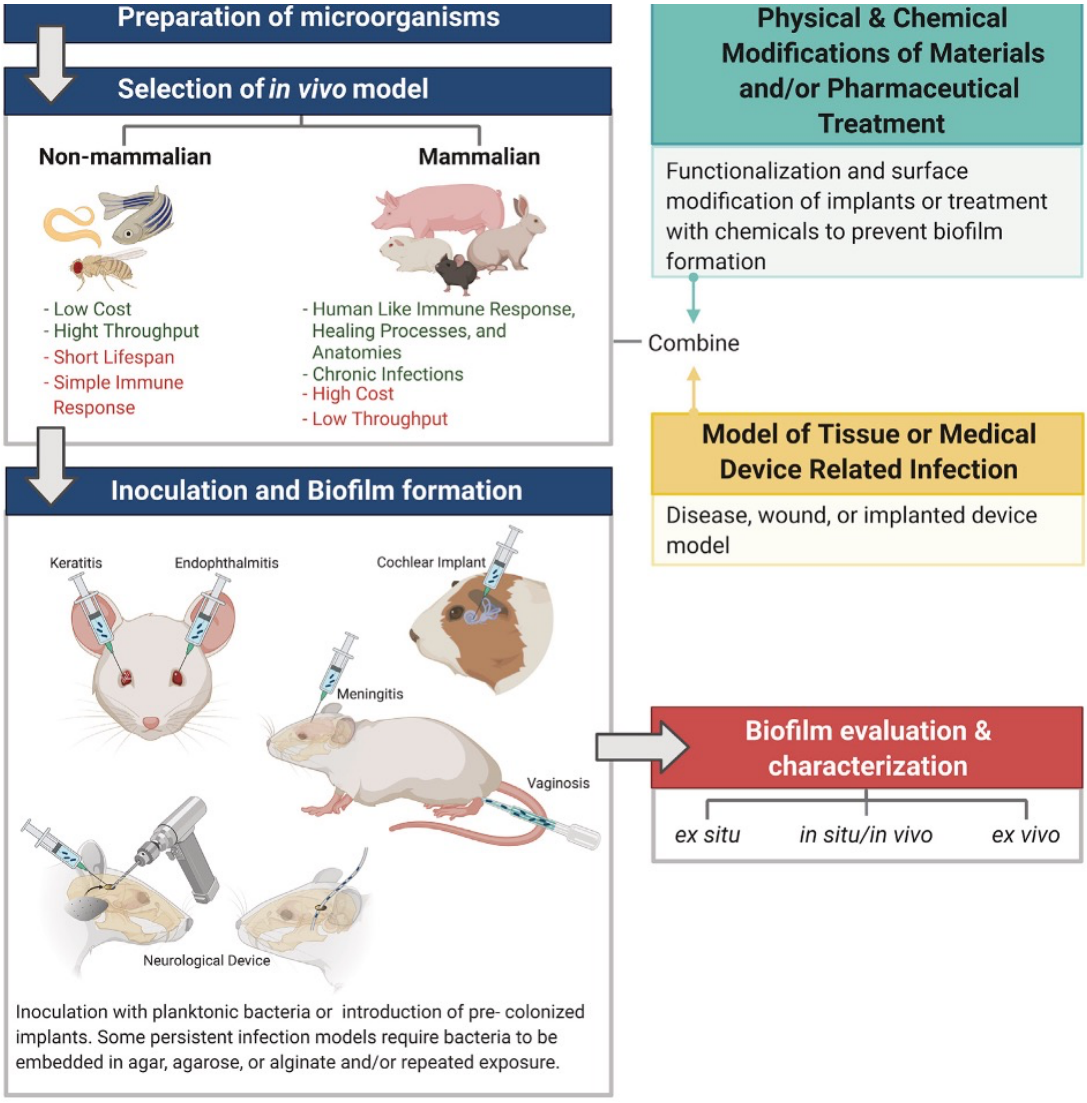

Figure 10. Schematic depiction for the overall steps involved in the design of *in vivo* protocols of biofilm formation and characterization.

2. Recently developed *in vivo* biofilm models.

Many tissue-related infections and commonly used medical devices have well-established animal models that allow the study of biofilm-related disease progression and testing of new drugs, treatments, materials, and coatings. However, over the last decade, there has been a push to develop new models that address the shortcomings of available models or fill the holes where no model currently exists. In **Table 3**, we

highlight several new *in vivo* biofilm models, which allow for the study of tissue- and device-related infections.

Table 3. Sample table of the recently developed *in vivo* biofilm models included in this review.

Description	Application	Microorganism(s)	Biofilm analysis	Outcome(s)
Recent *in vivo* biofilm models for tissue-related infection				
Endophthalmitis (Sadaka et al., 2014)				
The anterior chamber of the right eye is inoculated with *S. aureus* using a 35-G needle on a NanoFil syringe just anterior to the limbus without touching the iris. The left eye is used as an untreated control. Animals: ♀C57BL/6J mice	Investigate the impact of CodY deletion on *S. aureus* virulence in a murine anterior chamber infection model	*S. aureus* (MS7/SA564/CDM7) Initial cell density: 1 μL of OD_{600nm} = 0.4–0.8	• Bacterial growth assessed after 24 h by extraction and homogenization of the entire eye followed by quantitative plating • Light microscopy of histological samples	• Developed a model of anterior chamber infection, characteristic of endophthalmitis • Revealed a link between branched-chain amino acid responsive transcription regulator CodY and endophthalmitis repression • Addition of branched-chain amino acids to postoperative eyedrops could reduce progression of endophthalmitis

D. ROADMAP FOR THE SELECTION OF MORE REPRESENTATIVE BIOFILM MODELS

The more we learn about the underlying complexity of biofilm formation in living organisms, the more evident is the need to further advance in developing *in vitro* models that more closely mimic the *in vivo* setting where biofilms form and mature. It is clear that a ‘‘one-fit-all’’ approach is certainly unrealistic and not practical. Further, when presented with the choice of selecting or developing an *in vitro* biofilm; the first step should be assuming that no model will ever be able to fully recapitulate how bacteria will be challenged *in vivo*. Next, deciding on what critical factor(s) must be incorporated in an *in vitro* setting (**Figure 11**) is equally important as acknowledging the intrinsic limitations of that specific model.

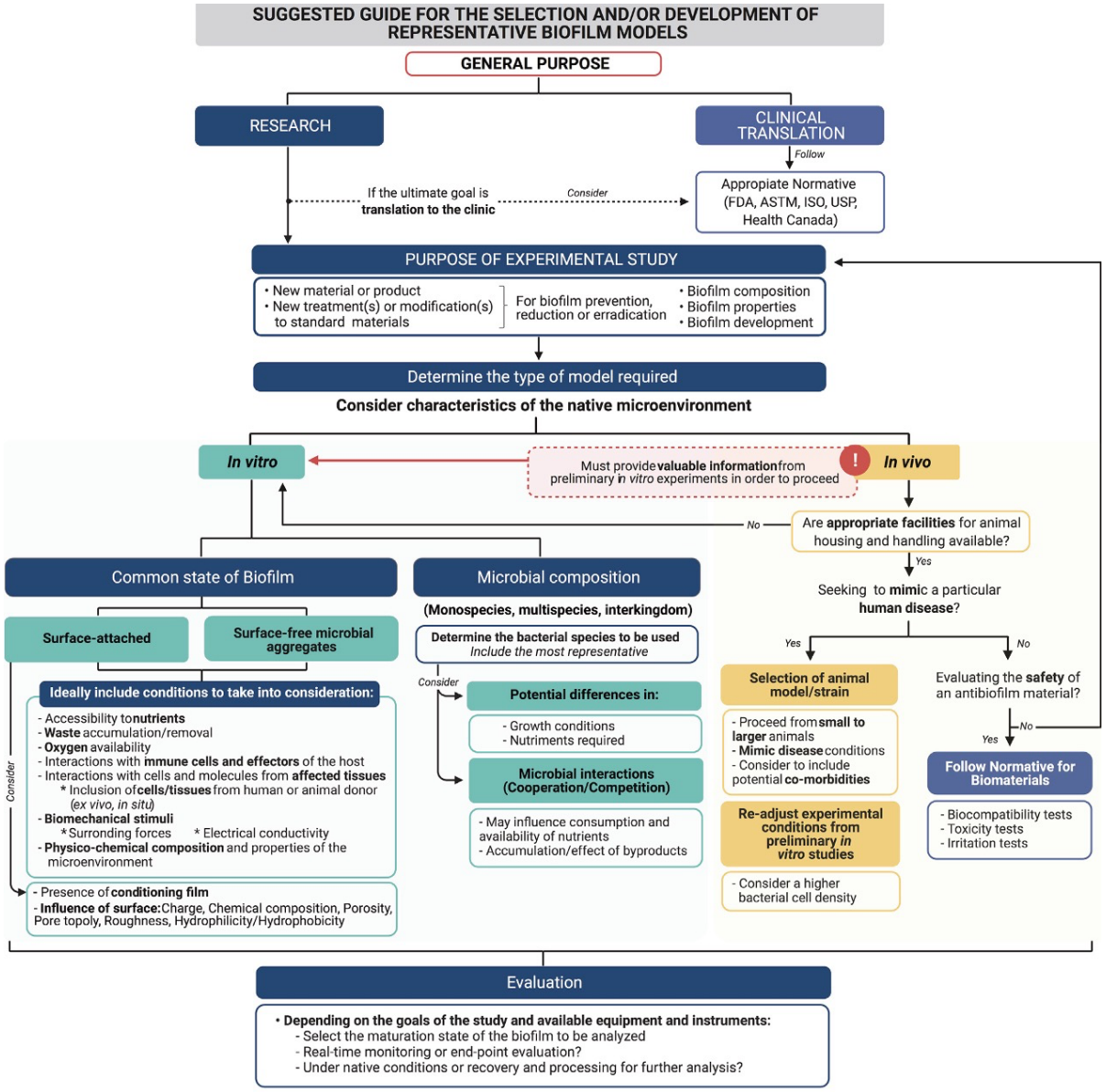

Figure 11. Suggested decision-making system for selecting a biofilm model.

E. GENERAL LIMITATIONS OF *IN VIVO* AND *IN VITRO* BIOFILM MODELS

The overall advantages and drawbacks of currently available *in vitro* and *in vivo* biofilm models were summarized in **Figure 12,** to provide a visual aid of the main points that could be considered when choosing or developing an experimental model for biofilm studies.

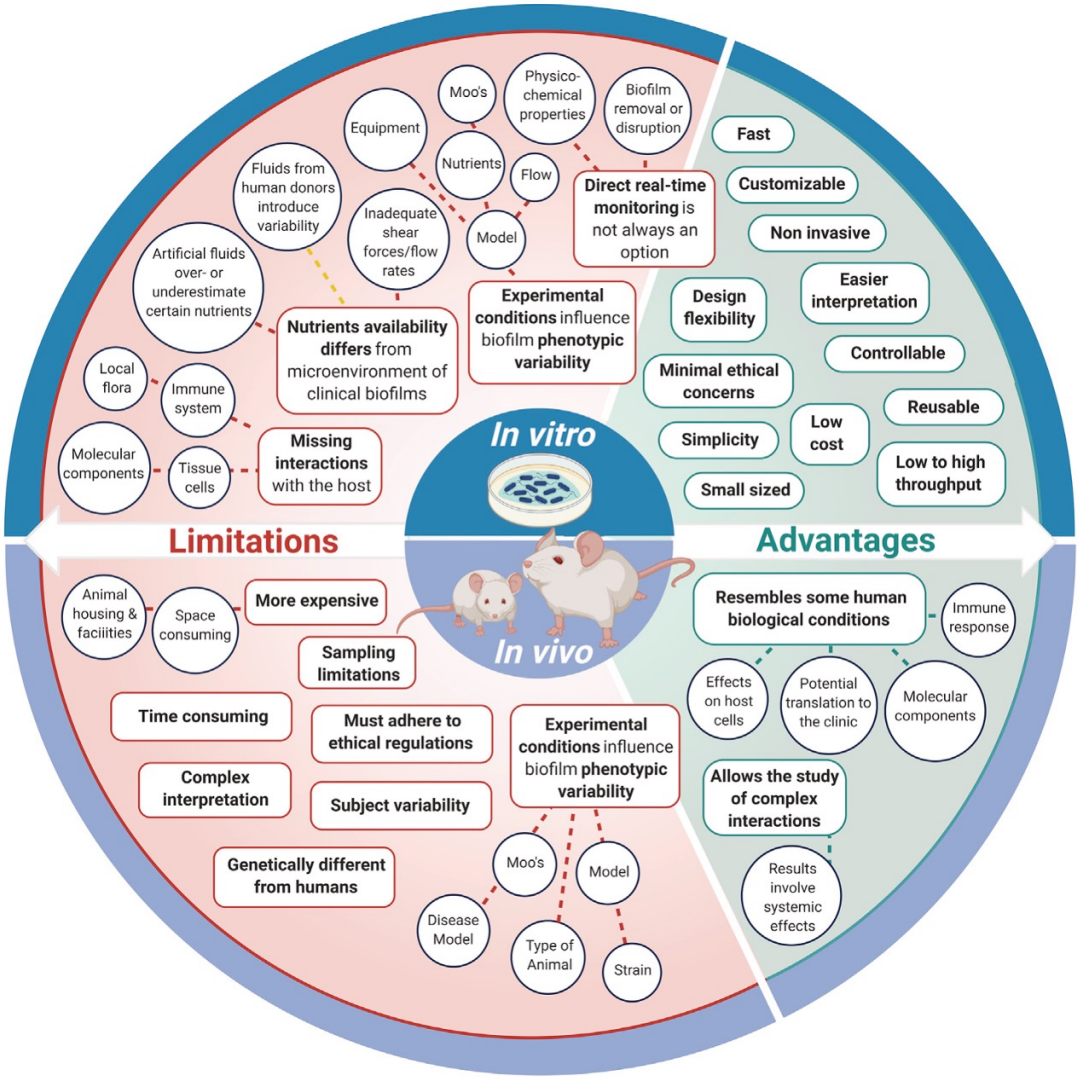

Figure 12. Schematic representation for the limitations and advantages of *in vitro* and *in vivo* biofilm models.

CHAPTER 2 | NANOTECHNOLOGY

2.1 INTRODUCTION

2.1.1 Nanomaterials

Despite being extensively used in research studies and some of them being commercially available, nanomaterials (NMs) still lack from a unanimous and clear definition (Miernicki *et al.*, 2019). Although materials with a length of 1-1000 nm in at least one dimension are sometimes defined as NMs, in the practice is common to find NMs described as those with a diameter in the range of 1 to 100 nm (Auffan *et al.*, 2009; Jeevanandam *et al.*, 2018). Here, the latest definition has been considered as criteria for the selection of nanoparticles (NPs) produced.

Properties of materials at the nanoscale significantly differ from those of their bulk counterparts. Due to the small size of NPs, their surface area to volume ratio is higher than in bulk materials (Phan & Haes, 2019). This is the basis of most of the advantageous characteristics of NPs. Mainly, an increased surface energy (Jolivet *et al.*, 2004; Phan & Haes, 2019); hence, a higher reactivity which provides them with easy variation of surface properties and higher carrier capacity (Ferdous & Nemmar, 2020). As consequence, NPs have a better chance to interact with cells, making them outstanding candidates for biomedical applications (Varier *et al.*, 2019).

NMs can be classified depending on their primary source (Jeevanandam *et al.*, 2018), being inorganic NPs, particularly metallic NPs, of special interest as they have found important applications in biomedical sciences and engineering (Mody *et al.*, 2010). Among them, silver nanoparticles (AgNPs) have been studied most widely. Due to their

distinctive properties, apart from being used in household utensils, and food and health care industries, AgNPs have been employed in biomedical applications as wound dressings, surgical instruments, and disinfectants (Ferdous & Nemmar, 2020).

2.1.2 Silver Nanoparticles (AgNPs)

Some of the main applications of AgNPs include chemical and biological sensing, pollutant removal through catalysis and antimicrobial activity (Mukherji *et al.*, 2019). Part of their popularity is due to the fact that AgNPs synthesis can be designed to include slight experimental variations to allow their formation in particular sizes and shapes (Khodashenas & Ghorbani, 2019). Morphology of AgNPs include spherical (Alarcon *et al.*, 2012; Husanu *et al.*, 2018), wire (Sivakala *et al.*, 2021), cubic (Tao *et al.*, 2006), prism (Alarcon *et al.*, 2016; Tao *et al.*, 2006), rod-like (Cheng *et al.*, 2016), elliptical (Thapa *et al.*, 2017), triangular (Alarcon *et al.*, 2016) and pyramidal geometries (Wiley *et al.*, 2006). It is precisely this variability in size and shape what determines their wide range physical, electronic, catalytic and optical properties which in turn dictates their potential applications (Mukherji *et al.*, 2019), including their resulting biological activities (Ashkarran *et al.*, 2013; Restrepo & Villa, 2021). Hence, when referring to AgNPs, these must be considered as a diverse group, and as such, their properties will be dependent on the chosen synthesis method and physical characteristics of the final product obtained.

2.1.2.1 Synthesis of AgNPs

There is a variety of methods available for the synthesis of AgNPs, being chemical reduction one of the most commonly used (Zhang *et al.*, 2018). It offers the advantage of being able to finely tune the size and shape of AgNPs depending on the nature and concentration of the reagents involved (Beaton *et al.*, 2020). Moreover, among the chemical reduction methods available, we can find differences in experimental conditions (e.g. temperature, type and rate of mixing/stirring, reaction time, etc.) which ultimately affect the type of AgNPs produced (Pinto *et al.*, 2010).

Chemical reduction methods for the synthesis of AgNPs require the inclusion of an agent that acts as silver source, commonly silver nitrate ($AgNO_3$), a reducing agent, and a substance that will provide stability to AgNPs during their synthesis and once produced. In some cases, the reducing agent meets both of these functions, as in the case of citrate (Levard *et al.*, 2012; Pinto *et al.*, 2010). From these methods, the photochemical synthesis of AgNPs represents a simple, clean, and fast alternative (Pacioni *et al.*, 2015). Apart from the above-mentioned components, the light assisted formation of AgNPs also requires the inclusion of a substance able to respond to this stimulus: the photosensitizer. After being exposed to light, photosensitizers can absorb the energy from this source and then transfer it (donors) to other molecules (acceptors) for their activation, causing them to undergo particular chemical reactions, such as polymerization and isomerization (Ravve, 2006). Specifically, photosensitized methods are based on the following mechanisms (Pacioni *et al.*, 2015):

a) Formation of reactive excited states.

b) Generation of organic radical species due to photoinduced bond cleavage reactions of the sensitizer molecule.

Ketones are good photosensitizers for the synthesis of AgNPs because of their ability to function under the second mechanism, favoring the generation of reducing free radicals (Scaiano *et al.*, 2009). Although there are different photosensitizer molecules available, various aromatic compounds have been reported to be the most useful (Ravve, 2006). Particularly, among the family of ketones, benzoines have been widely used due to their tunable solubility (Scaiano *et al.*, 2009). Dr. Scaiano and collaborators have reported several studies in the area of photochemistry for the customized synthesis of Ag and Au NPs, where their size and shape were easily modulated using the benzoin derivative 2-hydroxy-4′-(2-hydroxyethoxy)-2-methylpropiophenone (Irgacure-2959, I-2959) and different light sources (Gonzalez *et al.*, 2009; McGilvray *et al.*, 2006; Scaiano *et al.*, 2009; Stamplecoskie & Scaiano, 2010). The use of this highly efficient photoinitiator offers many advantages, the main ones being that it is a good source of ketyl radicals, has great solubility in water, possesses excellent absorption properties in the UVA region, is not cytotoxic, shows minimal immunogenicity, and is commercially available (Alarcon *et al.*, 2012; Choi *et al.*, 2019; Maretti *et al.*, 2009; Scaiano *et al.*, 2009). **Figure 2** presents a schematic illustrating the main functions of the components employed during the synthesis of AgNPs by a previously reported photochemical method (Alarcon *et al.*, 2012; Stamplecoskie & Scaiano, 2010).

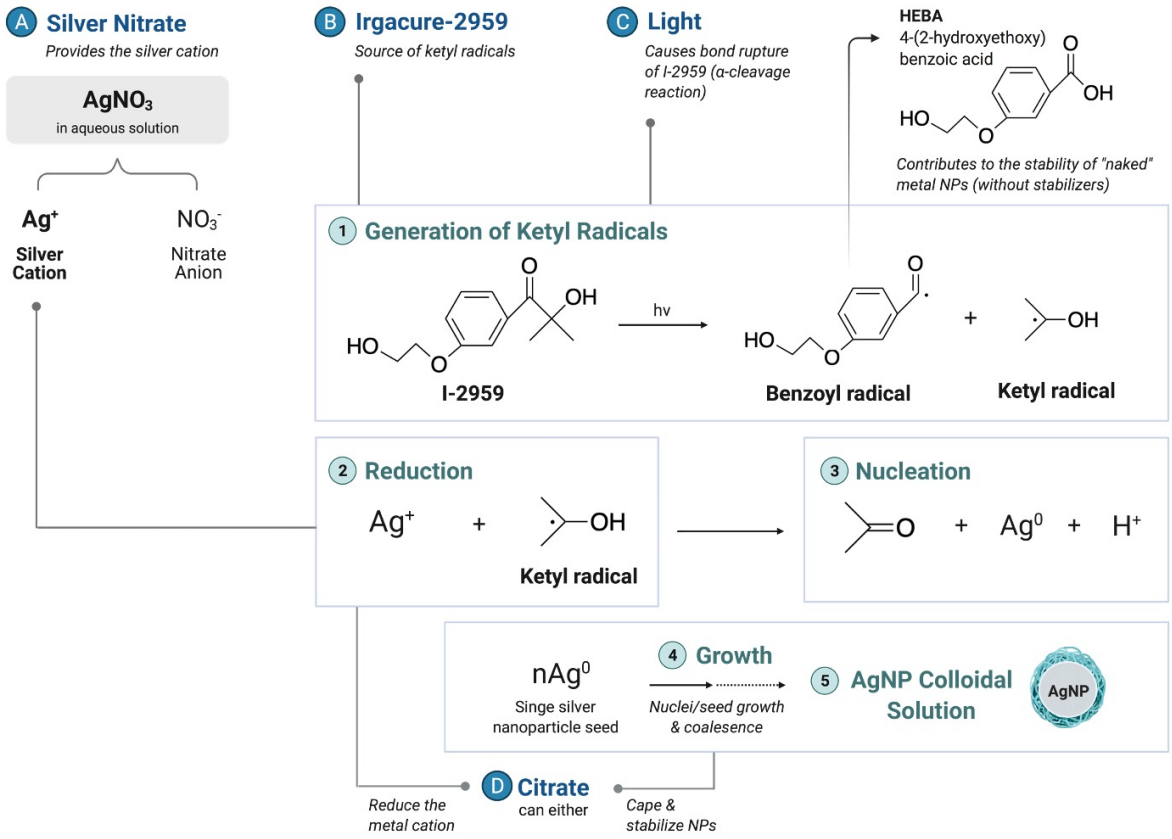

Figure 2. Synthesis of AgNPs by photochemical reduction via ketyl radicals.

This particular approach is based on the use of I-2959, which once exposed to UVA light undergoes an α-cleavage reaction causing the production of benzoyl and ketyl radicals **(1)** (Jockusch *et al.*, 2001; Scaiano *et al.*, 2012). The later are strong reducing agents which will cause the metal Ag cation reduction **(2)** (Maretti *et al.*, 2009). After this, the zero-valent state Ag undergoes a nucleation process, forming a single NP seed **(3)** which will grow and coalesce **(4)** into oligomeric clusters, leading to the formation of colloidal AgNPs **(5)** (Alarcon *et al.*, 2012; Lee & Jun, 2019; Scaiano *et al.*, 2012). Nuclei growth is regulated, among other factors, by the capping agent being utilized and its concentration (Mukherji *et al.*, 2019; Scaiano *et al.*, 2012), where citrate has shown to

contribute both to the stabilization of AgNPs during their formation and further reduction of Ag cations (Alarcon *et al.*, 2012; Mukherji *et al.*, 2019). Moreover, the benzoyl radical formed after I-2959 bond cleavage produces the corresponding carboxylic acid 4-(2-hydroxyethoxy) benzoic acid (HEBA), which contributes to the stabilization of metal NPs that were not protected by the capping agent (Scaiano *et al.*, 2012). In summary, light-assisted formation of AgNPs is a convenient alternative which offers important advantages over other methods, mainly (Maretti *et al.*, 2009; Pacioni *et al.*, 2015; Stamplecoskie & Scaiano, 2010):

- Ability to control the rate of metal reduction by simply regulating the incident light intensity and duration.
- Large versatility; easier control of AgNPs size and shape.
- Does not require harsh reaction conditions (such as boiling temperature) nor the use of strong (potentially toxic) reducing agents.
- Photochemical reduction reactions are usually carried out at room temperature.
- Allows the synthesis of AgNPs utilizing different synthetic and biological protecting agents.
- Relatively inexpensive method.

2.1.2.2 Limitations of AgNPs

Despite the simplicity and versatility offered by synthesis methods of AgNPs, there is an important fact to be considered. Compared to their bulk counterparts, materials at the nanoscale are found in a non-thermodynamically favored state under standard temperature and pressure conditions (Phan & Haes, 2019). Moreover, as the size of NPs

decreases, these become more susceptible to oxidation reactions and instability (Desireddy *et al.*, 2013; Levard *et al.*, 2012), limiting their applicability.

2.1.3 Need of capping agents for stabilization of AgNPs

To prevent the formation of unstable AgNPs, different substances have been proposed to be used as coatings, acting as protective factors. These substances are often referred to as capping agents. Some of them include carboxylic acids derivatives, polymers, surfactants, plant extracts, small ligands, dendrimers, cyclodextrins, and peptides (Javed *et al.*, 2020; Levard *et al.*, 2012; Restrepo & Villa, 2021). Apart from helping to avoid undesired effects, such as agglomeration of NPs, the use of capping agents offers several beneficial functions which are summarized in Figure 3.

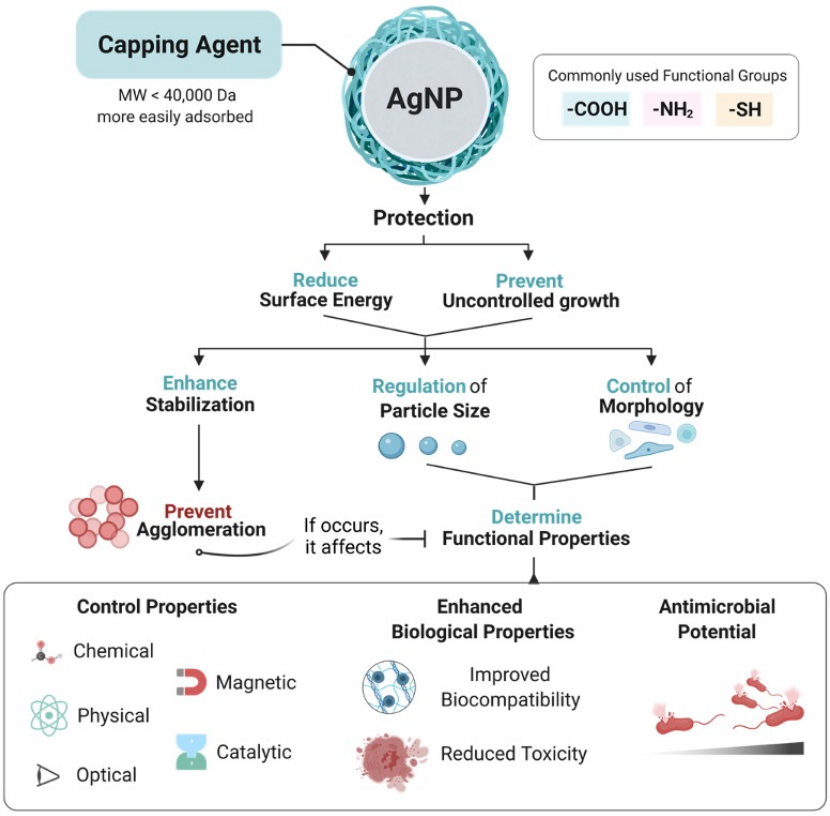

Figure 3. Functions of capping agents on synthesis and properties of AgNPs.

Hence, by selecting the appropriate capping agent, it is possible to not only produce stable AgNPs but to modulate their functional properties depending on the research goals pursued (Restrepo & Villa, 2021; Tanner *et al.*, 2015).

2.1.4 CLKRS as capping agent

The use of peptides as capping agents has proven to be an effective option for protection of AgNPs while providing them with selected additional properties (Kalakonda & Banne, 2018; I. Pal *et al.*, 2019; Restrepo & Villa, 2021). The peptide of interest can be used to produce a reaction of capping agent exchange by directly adding it into colloidal AgNPs, which have been previously synthesized by the method of preference (McLaughlin *et al.*, 2016; Rossi *et al.*, 2018). Alternatively, it can be incorporated as part of the AgNPs reaction mix before the synthesis takes place (Khatoon *et al.*, 2020; Vignoni *et al.*, 2014). It has been previously reported by our group that the pentapeptide CLKRS shows high affinity to the surface of AgNPs, contributing to their stabilization by acting as a capping agent (Poblete *et al.*, 2016). Moreover, we recently published the use of this short peptide for the rapid and easy *in situ* formation of CLKRS-capped AgNPs onto pre-made collagen corneal implants (Khatoon *et al.*, 2020). Apart from stabilizing AgNPs, such materials exhibited enhanced properties such as good biocompatibility, non-inflammatory response, and antimicrobial activity against planktonic and biofilm bacteria related to corneal infection.

2.2 NEXT GENERATION OF CLKRS PEPTIDES

2.2.1 HYPOTHESIS

We hypothesize that by increasing the structural complexity of CLKRS peptide, its properties as capping agent will be improved.

2.2.2 OBJECTIVE

To evaluate the use of newly designed CLKRS peptides as capping agents of AgNPs in colloidal solutions.

2.2.3 METHODOLOGY

Nine structurally different CLKRS peptides (**Figure 4**) were designed and synthesized by Dr. Marcelo Munoz, at the Bioengineering and Therapeutic Solutions (BEaTS) Laboratory of the University of Ottawa Heart Institute.

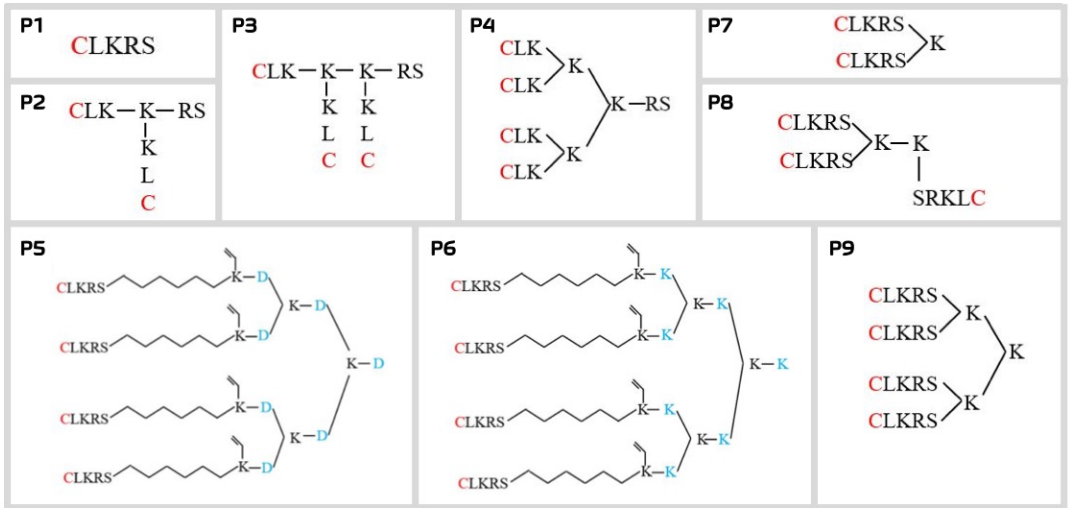

Figure 4. Semicondensed structures of the second generation of CLKRS peptides. To facilitate the identification of modified CLKRS peptides, these were labelled from P1 to P9. C: Cysteine, L: Leucine, K: Lysine, R: Arginine, S: Serine, D: Aspartic Acid.

These peptides were used as capping agents during the synthesis of AgNPs. Next, stability of the obtained colloidal solutions was evaluated (Figure 5).

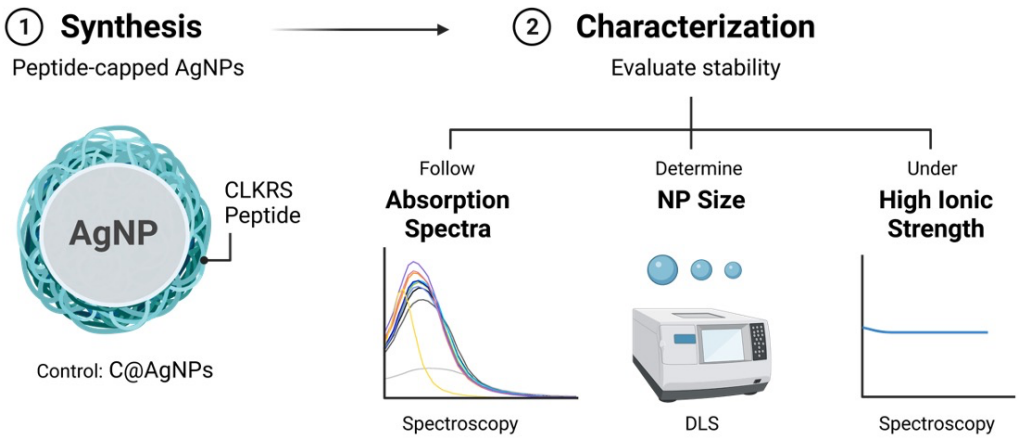

Figure 5. Methodology followed for assays part of the Nanotechnology chapter.

2.2.3.1 Peptide synthesis

The second generation of CLKRS peptides was synthesized using microwave assisted Fmoc solid phase peptide synthesis in a Liberty Blue automated system. Fmoc protected amino acids and Wang resin with preloaded amino acids were purchased from CEM. Briefly, the required amount of resin was swelled with DMF in the system for 5 min. Next, Fmoc deprotection was carried out with 20% piperidine at 90°C for 60s while standard coupling cycles using DIC/Oxyma Pure were run at 90°C for 240s for each amino acid that was added to the sequence. Peptides were cleaved from the resin and deprotected with 92.5/2.5/2.5/2.5% v/v TFA/TIS/EDT/H2O at 42°C for 30 min and then precipitated in -20°C diethyl ether. Peptide crude products were then dried under vacuum overnight and purified by Reversed Phase-High Performance Liquid Chromatography (RP-HLPC) in a Waters 1525EF semi-preparative system with a 21.6x250 mm C18 column at 20 mL/min. Peptide purity and identity was confirmed via

RP-UPLC-UV/MS in a Waters Acquity UPLC Xevo TQD using a 2.1x100 mm UPLC BEH C8 column. A purity of >95% was determined through ultraviolet (Suvarnapathaki *et al.*) peak analysis.

2.2.3.2 Synthesis of AgNPs

2.2.3.2.1 Citrate capped AgNPs (C@AgNPs)

C@AgNPs were synthesized as previously described (Alarcon *et al.*, 2016; Stamplecoskie & Scaiano, 2010). Briefly, a deoxygenated aqueous solution (30 min under N_2) composed of 0.2 mM $AgNO_3$, 0.2 mM Irgacure-2959 (I-2959), and 1.0 mM sodium citrate was irradiated with UVA light (14 lamps, in a Luzchem LZC-4 photoreactor at 25.0 ± 0.5°C) for 30 minutes. Clear yellow colloidal solutions were obtained and stored at room temperature, protected from light.

2.2.3.2.2 Peptide capped AgNPs

All the synthesized CLKRS peptides were used as capping agents during the synthesis of AgNPs. Previously reported conditions (**Supplementary Table 1**, (Khatoon *et al.*, 2020)) were evaluated for P3, as reference, by absorption spectroscopy (**Supplementary Figure 1**). The following mix composition was considered for further experiments: 0.6 mM $AgNO_3$ as source of silver and 0.6 mM of the photoinitiator I-2959. Twelve peptide concentrations (1, 2, 3, 4, 5, 6, 7.5, 15, 25, 50, 75, and 100 µM) were evaluated for the 9 CLKRS peptides. For this, 1 mL of each different condition was

individually exposed to UV irradiation in a 2 mL glass vial for 5 min using a Luzchem Photoreactor (LZC-4V, 14 UVA lamps, centered at 350 nm).

2.2.3.3 Characterization of AgNPs by absorption spectroscopy

Absorption spectra of the colloidal solutions obtained for all the CLKRS peptides at the different concentrations tested were obtained by reading 200 µL of each in a 96 well plate, using a SpectraMax M2 (Molecular Devices) microplate reader. To obtain the surface plasmon band (SPB), absorbance was read at room temperature in a wavelength range from 350 nm to 750 nm, with 10 nm increments.

2.2.3.4 Size of AgNPs by Dynamic Light Scattering (DLS)

Particle size of colloidal AgNPs was determined by DLS utilizing a DynaPro plate reader-II (Wyatt Technology). Setup conditions were determined after analyzing colloidal P3@AgNPs (due to availability) at different acquisition numbers and acquisition times (Software: Dynamics 7.1.9), at a temperature of 25°C. Each one of the correlation plots of every acquisition for each sample (10 acquisitions per sample per triplicate) were compared to the different types of correlation functions (DYNAMICS User's Guide M1400 Rev.K) to determine the quality of the measurements obtained (Wyatt, 2010). This way, a more accurate selection of the required parameters for DLS measurements was done and considered for further experiments. The best condition for peptide capped AgNPs consisted of 15 acquisitions per sample and an acquisition time of 1s. Then, 125 µL of freshly prepared colloidal AgNPs solutions for each one of

the 9 CLKRS peptides and corresponding 12 concentrations, were analyzed in 96-well half area black/clear flat bottom polystyrene microplates (Corning® 3880). The hydrodynamic diameter of AgNPs was determined by calculating an arithmetic average of 3 replicates under the above-mentioned settings.

2.2.3.5 AgNPs stability under high ionic strength

From the previously tested CLKRS peptides and concentrations, peptides P5, P6, and P9 were selected for further experiments. Particularly, peptide concentrations of 3, 4, 5, 6, and 7.5 µM were considered for evaluating stability of the corresponding colloidal AgNPs under a high ionic strength to simulate *in vivo* conditions (Regini *et al.*, 2004). For this assay, the SPB was followed every minute for up to 8 hours at a wavelength of 420 nm after the addition of 150 mM NaCl, in a 96-well plate (final volume of 200 µL).

2.2.4 STATISTICAL ANALYSIS

All the experiments were done at least in triplicates. Plots represent the mean and error bars correspond to standard deviation of the mean. Statistical comparisons between groups were done in Kaleida Graph v4.5.2 using Student t test for unpaired data with unequal variance. Significance was considered as $p<0.05$.

2.2.5 RESULTS AND DISCUSSION

2.2.5.1 Effect of capping agent on stability of AgNPs

As previously mentioned, size and shape of AgNPs can be controlled by surface modification, affecting as consequence their physicochemical, optical, electrical, magnetic, mechanical, thermal and catalytic properties (Beaton *et al.*, 2020; Phan & Haes, 2019). Regarding to optical properties, metal NPs present a phenomenon which is caused by the collective oscillation of conduction electrons when these are disturbed from their equilibrium positions (Lu *et al.*, 2009). During this event, the electron cloud oscillates on the NP surface, absorbing electromagnetic radiation (Smitha *et al.*, 2008). This is referred to as surface plasmon resonance (SPR). The colorful appearance of metallic NPs, red for gold (Au) and yellow for Ag, is a consequence of their SPR due to absorption of electromagnetic radiation at a particular energy (Stamplecoskie & Scaiano, 2012). Some transition metals, including cupper (Camci-Unal *et al.*), Ag, and Au, present SPR in the visible region (Lu *et al.*, 2009). For this reason, UV-Vis absorption spectroscopy is one of the most common methods for evaluating changes in the optical properties of AgNPs due to surface functionalization, as this affects surface polarization which causes alterations of the SPB (Smitha *et al.*, 2008). The absorption peak position for AgNPs, at about 400 nm for spherical NPs, is greatly dependant on their size, shape, surface charge, state of aggregation, and the surrounding dielectric medium (Jiang *et al.*, 2014; Smitha *et al.*, 2008). Some of the main variations that can be observed for AgNPs and their potential interpretations are summarized in **Figure 6**, which was designed based on previously published studies (Agnihotri *et al.*, 2014; Beaton *et al.*,

2020; Bélteky *et al.*, 2019; Krishnaprabha & Manjunatha, 2017; Levard *et al.*, 2012; Pinto *et al.*, 2010; Rycenga *et al.*, 2011; Smitha *et al.*, 2008; Sökmen *et al.*, 2017; Tejamaya *et al.*, 2012). It is important to highlight that this figure was based on the most common assumptions reported for this type of SPB curves and as such, it is merely intended to serve as a guide for an initial characterization step of AgNPs. Depending on the questions that want to be answered, specialized techniques would be required in order to provide more accurate assumptions.

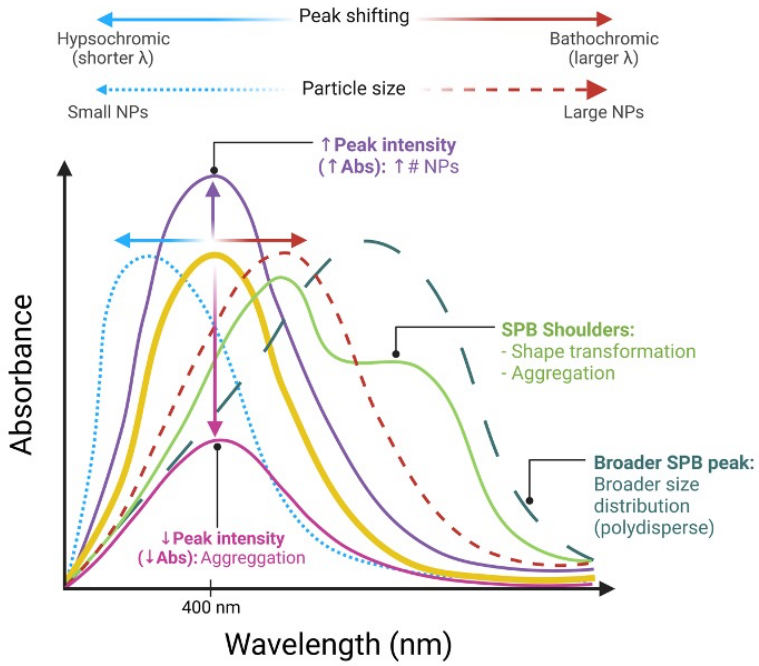

Figure 6. Potential interpretation of most common changes observed on the plasmon band of AgNPs.

After utilizing different concentrations of capping agents, namely CLKRS peptides, for the synthesis of colloidal AgNPs, their efficacy to produce stable NPs was evaluated by following the SPB by UV-Vis spectroscopy (**Figure 7**). From these plots and having the control C@AgNPs as reference, it can be noted that:

- In most of the conditions evaluated, produced AgNPs showed a red-shifted and broader SPB peak which is usually associated with larger particle size(s)

(Agnihotri *et al.*, 2014; Mlalila *et al.*, 2016) and polydispersity (Agnihotri *et al.*, 2014; Tejamaya *et al.*, 2012), respectively.

- Peptides P1, P2, P3, P7, and P8 showed a tendency to favor agglomeration of AgNPs at lower concentrations, specifically from 1 to 6 µM and up to 15 µM for the reference CLKRS peptide P1. This is observed as a reduced absorbance at the SPB peak position and at longer wavelengths. A decrease in intensity may be an indication of particle destabilization (Restrepo & Villa, 2021).

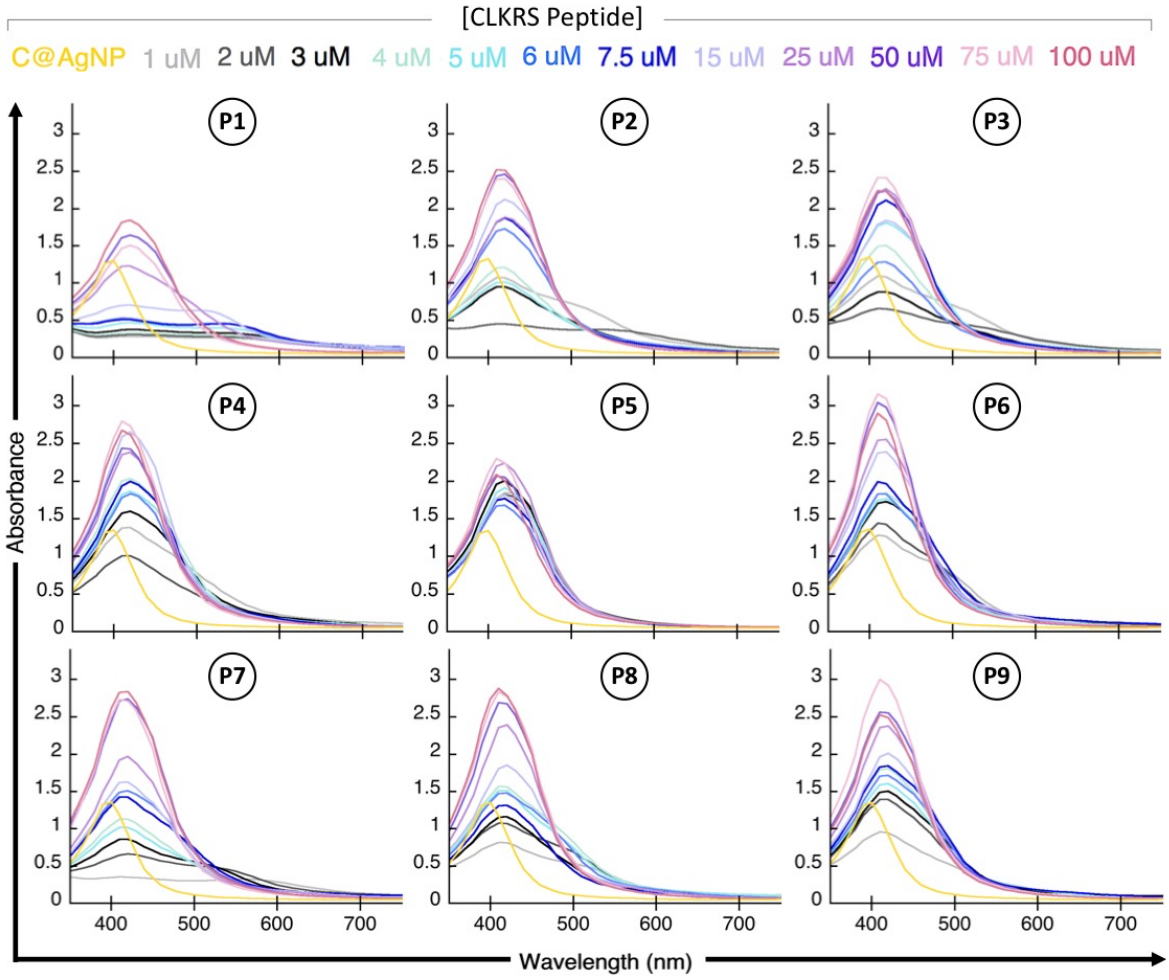

Figure 7. SPB of peptide capped AgNPs at different concentrations.

- There are higher absorbance values in most of the colloidal solutions prepared (with exception of the above-mentioned peptides and concentrations), which could be related to an increased number of AgNPs (Krishnaprabha & Manjunatha, 2017; Sökmen *et al.*, 2017).
- Peptides P1, P2, P3, P6, P7, and P8 presented a small shoulder at certain (low) concentrations and this has been previously associated with the presence of different shapes of AgNPs (non-spherical) (S. Pal *et al.*, 2007).
- CLKRS peptides with more complex structures (P4, P5, P6, and P9) produced apparently stable AgNPs at the lowest concentration evaluated (1 µM).

In brief, AgNPs synthesized in the presence of peptides P4, P5, P6 and P9 as capping agents required a minimal concentration of 1 µM. From these, the last 3 peptides also allowed the synthesis of AgNPs with higher absorbance intensity.

2.2.5.2 Size of peptide capped AgNPs by DLS

DLS is a frequently used technique for physicochemical characterization of AgNPs as it allows the estimation of particle size and size distribution (Shnoudeh *et al.*, 2019). The hydrodynamic size of AgNPs, produced at 12 different concentrations of CLKRS peptides, was determined by DLS analysis of the colloidal solutions. **Figure 8** include the plots for size of AgNPs capped with P5, P6, and P9, as these presented NP diameters below 100 nm at all the concentrations evaluated. Results for each of the 9 peptides tested are shown in **Supplementary Figure 2**.

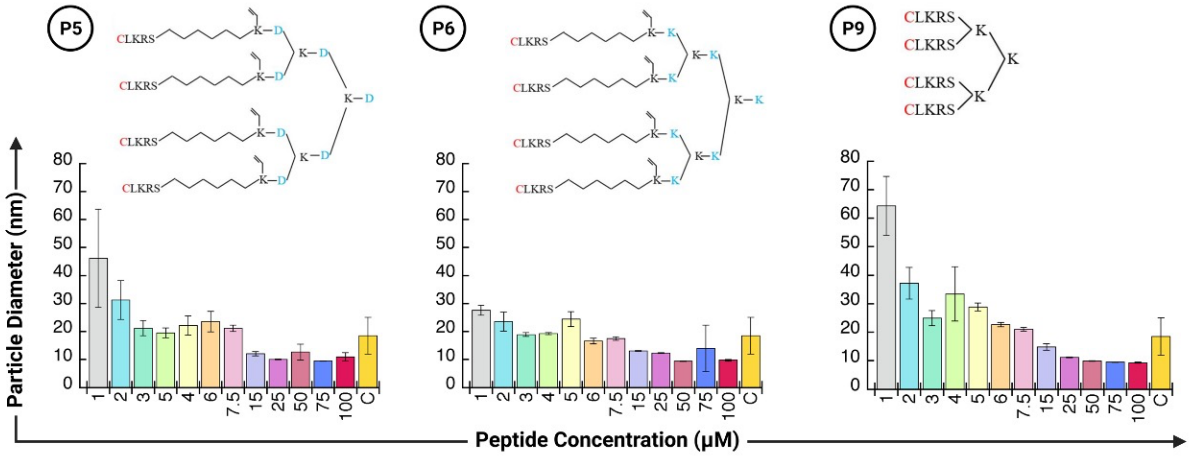

Figure 8. Hydrodynamic size of AgNPs produced with different concentrations of P5, P6, and P9 peptides. C: C@AgNPs.

The main findings that can be drawn from this assay include:

- Decrease in particle size as peptide concentration increased. No further decrease in NP size from concentrations equal or higher than 25 μM.
- Peptide P7 produced the largest AgNPs.
- Peptides P5, P6, and P9 fell into the size range that meets the definition of NP (below 100 nm in diameter), at all the concentrations tested.
- Concentrations from 3 to 7.5 μM of these peptides produced AgNPs with a similar size to those synthesized with citrate (C@AgNPs) as capping agent via traditional photochemical method (**Supplementary Table 2**).

2.2.5.3 Stability of peptide capped AgNPs under high ionic strength

It has been previously stated that stability of AgNPs must be considered during their synthesis and storage conditions but, the environment where these will be finally utilized must be also considered as this will ultimately determine their properties. One of the most common ways of evaluating this is to combine NPs with diverse biologically relevant solutions and microenvironmental conditions. Then, their SPB is monitored at different times to assess stability. We evaluated peptide capped AgNPs under physiological ionic strength (150 mM NaCl) (Regini *et al.*, 2004). **Figure 9** shows the plots for the slope obtained from the absorbance decay at λ=420 nm during the first 15 min post-incubation, which in this case where the most representative.

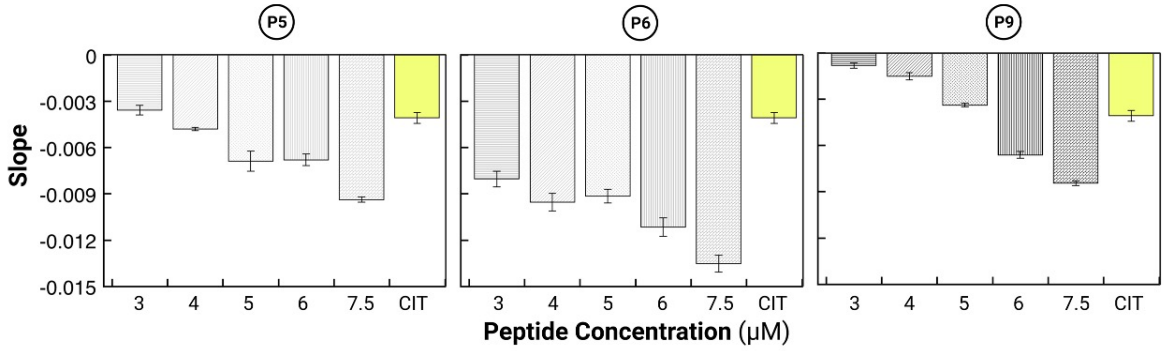

Figure 9. Ionic strength assay of peptide capped AgNPs. Values correspond to the mean of 3 repeats and error bars indicate the standard deviation of the mean. CIT: C@AgNP. In all cases, difference between the lowest and any other concentration was statistically significant ($p<0.05$).

For interpretation of these results, it was considered that the larger the slope values, the steeper it is, and for our data, it would represent a more pronounced decay in absorbance. This would be an indicative of less stable AgNPs. Hence, as observed in **Figure 9**, stability of AgNPs is concentration dependant, with a value of 3 μM being the best concentration for the three peptides evaluated.

2.2.6 CONCLUSIONS

All the CLKRS peptides evaluated showed to be effective for their use as capping agents at most of the concentrations tested. From these, peptides of higher structural complexity (4-leg peptides) produced more stable AgNPs. Peptides (P5, P6, and P9) favoured the production of AgNPs with diameters below 100 nm, even at concentrations as low as 1 μM. Finally, these peptides rendered AgNPs which showed to be more stable at a concentration of 3 μM under physiologically relevant conditions. Hence, after synthesis and characterization of AgNPs, the available capping agents were narrowed down to three peptide candidates to be used in further experiments for functionalization of biomaterials.

CHAPTER 3 | BIOMATERIALS FOR CORNEAL REPAIR

3. 1 INTRODUCTION

As previously mentioned in Chapter 1, there is a high prevalence of corneal associated diseases which may culminate in corneal blindness. In fact, corneal opacities occupy the fourth position among the leading causes of blindness worldwide, right after cataracts, glaucoma, and macular degeneration (Jeng & Ahmad, 2021). Moreover, not only the long waiting lists for human donor corneas but also the potential occurrence of post-operative complications denote an urgent need for the development of alternative options to treat and replace damaged corneas. Some of the main biomaterial-based strategies for corneal repair that have been proposed include the use of cell-based and cell-free scaffolds, natural, synthetic and hybrid materials, hydrogels, bioengineered prosthetic devices, contact lenses, bioprinting, and drug delivery systems (Hancox *et al.*, 2020; Palchesko *et al.*, 2018; Tsai *et al.*, 2015). Tissue transplantation from non-human donors (allogenic tissues) may represent an attractive option to uphold the shortage of corneal tissue. However, there is an associated risk of immune reaction and potential ethical concerns which limit its applicability. Hence, cell-free biomaterials with enhanced properties to prevent post-surgery complications would provide a safe alternative to treat corneal blindness. Furthermore, there are several considerations that must be taken into account when designing biomaterials intended to be used in corneal repair and replacement strategies. Mainly, biodegradability, biocompatibility, mechanical properties, cell attachment suitability, water permeability, transparency and porosity (Hancox *et al.*, 2020).

Collagen hydrogels have proved to be a suitable option to produce cornea-shaped lenses which may be used as a replacement for human donor corneas (Liu *et al.*, 2006). Furthermore, the incorporation of AgNPs into collagen hydrogels has shown to prevent and/or reduce the development of microbial infections (Alarcon *et al.*, 2016). Recently, our group reported a rapid and facile method for the *in situ* formation of peptide-capped AgNPs onto pre-made collagen corneal implants (Khatoon *et al.*, 2020), increasing the possibilities of clinical applicability.

3.2 RATIONALE

To contribute to the alternative approaches required for the demanding need of corneal repair and replacement, the combined use of cell-free biomaterials and NPs is proposed.

3.3 HYPOTHESIS

We hypothesize that CLKRS peptides of higher structural complexity will act as capping agents during the *in situ* functionalization of premade collagen-based hydrogels with AgNPs, to provide them with improved antimicrobial properties.

3.4 OBJECTIVE

To produce and functionalize two types of collagen-based hydrogels (Figure 10), specifically, compressed collagen hydrogels to be used as corneal patches in injured corneas and, cornea-shaped hydrogels to prevent post-operative microbial infections after transplantation.

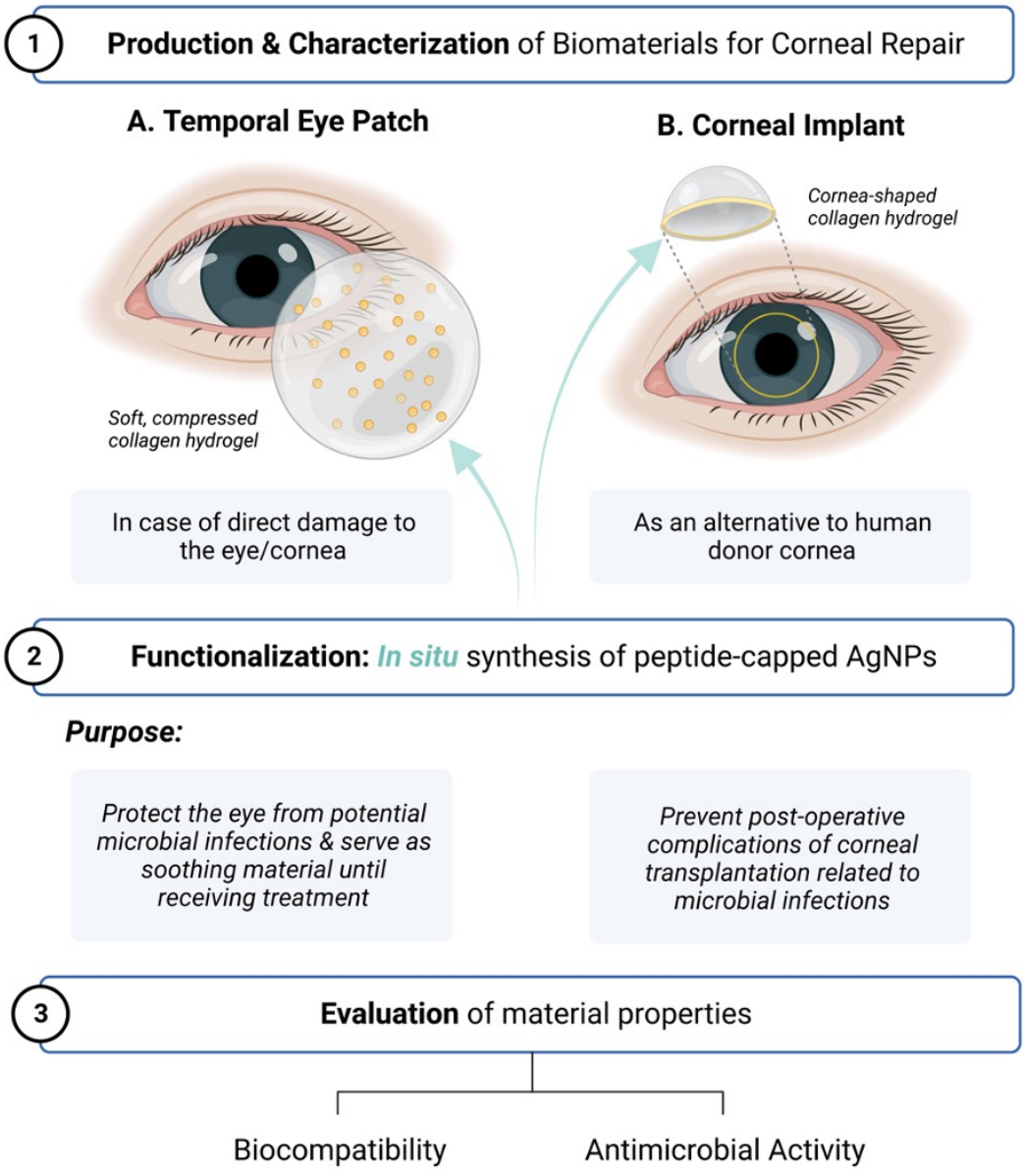

Figure 10. Schematic representation of the rational and objectives of Chapter 3.

3.5 METHODOLOGY

Chemicals and reagents

Unless otherwise indicated, all common laboratory chemicals and reagents were purchased from Sigma®.

A. COMPRESSED COLLAGEN HYDROGELS

The methodology followed for producing and evaluating compressed collagen hydrogels is represented in **Figure 11** schematic.

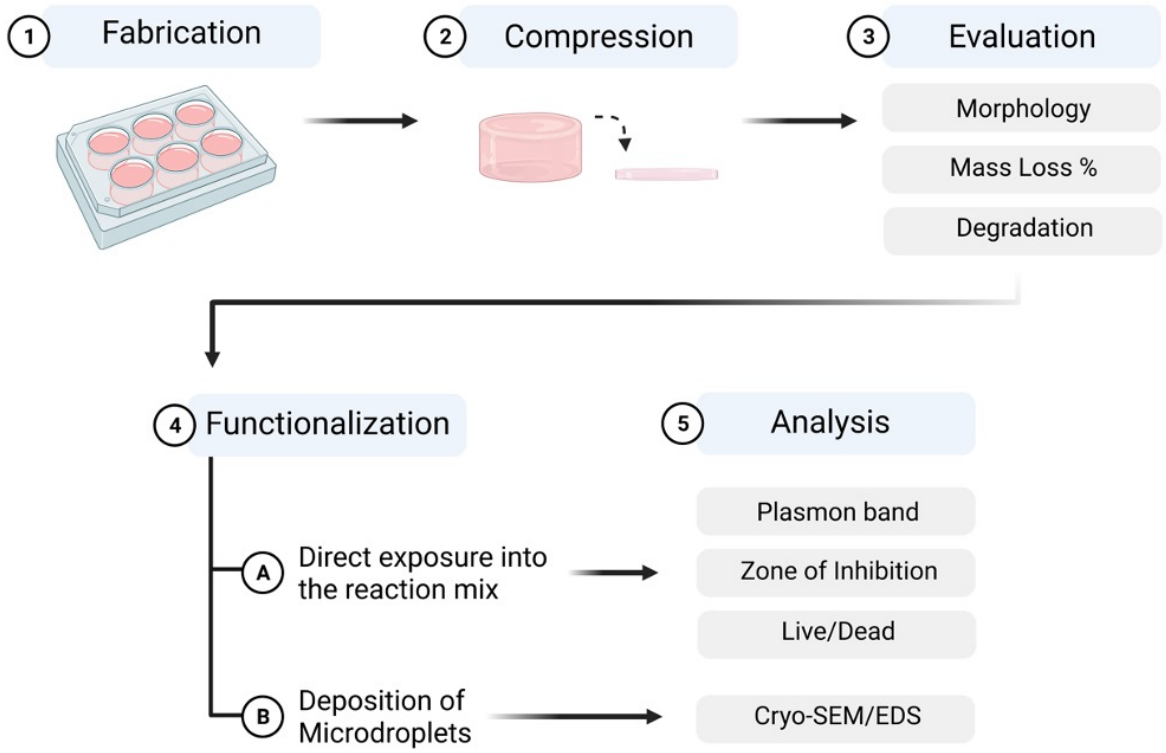

Figure 11. Methodology for compressed collagen hydrogels.

A.1 Solutions

All solutions were prepared with Milli-Q water, unless otherwise indicated.

- **10X Collagen medium:** Composed of 9mL of 10X DMEM (pH 7.2, Gibco), 9mL of 1 M HEPES (pH 7, Gibco), 10mL of FBS (Gibco), and 0.1mL of Gentamycin (Gibco). Mix all components in appropriate volumes and sterile filter into 50 mL Falcon tubes. Store at -20°C until use.
- **1X PBS:** According to manufacturer, corresponds to a solution composed of 137 mM NaCl, 2.7 mM KCl and 10 mM phosphate buffer.
- **0.1 M Tris-HCl buffer:** 0.1 M Tris Base complemented with 5 mM $CaCl_2$, pH 7.4 adjusted with 12.1 M HCl.

A.2 Collagen-based hydrogel preparation

Collagen hydrogels were prepared in sterile biosafety cabinets according to a previously published protocol from our group (Lazurko *et al.*, 2020), with slight modifications. Briefly, hydrogels were prepared by combining 6 mL of 1% type I porcine collagen (TheraCol, Sewon Cellontech Co.) with 1 mL of 10X collagen medium in a 20 mL glass vial. As the presence of air bubbles interfere with crosslinking of this type of hydrogels, their formation was prevented by utilizing a 5 cm stirring bar in vertical position and gently mixing at low speed for short periods of time. Note that collagen was kept on ice throughout the experiment. Next, 600 µL of 1X PBS were added to the solution. After this, pH of the solution was adjusted to 7.2-7.4 with 1 N NaOH in 10 µL increments, using pH paper strips (Fisherbrand™ pH Test Paper Rolls, Cat. No. 13-640-

507). Next, 200 μL of 1.5% glutaraldehyde (crosslinking agent) were incorporated in 2 addition steps (100 μL at a time) and incubated on ice in dark conditions (covered with aluminum foil) for 15 min. Then, 500 μL of 20% glycine were added and solution was allowed to sit for 30 min prior to use to quench the unreacted glutaraldehyde. After this time, the still liquid solution was transferred into a 6-well plate by pouring 3 mL of the mix per well. Hydrogel formation was done after incubating the plate at 37°C for 1 hour.

A.3 Compression of Collagen Hydrogels

Once the hydrogels were obtained, these were scooped out of the 6-well plate and placed onto a glass Petri dish. Then, a circular piece of absorbent filter paper (Whatman® Chromatography paper, 3030 917) of 3.4 mm diameter was sit on top of the hydrogel and used to transfer it to the paper by flipping the plate upside down. A total of 5 layers of filter paper were arranged both on top and bottom of the hydrogel and placed into a 60x15 mm tissue culture plate lid. Next, a custom 3D printed plastic piece was placed and centered on top of the paper portion where the hydrogel was located to serve as support for the load to be used for compression. Afterwards, a metallic piece of 198.07 g was placed on top of the plastic device to exert pressure onto the hydrogel. The calculated total pressure reached using this set up was 2285.06 N/m^2. **Supplementary Figure 3** illustrates the setting of materials used for this purpose. Different compression times were evaluated: 5 min, 10 min, 15 min, and 30 min. After obtaining experimental information about mass loss and degradation by collagenase of these hydrogels, only one of the compression times was considered for further

experiments. Once ready, compressed collagen hydrogels were stored in 1X PBS at 4°C.

A.4 Mass loss after compression

Mass of hydrogels was measured before and after compression to estimate mass reduction in the final product. The following formula was used to calculate the mass loss percentage after compression, where m_0 corresponds to the initial mass (before compression) and m_t to mass at a subsequent time (after compression).

$$Mass\ Loss\ \% = \frac{m_t - m_0}{m_0} \times 100$$

A.5 Scanning Electron Cryo-Microscopy (Cryo-SEM) of compressed hydrogels

After compression, a sample hydrogel was processed for cryo-SEM to perform microstructure analysis. Assessment was done at the Nano Imaging Facility (NIF) of Carleton University by Dr. Jianqun Wang. Briefly, image capture was done with a TESCAN scanning electron microscope, Model VegaII XMU, with a backscattered electron detector using cryo operation at a low-vacuum condition. Setting conditions included an acceleration voltage of 20KV, CryoStage temperature around -50°C (below -40°C), and chamber vacuum around 40Pa.

A.6 Hydrogel degradation by collagenase

Samples of compressed collagen hydrogels were obtained by cutting out 6 mm diameter circular pieces, using a sterile disposable biopsy punch (Integra Miltex®, REF 33-36), and rinsed with 1X PBS. The mesh part of a 70 µm Nylon Mesh Cell Strainer (FisherBrand, Cat# 22363548) was used for this purpose and excess water was removed by pressing the mesh against a Kimwipe®. Disposable 24-well Millicell® Hanging Cell Culture Inserts (0.4 µm PET, Millipore, Cat# PIHT12R48) were used as hydrogel holders to facilitate their manipulation while allowing exposure to solutions and easier removal of these, without further disruption of the materials being tested. Once rinsed, hydrogels were transferred to the hanging inserts and allowed to stabilize in 0.1 M Tris-HCl buffer during 1 h at 37 °C. After this time, gels were taken out of the buffer, excess liquid was removed, and mass registered (m_0). Next, 300 µL of prewarmed 5 U/mL Collagenase solution (Type I Collagenase from *Clostridium histolyticum,* 235.00 Units/mg, Gibco) were added on top of the hydrogel and the 24-well plate with inserts was incubated at 37 °C. Solution was drained out of the inserts (by pressing against a Kimwipe®) at selected time intervals to measure the mass remaining (m_t). Collagenase solution was replaced after each sample was weighed throughout the selected time period (5, 10, 15, 60, 120, 300, 420, and 480 min). To calculate collagen degradation (reported as residual mass percentage), the following equation was used:

$$Residual\ Mass\ \% = \frac{m_t}{m_0} \times 100$$

A.7 *In situ* functionalization of compressed collagen hydrogels

Functionalization of compressed collagen hydrogels was proposed to be done by testing the efficacy of different CLKRS peptides to act as capping agents during the synthesis of AgNPs directly onto the hydrogels. Two strategies were evaluated: direct exposure of all components to photoirradiation, and deposition of AgNPs onto the hydrogels after their formation in microdroplets.

A.7.1 Direct exposure into the AgNPs reagent mix

Collagen hydrogels were prepared and compressed as previously described. Then, pieces of 6 mm in diameter were obtained from these gels using a sterile disposable biopsy punch (Integra Miltex®, REF 33-36). The best peptide concentration obtained from SPB, size, and ionic strength stability results from chapter two was considered for functionalization of hydrogels with peptide capped AgNPs. From the same set of experiments, 3 peptides were selected for the *in situ* synthesis of AgNPs on hydrogels. Hence, peptides P5, P6, and P9 were individually used at a 3 µM concentration to serve as capping agents during the *in situ* formation of AgNPs directly on the hydrogels. The AgNPs reagent mixture was composed of 3 µM peptide (either P5, P6, or P9), 0.6 mM $AgNO_3$ and 0.6 mM I-2959, prepared in sterile Milli-Q® water. Next, the compressed hydrogel samples were rinsed 5 times in Milli-Q® water to remove any leftover of PBS, as this may interfere with formation of AgNPs. The mesh part of a 70 µm Nylon Mesh Cell Strainer (FisherBrand, 22363548) was used for this purpose and excess water was removed by pressing the mesh against a Kimwipe®. Then, gels were placed into 4 mL

of the AgNPs reagent mix in a glass vial and exposed to UV irradiation during 5 minutes in a Luzchem Photoreactor (LZC-4V, 14 UVA lamps, centered at 350 nm). This procedure was repeated at least 3 times for each peptide using different batches of compressed hydrogels. Finally, the functionalized gels obtained after the *in situ* formation of peptide capped AgNPs were analyzed by spectrometry for analysis of SPB. Freshly functionalized hydrogels were prepared when required for further experiments; namely, antimicrobial activity and biocompatibility assays.

A.7.1.1 Plasmon band of functionalized compressed hydrogels

To evaluate the potential presence of AgNPs in the functionalized compressed hydrogels, the excess of irradiation solution was removed, and gels were placed into individual wells of a 96-well plate. Non treated compressed hydrogels were used as negative control (Blank Gels). Further, a sample (200 µL) of the irradiation solution where each peptide was exposed, was also evaluated. Different conditions were considered to serve as controls for these solutions. Specifically, C@AgNPs; No gel-No peptide (NG-NP): Mix with all components, except peptide; Gel-No peptide (G-NP): Mix with all components, including hydrogel, and missing peptide; No gel-peptide 5 (NG-P5): Mix with all components, except gel; No gel-peptide 6 (NG-P6): Mix with all components, except gel; and No gel-peptide 9 (NG-P9): Mix with all components, except gel. Spectra of the hydrogels were obtained by following absorbance readings in a wavelength range from 350 nm to 750 nm, using a SpectraMax M2 (Molecular Devices) microplate reader.

A.7.1.2 Zone of inhibition (ZOI) assay

The potential antimicrobial activity of compressed hydrogels functionalized with peptide capped AgNPs was evaluated by means of a ZOI assay (Haq *et al.*, 2020). Briefly, it consists in placing small circular pieces of sterile filter papers that have been previously soaked into the substance of interest, onto an agar plate with freshly spread bacterial suspension to test its potential as antimicrobial agent. Different concentrations and conditions can be evaluated using the same agar plate by dividing it into sections. After incubation at optimal temperature for the bacteria being evaluated, a clear halo with no bacterial growth (ZOI) is observed around those treatments that resulted effective against bacterial colonization (Vaughan *et al.*, 2011). Next, antimicrobial activity may be visually assessed or, if a semi-quantitative analysis is preferred, the diameter of such clear halos is measured to establish group comparisons. Here, both approaches were performed.

Bacterial strains

Staphylococcus aureus ATCC 25923 and *Pseudomonas aeruginosa* PAO1 were used for testing the potential antibacterial activity of compressed collagen hydrogels functionalized with peptide capped AgNPs. ATCC 25923 had been previously obtained from the American Type Culture Collection (ATCC), while PAO1 strain had been kindly donated by Dr. Thien Fah Mah (Faculty of Medicine, University of Ottawa) to our laboratory. Both were available as bacterial stocks prepared in 25% glycerol and stored at -80°C.

Bacterial culture obtention

The protocol followed to prepare the bacterial cultures used in this and other antimicrobial testing experiments consisted in transferring a loop full of bacteria from the -80°C aliquots into 5 mL of previously warmed up Luria Bertani (LB) broth. Next, this tube was incubated overnight at 37°C, under aerobic conditions and constant agitation using an orbital shaker device (Innova®40, New Brunswick Scientific) set at 230 rpm. The day after, a loop full of the obtained bacterial suspension was distributed onto an LB agar plate using the strake plate method to isolate individual colony forming units (CFU). Plates were incubated overnight at 37°C in an upside-down position. Then, a single CFU of the corresponding bacterial strain was recovered using a metallic loop, transferred into 5 mL of previously warmed up LB broth, and incubated overnight under the above-mentioned conditions for bacterial suspensions. The next day, bacterial cultures were ready to be used.

ZOI assay conditions

Mueller-Hinton agar (MHA) is recommended for testing antibacterial agents (Bauer, 1966; Vaughan *et al.*, 2011). Hence, individual MHA plates were used for both bacterial strains, in triplicates for each condition. A volume of 100 µL was transferred from the corresponding bacterial culture and spread all over the surface of the agar plate, using a glass spreader. Functionalization of compressed collagen hydrogels was done as previously described, utilizing peptides P5, P6, and P9 as capping agents for AgNPs.

Then, both the functionalized gels and the solution where these were exposed to photoirradiation were used for ZOI assays. Several conditions were evaluated.

Positive controls:

- Gentamicin at different concentrations: 50 µg/mL, 250 µg/mL, and 500 µg/mL.

Negative Controls:

- Sterile Milli-Q® water.
- Blank gel: Compressed collagen hydrogel; no treatment.
- Gel-No peptide (G-NP): Compressed collagen hydrogel exposed to photoirradiation in the AgNPs reaction mix with no peptide. From this group, two samples were used: Gel (G-NP_Gel) and Irradiation solution (G-NP_Sol).

Experimental groups (functionalized hydrogels):

- Compressed collagen hydrogels exposed to photoirradiation in the AgNPs reaction mix. Two samples were evaluated for each peptide (P5, P6, and P9) and identified as PX_Gel and PX_Sol for the functionalized hydrogel and the irradiation solution, respectively. "X" corresponds to the peptide number.

When the sample to evaluate was liquid, a sterile 6 mm diameter circular piece of absorbent paper was dipped into the solution, excess liquid removed and then placed on top of the agar plate with the recently spread bacterial suspension. For hydrogel samples, excess liquid was removed and once the samples were placed in their assigned spots, they were allowed to sit onto the agar for 10 minutes to be then incubated in an upside-down position at 37°C for 24 hours. The day after, pictures from the bottom of each plate were taken using a 3D printed support to make sure that the

distance from the camera to the plate was kept constant for all samples. Finally, samples were analyzed using the software Image J 1.53a (National Institutes of Health (NIH), USA). To obtain the ZOI values, circular/oval shapes were used to outline the sample and the clear zone limits. Their area was obtained and subtracted from each other to calculate the area of the ZOI. Hence:

$$ZOI = Area\ defined\ by\ the\ clear\ zone - Area\ of\ the\ sample$$

A.7.1.3 Live/dead assay

To evaluate the biocompatibility of compressed collagen hydrogels functionalized with peptide capped AgNPs, a cellular viability assay was done. Human Umbilical Vein Endothelial Cells (HUVEC) were seeded, grown, lifted, and passaged from T25 to T75 flasks until reaching an 80-90% confluency. Cells were maintained in complete M200 medium (Gibco, USA) with 1% penicillin–streptomycin, replacing half media every 48 hours. Once ready, cells were recovered and counted. Functionalized hydrogels were prepared the same day of cell assays and 1.5 cm diameter pieces were sampled to be transferred into a 24-well plate. A volume of 400 µL of medium was used to rinse the hydrogels. Then, 500 µL of cell suspension were added to each sample-containing well to seed a concentration of $1x10^4$ cells per well. Gels functionalized with P5@AgNPs, P6@AgNPs, and P9@AgNPs were tested and, to serve as negative controls, blank gel (non-treated) and G-NP groups were also included. The plate was incubated at 37°C with 5% CO_2 for 24 hours. Next day, cellular viability was assessed using a Live/Dead assay kit (Invitrogen). Cells were stained with a mix of 2 µM Calcein-AM and 4 µM

Ethidium homodimer (EthD-1) in 1X PBS, for 30 min at room temperature protected from the light. After this time, cells were observed under a Zeiss Axio Observer.A1 inverted phase contrast fluorescence microscope. Images were captured using the Axio Vision 4.8.2 software and then analyzed with Image J 1.53a (NIH, USA), using the "multi-point" option. Three replicates per group were considered and three pictures per sample were captured. As per the manufacturer product information, the cell membrane of live cells is permeable to Calcein-AM, which is converted by enzymatic (esterase) activity into fluorescent calcein, producing an intense uniform green (ex/em ~495 nm/~515 nm). On the other hand, EthD-1 is excluded by live cells but it is able to penetrate cells with disrupted/damaged membranes, binding itself to nucleic acids to produce a bright red fluorescence (ex/em ~495 nm/~635 nm. Hence, cells stained in green correspond to live cells, while orange-red cells are assumed to be dying and dead cells.

A.7.2 Deposition of peptide capped AgNPs formed in microdroplets

A different approach for the *in situ* formation of peptide capped AgNPs onto compressed collagen hydrogels was proposed to avoid the exposure of these gels to the photoirradiation process. The new strategy consisted in testing if AgNPs could be synthesized directly in the microdroplets formed after flushing the reaction mix through a spray nozzle while exposed to UV light. Briefly, 100 µL of the AgNPs reaction mix with a 3 µM P6 peptide concentration were delivered through a nozzle using an electric air pump to form a fine spray. Right at the moment of microdroplets formation, two UV lamps (365 nm) positioned on each side of the nozzle were turned on during the time

required to flush the mix (~9 to 10 seconds). A plate containing 8 mm diameter samples of compressed collagen hydrogels (previously rinsed 5X in Milli-Q water®), was placed below the nozzle and between the two UV lamps to recover the UV-exposed sprayed microdroplets. This was done on each side of the hydrogel. Then, exposed hydrogels were allowed to sit for 15 min at room temperature. After this time, hydrogels were stored in 1X PBS at 4°C and solution was replaced daily for up to 3 days to remove non adsorbed AgNPs, if formed.

A.7.2.1 Cryo-SEM/Energy Dispersive Spectroscopy (EDS) analysis

Compressed collagen hydrogels processed for the *in situ* formation of AgNPs using the microdroplets approach were analyzed at the NIF of Carleton University by Dr. Jianqun Wang, as described in Section A.5. Elemental analysis was performed using an Energy Dispersive X-Ray Spectroscopy Detector (INCA X-Act, Oxford Instruments).

B. CORNEA-SHAPED HYDROGELS

Figure 12 presents a schematic of the general methodology followed for the functionalization and analysis of processed collagen implants.

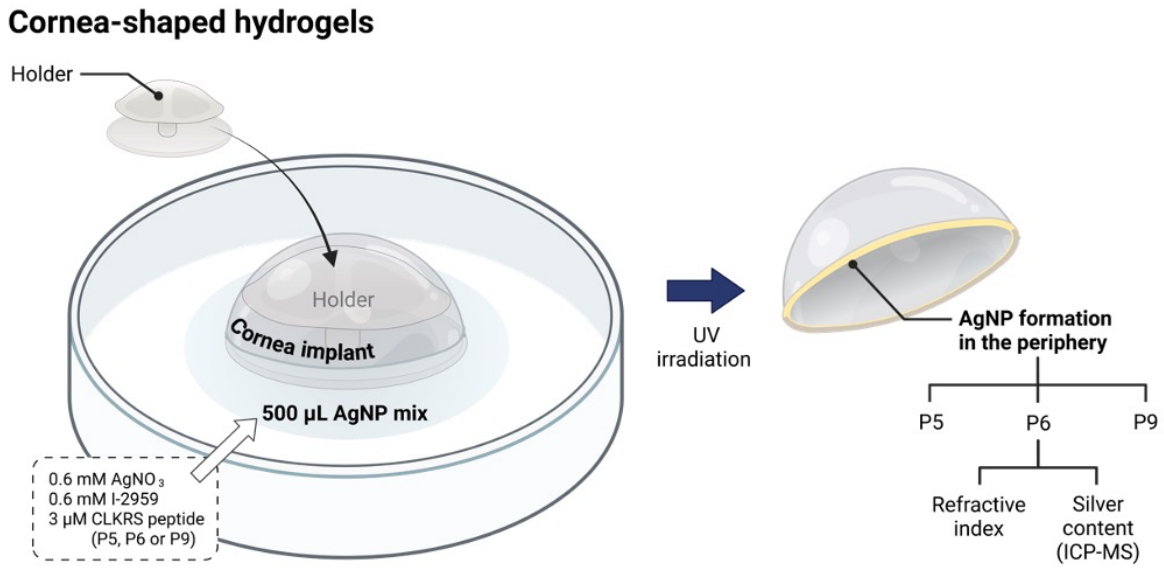

Figure 12. Schematic of the functionalization and analysis of processed cornea shaped hydrogels.

B.1 Preparation of solutions

Solutions were prepared with Milli-Q® water, unless otherwise noted.

- **1X PBS:** According to manufacturer, corresponds to a solution composed of 137 mM NaCl, 2.7 mM KCl and 10 mM phosphate buffer.
- **10% w/v collagen solution:** A volume of 1% Theracol solution is freeze-dried for 5 days and used after to prepare a 10% w/v solution in molecular grade water (HyClone™ - GELifeSciences).
- **Carbonate buffer:** 0.036 M Na_2CO_3 + 0.064 M $NaHCO_3$.

B.2 Preparation of cornea-shaped hydrogels

Collagen based cornea-shaped hydrogels were prepared as previously reported (Alarcon *et al.*, 2016; Koh *et al.*, 2013). To prepare this type of hydrogels, a collagen solution was crosslinked with 1,4-butanediol diglycidyl ether (BDDGE) and casted to obtain the desired shape. First, a T-piece system was primed with carbonate buffer (pH 10) and the remaining solution was mixed with 400 µL of 10% w/v type I porcine collagen solution (Sewon Cellontech Co.) until obtaining a cloudy mix. Then, pH was adjusted to 11 by adding 10-20 µL increments of 2N NaOH until collagen solution became transparent. The corresponding volume of BDDGE (depending on the mass of collagen solution being used) was incorporated to the T-piece system and mixed 75 times. The product obtained was rapidly distributed into 4 hemispherical molding plastics (500 µm spacers) which had been previously sit over the bottom part of a metallic press. Next, the molds were covered with a second molding plastic, and the top part of the metallic press was placed and screwed tightly. Then, the entire casting system was placed in a humidity chamber at 4°C for 18-20 hours. The day after, the molding plastics were released from the press and transferred into a container with 1X PBS at 4°C under agitation for up to 5 days to remove any excess of unreacted crosslinker. PBS was replaced daily. Finally, the cornea-shaped collagen hydrogels were unmolded and stored in 1X PBS at 4°C until use.

B.3 *In situ* functionalization of cornea-shaped collagen hydrogels with peptide capped AgNPs

Different strategies were evaluated to achieve the *in situ* formation of peptide capped AgNPs in a particular region of the cornea-shaped hydrogels, specifically in the periphery, and functionalize them with antimicrobial properties. Here, the one that showed to be more promising is described.

The AgNPs reagent mix was composed of 3 μM peptide (either P5, P6, or P9), 0.6 mM $AgNO_3$, and 0.6 mM I-2959, prepared in sterile Milli-Q® water. 3D printed cornea holders were used to expose only the periphery of the implant when this was placed in a horizontal position (dome pointing upwards) onto the AgNPs reaction mix.

Cornea-shaped hydrogels were rinsed 5 times with Milli-Q® water and excess liquid was removed. Then, these were placed on top of the plastic holders. Due to the holder design, only the periphery of the implant was directly exposed to the reaction mix. The implant plus holder were placed in a glass Petri dish, where a volume of 500 μL of AgNPs reaction mix was distributed around these to be then exposed to UV irradiation in a Luzchem Photoreactor (LZC-4V, 14 UVA lamps, centered at 350 nm). Different photoirradiation times were evaluated, specifically 5, 10, 15, and 30 minutes. Successful *in situ* formation of AgNPs was evaluated as the presence of a yellow halo around the bottom part of the cornea-shaped collagen implants.

B.3.1 Refractive index (RI) of functionalized corneal implants

During the photoirradiation process of corneal implants, part of these is not in contact with a liquid environment. To test whether the exposure of this area to UV irradiation in such conditions may cause a detrimental change in the transparency of the implant or not, RI measurements were taken. Samples of 0.6 mm and 0.4 mm in diameter, from the central and peripheral portions, respectively, of the processed implants (5 minutes exposure time). Sample analysis was done in an Abbemat 300 refractometer (Anton Paar) at 37°C. Blank (non-treated) corneal implants were used as controls.

B.3.2 Inductively Coupled Plasma-Mass Spectrometry (ICP-MS)

Functionalized corneal implants were rinsed daily in 1X PBS for up to 3 days to remove any excess solution and non-adsorbed AgNPs, if formed. Next, 8 mm diameter samples were cut out of the central part of the implants to evaluate if the synthesis of AgNPs had been done exclusively in the periphery. Then, the central and peripheral portions of functionalized and non-treated corneal implants were freeze dried for ICP-MS analysis. Samples were analyzed by Dr. Emmanuel Yumvihoze at the Center for Advanced Research in Environmental Genomics of the University of Ottawa. Samples were processed as previously reported (Alarcon *et al.*, 2015). Briefly, samples were digested in a DigiPrep MS system (SCP Science) and analyzed in an Agilent 7700x ICP-MS system. Silver content was determined by monitoring the 107 m/z signal (100 ms integration) and Argon was used as the carrier gas (0.75 ml/min, Ar plasma gas flow: 15 L/min). The limit of detection (LOD) of silver was determined as 0.0024 μg/L.

3.6 P6 PEPTIDE ANALYSIS

To confirm the safety and antimicrobial potential of the CLKRS peptide P6 *per se*, independently of its use as capping agent for AgNPs, a set of experimental assays was considered.

3.6.1 Proliferation of human corneal epithelial cells (HCEC)

A culture of HCEC expressing green fluorescent protein (GFP-HCEC) was grown in keratinocyte serum free medium (k-SFM, Gibco®) supplemented with human recombinant Epithelial Growth Factor (rEGF) and Bovine Pituitary Extract (BPE) at final concentrations of 5 ng/mL and 50 μg/mL, respectively, until reaching an 80-90% confluency. Once lifted and counted, cells were seeded in a 96-well plate as $2.5x10^3$ cells per well and incubated at 37°C with 5% CO_2 for 24 hours to allow the cells to become attached to the plate. The day after, media was discarded and a volume of 150 µL of a P6-medium mix was added. The P6 peptide concentrations evaluated were 1, 3, 10, 25, 50, and 100 µM. Right after cells became in contact with the P6-medium mix (time 0), images were obtained using a Zeiss Axio Observer.A1 inverted phase contrast fluorescence microscope (Axio Vision 4.8.2 software). Next, cells were incubated at 37°C with 5% CO_2 for 48 hours and images were captured in a Juli FL Microscope (NanoEntek). Three representative microscopic images per well were taken at both times and cell proliferation was evaluated by counting the number of cells with Image J 1.53a software (NIH, USA). Each peptide concentration was tested in triplicate.

3.6.2 Evaluation of antimicrobial activity by turbidimetry

Staphylococcus aureus ATCC25923 was cultured as previously described (Section A.7.1.2). The absorbance of a 1 mL sample of bacterial suspension was read using a quartz cuvette in a SpectraMax M2 (Molecular Devices) spectrophotometer at a wavelength (λ) of 600 nm. In the meantime, the remaining bacterial suspension was centrifuged at 1500 rpm for 10 minutes and supernatant was discarded. Next, the bacterial pellet was resuspended in the corresponding volume of pre-warmed LB medium to reach an Optical Density (OD) of 0.7 (λ= 600 nm). A 1:10 dilution of the OD-adjusted ATCC25923 bacterial suspension in 10% LB medium was used. A volume of 50 µL of P6 peptide was combined with 50 µL of the corresponding bacterial dilution for a final volume of 100 µL per well in a 96-well plate. The final P6 peptide concentrations evaluated were 1, 3, 10, 25, 50, and 100 µM. Next, the plate was incubated at 37°C for 24 hours. After this time, OD values were read at a λ of 600 nm.

3.7 RESULTS AND DISCUSSION

3.7.1 COLLAGEN HYDROGEL COMPRESSION

The method of plastic compression of collagen hydrogels was reported over 15 years ago (Brown *et al.*, 2005). It consists in removing unbound water from the hydrogels to produce thin collagen sheets, improving their mechanical properties and resistance to degradation by collagenase (Ajalloueian *et al.*, 2018; Tsintou *et al.*, 2018).

We considered the evaluation of different compression times: 5-, 10-, 15-, and 30-min. Hydrogel thickness was reduced from 3.30±0.05 mm to less than 1 mm (~0.5 mm), with a mass loss of at least 80% in all cases (85.61% average) (**Figure 13**). A period of 15 min was found to be the minimum time required to successfully reach *full compression* (Brown *et al.*, 2005; Sarrigiannidis *et al.*, 2021). No difference was observed with a compression time of 30 minutes.

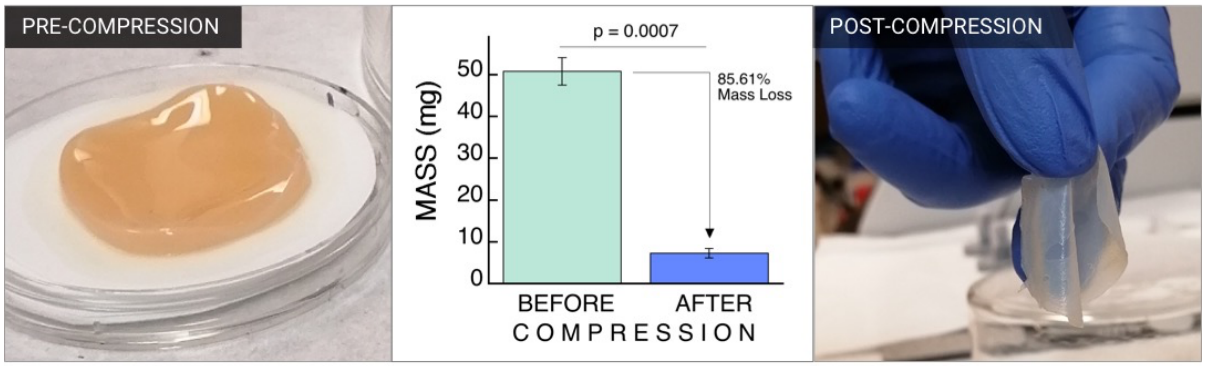

Figure 13. Compression of collagen-based hydrogels. Left and right panels show representative pictures of the obtained hydrogels before and after compression, respectively. Mass reduction percentage post-compression is represented in the central panel (n=3).

3.7.1.1 Microstructure of compressed hydrogels by Cryo-SEM

The collagen-based hydrogels used for compression have been previously characterized by our group (Lazurko *et al.*, 2020). Some of the assays performed in such study included water content, structure, denaturation temperature, degradation by collagenase, and pore size of this and other hydrogels. Here, an exploratory analysis of the microstructure of collagen hydrogels post-compression was done by cryo-SEM imaging (**Figure 14**). Although not clear structural details are available in the left side pictures (A & C), it can be observed that there are certain areas where the hydrogel seems to be folded, potentially as consequence of the mechanical action exerted by the load used during compression. Moreover, it can also be noted that there is an uneven distribution of hydrogel pores along the surface of the material. Pore size and distribution are part of the main characteristics to be taken into account during the design and optimization of biomaterials (Ahumada *et al.*, 2019). In Lazurko's report (Lazurko *et al.*, 2020), pore size of non-compressed collagen hydrogels obtained by SEM analysis was equal to 16±4 μm, significantly larger compared to the 9.8±4 μm of the compressed hydrogel analyzed (p=0.0024), **Figure 14C**. The purpose of this analysis was mainly qualitative, being the overall morphology of the hydrogel after compression of particular interest. To properly analyze and compare the produced materials, it would be required to increase sample size, the number of images captured per sample, and to do pore size measurements from them. Furthermore, a strategy that could be tested with the purpose of regulating pore distribution and reducing the degree of folding of the hydrogel would be to increasingly augment the load used for

compression. This way, the hydrogel may gradually lose mass without a significant displacement of pores.

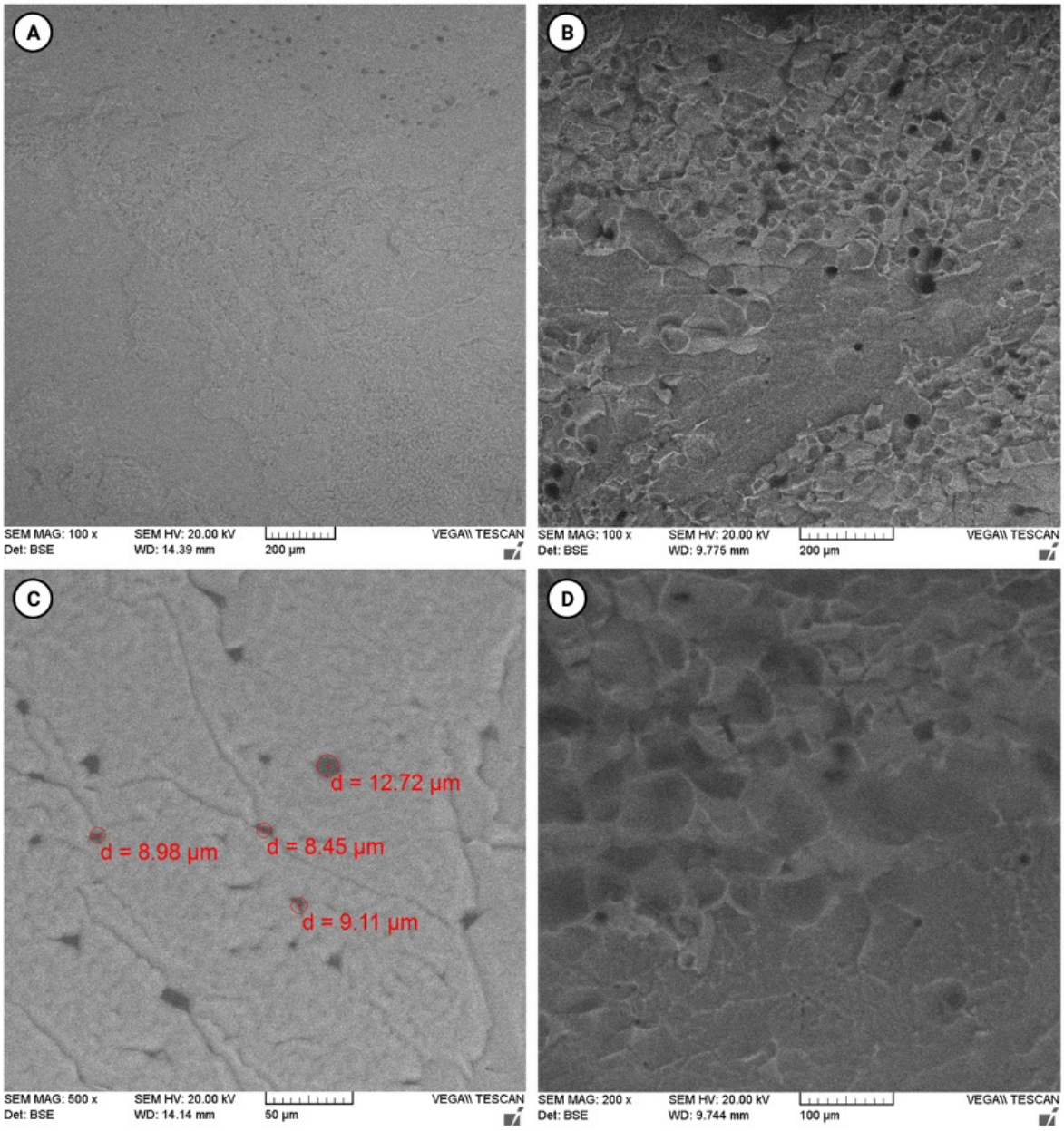

Figure 14. Representative cryo-SEM image captures at different magnifications showing the resulting microstructure of compressed hydrogels. Left and right panels show results from two independent analysis.

3.7.1.2 Hydrogel degradation by collagenase

The degradation extent of biomaterials due to enzymatic activity is commonly assessed during their development process. This is of particular importance for hydrogels. Usually, the level of hydrogel resistance to degradation by collagenase is proportionally related to the crosslinking level and stiffness reached in the material being tested (Helling *et al.*, 2017; Sarrigiannidis *et al.*, 2021). Furthermore, by modulating the density and distribution of collagen fibrils, the enzymatic degradation of collagen-based hydrogels can be regulated depending on the final applications (Ng *et al.*, 2020). It has been previously reported that plastically compressed hydrogels exhibit a reduced susceptibility to degradation by collagenase (Tsintou *et al.*, 2018). The common range of collagenase concentration used for the *in vitro* degradation assays of biomaterials lies between 0.1 and 5 U/mL (Sarrigiannidis *et al.*, 2021). For soft tissue applications such as skin and cardiovascular tissue, a concentration of 2.5 U/mL has been reported (Camci-Unal *et al.*, 2013; Suvarnapathaki *et al.*, 2019). Here, the effect of a high collagenase concentration (5 U/mL) was evaluated on compressed collagen hydrogels (**Figure 15**) to simulate an accelerated biodegradation process (Islam *et al.*, 2016). Initially, non-compressed hydrogels were apparently more resistant to degradation by collagenase. However, as thickness of these was higher, a larger hydrogel mass was exposed to the same volume of collagenase solution used for compressed hydrogels. Despite of this, after one hour of incubation, non-compressed hydrogels had a similar mass reduction percentage to hydrogels that had been compressed for 15 min (COMP-15). After this point, non-compressed hydrogels showed

to be significantly more susceptible to degradation by collagenase than COMP-15 hydrogels, as observed by an increased mass loss percentage.

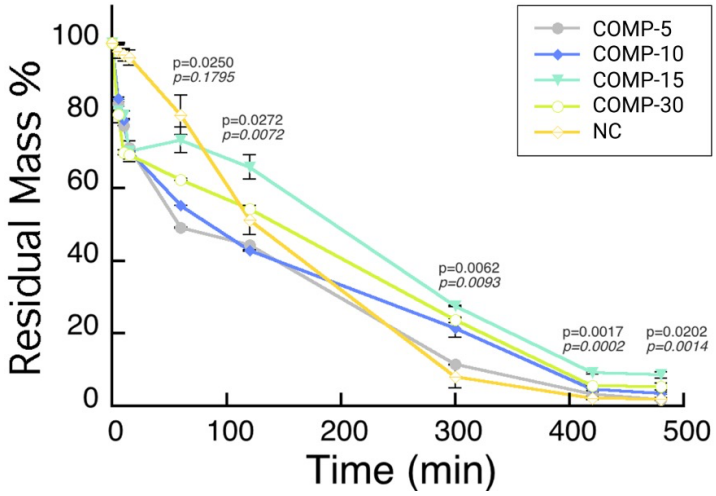

Figure 15. Compressed collagen hydrogel degradation by collagenase. Data is presented as the average residual mass percentage of 3 independent samples and error bars display the standard deviation of the mean. Significance values correspond to the comparison of a compression time of 15 min versus 30 min (top) and hydrogels compressed for 15 min versus non compressed hydrogels (bottom, italics). Plot legend box: COMP-5, COMP-10, and COMP-30 correspond to samples from collagen hydrogels compressed during 5, 10, 15, and 30 min, respectively. NC: Non compressed collagen hydrogels.

Moreover, from the results obtained for hydrogels compressed at different times it can be observed that COMP-5 and COMP-10 hydrogels had a greater mass reduction than COMP-15 and COMP-30 hydrogels. No apparent difference had been observed between the later after compression, however, COMP-30 hydrogels showed to be significantly more susceptible to degradation by collagenase. Hence, by applying a 200 g load onto collagen hydrogels during 15 min resulted to be ideal for reaching full compression while providing them with improved properties such as a higher resistance to enzymatic degradation. Finally, it is important to highlight that for biomaterials intended to be used as temporary drug carriers, *in vivo* biodegradability is desired for

an optimal performance (Ng *et al.*, 2020). Hence, the degradation rate of the compressed collagen hydrogels produced suggests these may be good candidates to be used as temporal patches.

3.7.2 *IN SITU* FUNCTIONALIZATION OF COMPRESSED HYDROGELS I

Exposure into AgNPs reagent mix

3.7.2.1 Plasmon absorption of functionalized compressed hydrogels

To evaluate if the *in situ* functionalization of compressed hydrogels had been achieved, SPB of each were evaluated. As it can be noted in **Figure 16**, all hydrogels presented increased absorbance readings between ~380 nm and 470 nm, with a peak around 410-420 nm. This is in accordance with the SPB obtained for colloidal solutions of AgNPs capped with CLKRS peptides. Hence, results suggest that the three peptides tested successfully contributed, at a similar level, to the *in situ* synthesis of AgNPs in this type of hydrogels.

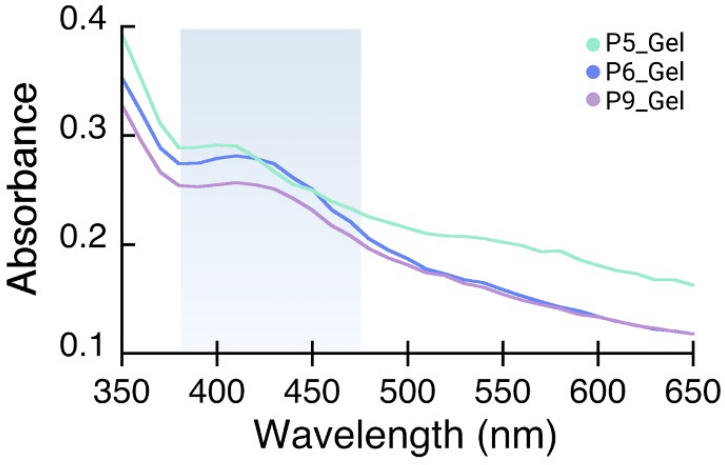

Figure 16. SPB of compressed collagen hydrogels after exposure to photoirradiation into the AgNPs reagent mix containing either P5, P6, or P9 to act as capping agents.

3.7.2.2 ZOI assay

The ZOI test is based on the disc diffusion antimicrobial susceptibility test developed by Bauer and Kirby over 5 decades ago (Bauer, 1966). There are several variations of this assay, with all of them having as main goal the creation of a confluent layer of the selected microorganism(s) to evaluate the effect of antimicrobial agents (Vaughan *et al.*, 2011). Depending on the research interests, interpretation of results from ZOI assays can be done by simple observation to determine the presence or absence of a clear halo around the treatment, which is related to the level of bacteriostatic effect of the treatment. Another alternative is to report the ZOI diameter for comparisons between samples, and one third option, is to measure both the area where the treatment was added and the one defined between the ZOI and the lawn of bacteria to determine the area that corresponds to the ZOI exclusively. Due to the irregular shape of some of the functionalized hydrogels, the latter method was followed. **Figure 17A-E** shows representative images of the ZOI obtained with functionalized hydrogels and controls in *S. aureus* ATCC25923, while ZOI area values are presented in **Figure 17F** for comparison. From these results, it can be observed that all functionalized hydrogels (either with P5, P6, or P9 capped AgNPs) generated a clear zone of growth inhibition compared to the sterile water controls, where such zones were not observable after 24 h. Also, the solutions where these gels were exposed to photoirradiation showed no halo of bacterial inhibition, which suggests that the observed effect was given by the functionalized hydrogels and not due to any potential leftover of the photoirradiated

solutions. However, it is important to note that collagen compressed hydrogels showed a minimal antibacterial activity *per se*.

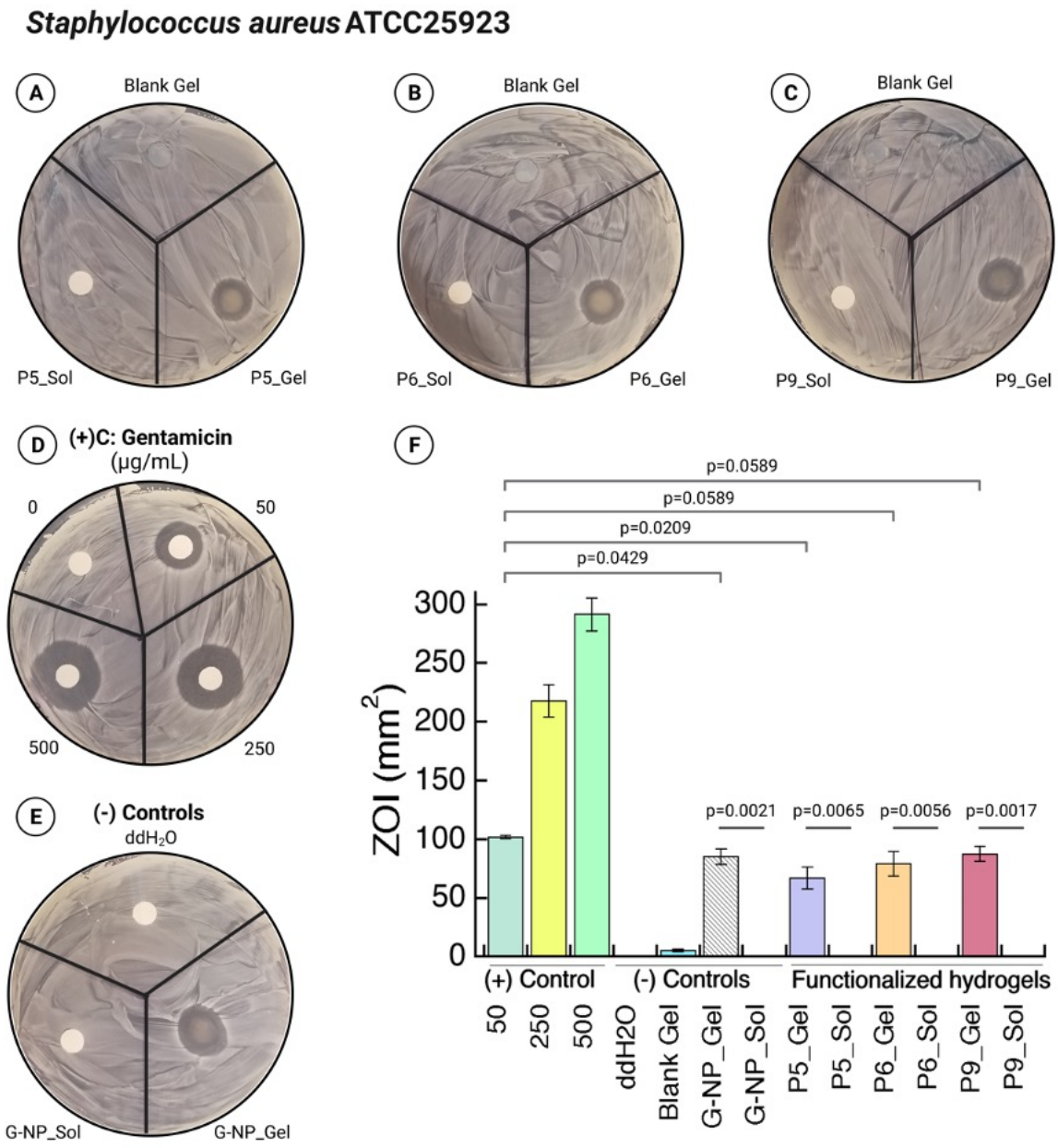

Figure 17. ZOI test results for functionalized compressed collagen hydrogels in the bacterial strain *S. aureus* ATCC 25293. Refer to section A.7.1.2 for sample coding and group description. (+)C: Positive control; Gentamicin at different concentrations (in µg/mL), indicated as 50, 250, and 500.

The area of bacterial inhibition of functionalized hydrogels was close to the one obtained with 50 μg/mL gentamicin. It can also be noted that the ZOI in the positive control at different concentrations (**Figure 17D**) was more clearly defined that in any of the experimental groups tested. It has been previously suggested that in order to improve the definition of the ZOI edge, a layered agar plate could be used (Vaughan *et al.*, 2011). This consists in having a bottom layer of sterile agar and then pouring a second layer of inoculated agar on top.

Furthermore, a ZOI was also obtained in one of the negative controls included (**Figure 17E**), which is in similar values to the functionalized hydrogels. This group consisted in adding all components to the AgNPs reaction mix with exception of the peptide. No peptide capped nor stabilized AgNPs may be present, as shown by the SPB of this control group (**Supplementary Figure 1**). For this and all other functionalized gels, a sample taken from the solution where the hydrogels were exposed to photoirradiation was analyzed to confirm the presence of stable AgNPs by following the absorption spectra. An additional control group where no gel and no peptide were included in the reaction mix was also analyzed. From these and ZOI results, it can be noted that functionalized compressed collagen hydrogels (Gel+AgNPs+Peptide) showed certain level of antibacterial activity (as per ZOI results). Further, stable AgNPs were formed in the solutions where hydrogels were functionalized but, these had no effect over bacterial growth (no ZOI). Moreover, no AgNPs were detected by following the SPB in solutions with no peptide added (either NG-NP or G-NP_Sol), and no ZOI was observed in the G-NP-Sol samples. However, a similar area of inhibition to those

obtained with functionalized peptides was obtained in the hydrogels under these conditions. Hence, this set of results suggests that the antimicrobial effect observed as ZOI in *S. aureus* ATCC25923 cultures was not due to the capped/non-capped AgNPs nor due to the gel itself. One alternative may be that certain chemical by-products were formed in the hydrogel as a consequence of the chemical reactions initiated by the photosensitizer molecules during the photoirradiation process. Moreover, despite that glutaraldehyde is a commonly used crosslinking agent, it might render materials which are not fully biocompatible if used in inadequate concentrations and conditions (Islam *et al.*, 2021). This could cause glutaraldehyde to become released out of the hydrogel or some of its structural components to become exposed on the surface of the hydrogel, leading to cytotoxicity (Gough *et al.*, 2002; Yoshioka & Goissis, 2008). Furthermore, it must be taken into consideration that the ZOI assay provides information about bacteriostatic (microbial inhibition), not bactericidal (microbial kill) effects (Vaughan *et al.*, 2011). Hence, ZOI assays are intended to be exploratory assessments and further analysis (such as turbidimetry, CFU counting, etc.) would have been required to evaluate antimicrobial properties, in case that the initial tests showed to be promising. Considering the ZOI results obtained for the functionalized collagen hydrogels, no further antimicrobial assays were proposed.

Originally, it had been planned to repeat the same set of experiments in *Pseudomonas aeruginosa* PAO1 cultures, as it is in one of the main microorganisms used to study chronic corneal infections *in vitro* (Elsahn *et al.*, 2020). Results obtained for this bacterial strain are presented in **Supplementary Figure 5**. As expected, the

effect of gentamicin was more pronounced in all the concentrations evaluated than values found for *S. aureus* (Tam *et al.*, 2006). However, as shown in the representative pictures of the same figure, the ZOI assay may not be suitable for this type of bacteria. The halos of inhibition were present, however, as the lawn of bacteria is somehow translucent, it is complicated to obtain quality pictures for further analysis. If comparisons are intended to be reported as ZOI diameter values, then it could be done manually taking care of properly identifying the edge defined by the ZOI.

3.7.2.3 Cell viability

To evaluate the level of biocompatibility of the functionalized compressed collagen hydrogels, an *in vitro* Live/Dead assay was performed (**Figure 18**). All groups exposed to photoirradiation presented a cell survival rate of less than 20%, which were significantly lower than the 97.5% survival value obtained for blank compressed collagen hydrogels. As these were not functionalized with peptide capped AgNPs nor exposed to photoirradiation, we can conclude that this type of hydrogels are biocompatible, as previously reported (Lazurko *et al.*, 2020). Hence, it may be possible that some of the reagents which are part of their chemical composition reacted during the photoirradiation process, causing the formation of toxic by-products. This would be in accordance with the results obtained from the ZOI assay for bacteria. Furthermore, it is important to consider that some of the processed hydrogels showed certain modifications in their appearance after photoirradiation. Specifically, these had increased diameters and were less facile to manipulate. To test this hypothesis, it would

be required to analyze the chemical composition of hydrogels before and after being exposed to UV light. Furthermore, evaluating the biocompatibility of both peptide capped AgNPs (in colloidal solutions) and peptides themselves should also be considered to confirm their safety and potential for future biomedical applications.

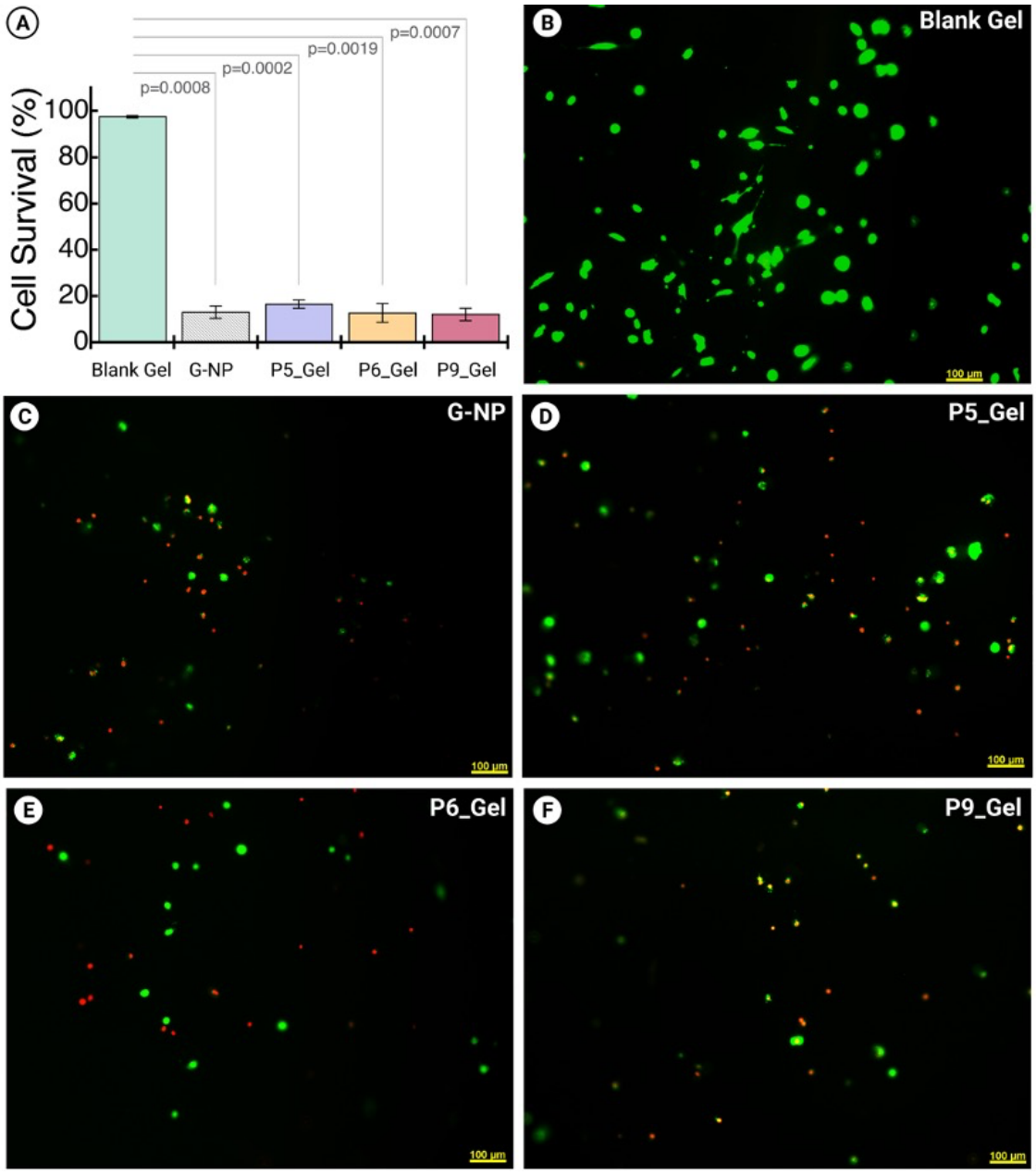

Figure 18. *In vitro* biocompatibility of compressed collagen hydrogels functionalized with peptide capped AgNPs in HUVEC culture after 24 h of incubation.

3.7.3 *IN SITU* FUNCTIONALIZATION OF COMPRESSED HYDROGELS | Microdroplets

As results obtained from previous experiments point towards compressed collagen hydrogels being not suitable to be used under photoirradiation processes, a different strategy for their functionalization with peptide capped AgNPs was proposed. The second approach consisted in using an air pump system and a small nozzle to pass the AgNPs reaction mix through it to create a fine spray (**Figure 19**). Then, at the precise moment when the solution is sprayed, a set of UV lamps was turned on to allow the microdroplets to interact with the light and potentially start the photochemical reaction process of AgNPs synthesis during their deposition time onto the compressed collagen hydrogels.

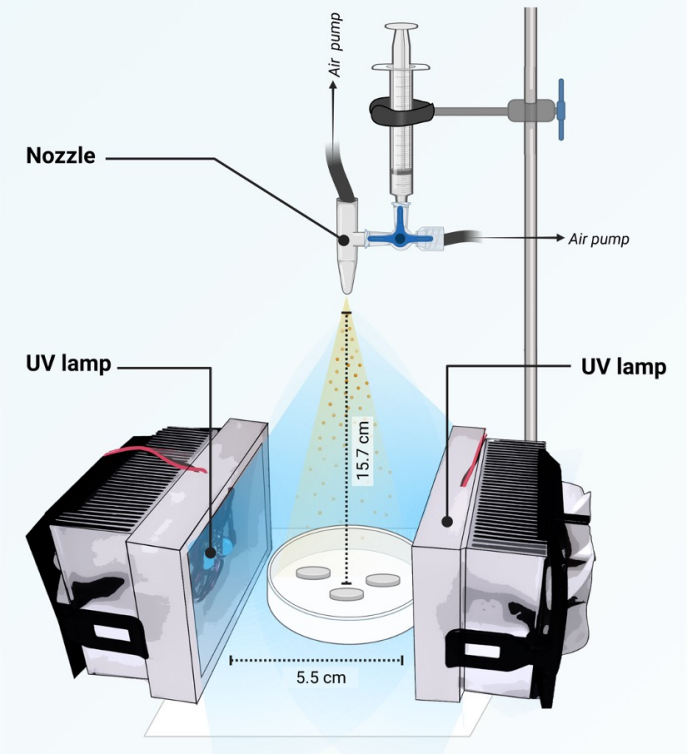

Figure 19. Schematic of the setting used for the *in situ* synthesis of peptide capped AgNPs in microdroplets for their deposition onto compressed collagen hydrogels.

3.7.3.1 Cryo-SEM/EDS analysis

To evaluate if functionalization of compressed collagen hydrogels using the microdroplets approach had been successful, these were scanned and analyzed for silver content by cryo-SEM/EDS (**Figure 20**). Despite being an interesting approach, no silver was detected in these samples.

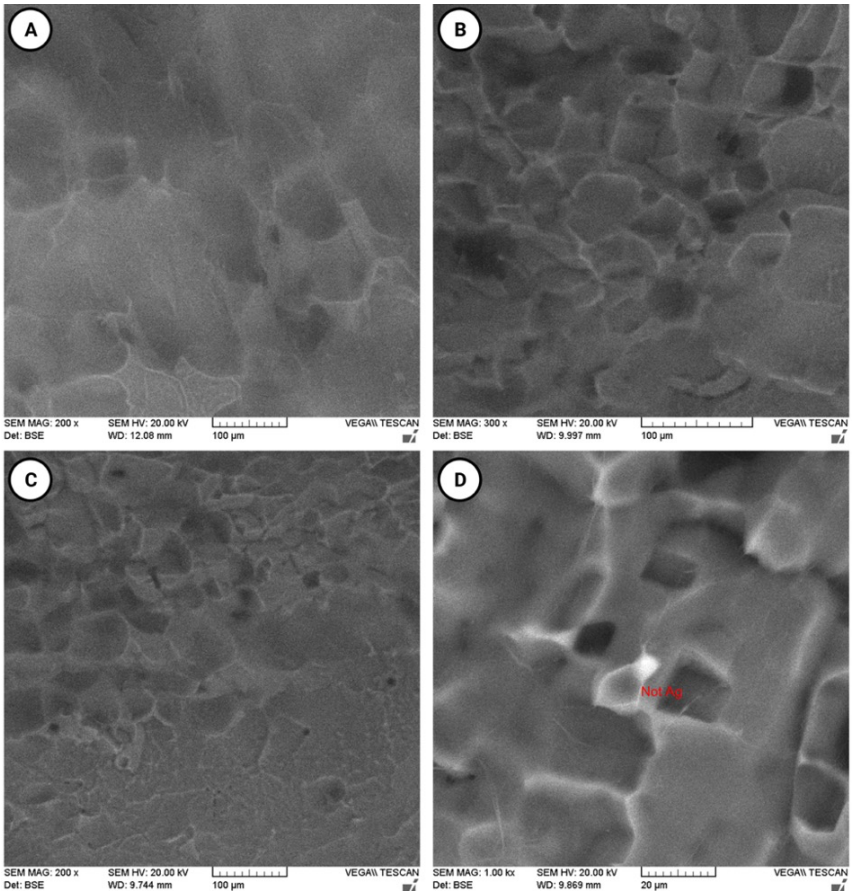

Figure 20. Cryo-SEM/EDS results of the *in situ* functionalization of compressed collagen hydrogels after deposition of microdroplets.

Further experimental design adjustments would be required to fully determine the potential of this strategy. For instance, it would be important to evaluate different microdroplet sizes, distance from the nozzle to the hydrogel, deposition time of the microdroplets, optimal distance of the UV lamps, intensity of these, etc.

3.7.4.1 *In situ* functionalization of cornea-shaped collagen hydrogels with peptide capped AgNPs

From the CLKRS peptides evaluated, only P6 caused a visible change in the periphery of corneal implants (**Figure 21**). A yellow coloration was expected as this is characteristic of colloidal AgNPs (Stamplecoskie & Scaiano, 2012) and it has also been observed in collagen based implants (Khatoon *et al.*, 2020). However, this coloration was only observed in the reaction mix, mainly closer to the contact area between the implant and the solution (**Figure 21A**), while a slightly hazy halo was present in the periphery of some of the implants exposed to photoirradiation (**Figure 21B-C**).

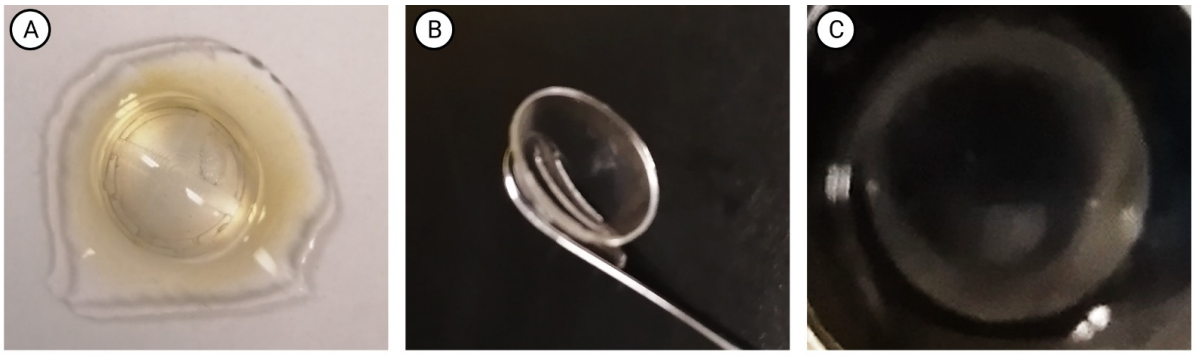

Figure 21. Representative images of the localized *in situ* functionalization of corneal implants (5 minutes of photoirradiation). A. Top view of the corneal implant onto the plastic holder. B. Corneal implant after the *in situ* synthesis of AgNPs. C. Zoom in of the functionalized corneal implant (from the bottom). *Note:* Brightness and contrast of pictures B and C were adjusted to show the mark obtained in the periphery.

3.7.4.2 RI of functionalized corneal implants

Measurements of the RI of functionalized corneal implants (**Figure 22**) were done with the purpose of evaluating if exposure of the dome part of the corneal implant to photoirradiation, when this is not fully contained in a liquid medium, may cause certain level of damage of the implant by reducing its transparency.

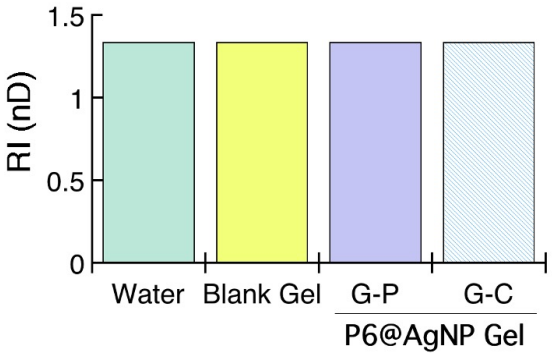

Figure 22. RI values of functionalized corneal implants. Water and blank gels were included as negative controls. G-P and G-C correspond to Gel-Periphery and Gel-Central part of the corneal implants functionalized with P6@AgNPs. Values are presented as the mean of 3 repetitions and error bars correspond to standard deviation of the mean.

No differences were observed between controls and processed samples, not even between the peripheral portion where the hazy halo was obtained and the central part, suggesting that transparency of the material was not significantly affected after functionalization.

3.7.4.3 ICP-MS

To explore if the mark observed at the periphery of corneal implants after the *in situ* synthesized AgNPs could become better defined, different exposure times were evaluated. Not evident hazy halo was observed in samples exposed to photoirradiation for longer times than 5 min. However, all samples were analyzed by ICP-MS (**Figure 23**). Both central and peripheral zones from the treated implants resulted positive for silver content, which in all cases was higher for samples from the periphery. This suggests that peptide capped AgNPs were potentially formed in the implants, mainly in the area directly exposed to the reaction mix. Further, a processing time of 5 min resulted enough obtain the highest levels of silver in the implant. However, no conclusions should be drawn as sample size was limited to one implant per group. Finally, in order to confirm the *in situ* formation of AgNPs, further analysis would be required. As AgNPs would be present in the surface of the corneal implants, modifying its topology as consequence, techniques such as SEM and Atomic Force Microscopy (AFM) may be useful to confirm their functionalization with AgNPs.

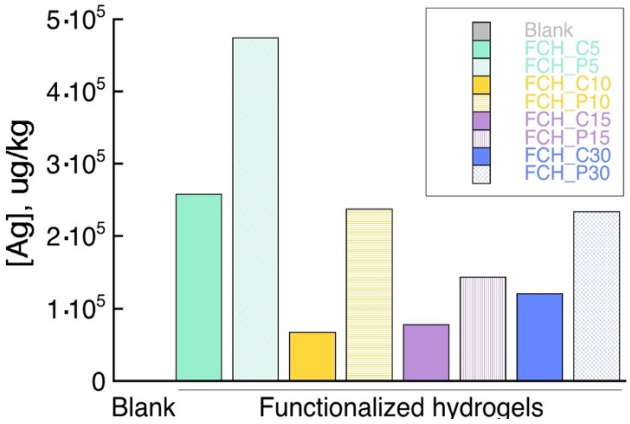

Figure 23. Silver content in functionalized corneal hydrogels. FCH: functionalized collagen hydrogel; C: Central part; and P: Peripheral portion. Numbers correspond to the time of exposure to photoirradiation (n=1).

3.8 P6 PEPTIDE ANALYSIS

Previous results from functionalization of compressed collagen hydrogels showed cell toxicity *in vitro*. Control groups included and additional sample analysis suggest that, most likely, such toxicity may be due to alterations in the chemical composition of compressed hydrogels after their exposure to photoirradiation and not due to the peptide capped AgNPs. However, to prove this, further experiments are required. As an attempt to evaluate if the peptides used for functionalization may had an influence on such detrimental effects and evaluate their individual performance, biocompatibility and antimicrobial tests were considered.

3.8.1 Proliferation of GFP-HCEC *in vitro*

From the 3 peptides evaluated for functionalization of hydrogels, P6 was selected for further experiments. Biocompatibility of P6 was assessed *in vitro* by following proliferation of GFP-HCEC for up to 48 h (

Figure 24). After addition of P6 peptide onto pre-seeded GFP-HCEC (allowed to attach for 24 h), concentrations of 50 and 100 μM showed immediate cell toxicity, while the number of cells in concentrations ranging from 1 to 25 μM were in similar levels to cells with no treatment. P6 concentrations of 3 and 25 μM presented a statistically significant higher number of cells per field of view (FOV) than the control group. As an effect on cell growth and division is not expected in the short term (<1 h), the observed difference might be associated to cell attachment rather than cell proliferation. Follow up image captures were obtained 48 h post incubation of cells with peptide. After this time, P6

concentrations below 10 µM resulted in the same proliferation rate as the control group, suggesting that it is safe to be used in that concentration range. The peptide concentration used as capping agent during the *in situ* synthesis of AgNPs on either of the hydrogels evaluated was of 3 µM. Hence, this suggest that the peptide used was not directly associated to the negative effect previously observed. This and additional experiments would be also required for the other peptides used, namely P5 and P9.

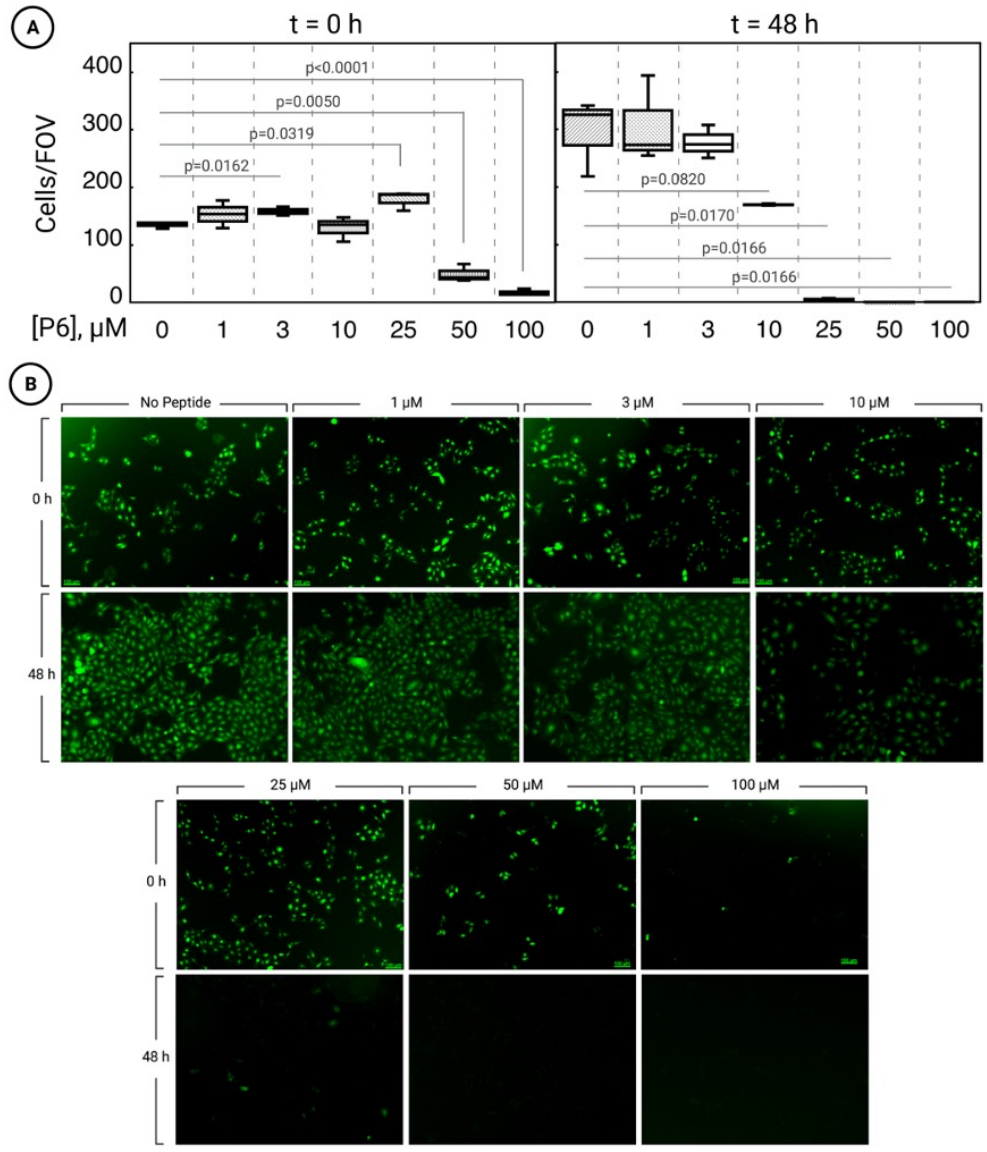

Figure 24. *In vitro* proliferation of GFP-HCEC after incubation with different concentrations of P6 peptide. A. Number of cells per FOV at t=0 (incubation day) and t= 48 h post-incubation. B. Representative images of GFP-HCEC incubated with varying concentrations of P6.

3.8.2 Antimicrobial activity by turbidimetry

The antimicrobial potential of P6, in a range from 1 to 100 μM, was evaluated in planktonic *S. aureus* ATCC25923 cultures by measuring the OD 24 hours post incubation **Figure 25**. No statistical differences were observed between any of the treated groups, nor against the control group with no peptide. Hence, results suggest that P6 peptide had no antimicrobial effects *per se*.

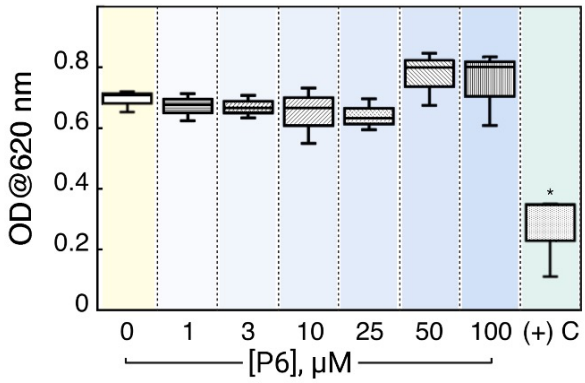

Figure 25. Antimicrobial activity of P6 evaluated by turbidimetry. (+)C: Positive Control, 50 μg/mL Gentamicin).

3.10 CHAPTER CONCLUSIONS

The strategies followed for the *in situ* functionalization of compressed collagen hydrogels with peptide capped AgNPs were not appropriate for these type of hydrogels. Furthermore, the localized formation of AgNPs on corneal implants resulted successful for the CLKRS peptide P6, which was proven to be biocompatible by itself. However, no antibacterial activity was detected for P6 by the methods utilized for analysis.

4. OUTLOOK AND FUTURE DIRECTIONS

The use of peptides as capping agents during the synthesis of AgNPs by photochemical methods is an attractive alternative. Diverse physicochemical properties can be modulated through the custom-design of peptides. Moreover, by combining peptide synthesis chemistry and nanotechnology, the final biological activity of the products obtained can also be modulated. This may find countless paths for biomedical applications. Here, we reported different approaches for the *in situ* functionalization of collagen-based hydrogels with peptide-capped AgNPs for their use as alternatives for corneal repair and replacement. Although not all these strategies resulted optimal for the intended applications, some insights were gained for the improvement of further studies. Developing *in silico* analysis to study the potential spatial organization of peptides when these interact with the surface of NPs may represent a suitable alternative to evaluate their potential biological activity. By doing this, the process of experimental evaluation could be expedited as the best candidates would be evaluated first.

5. REFERENCES

Agnihotri, S., Mukherji, S., and Mukherji, S. (2014). Size-controlled silver nanoparticles synthesized over the range 5–100 nm using the same protocol and their antibacterial efficacy. *RSC Advances,* 4 (8), 3974-83.

Ahumada, M., Jacques, E., Calderon, C.*, et al.* (2019), 'Porosity in Biomaterials: A Key Factor in the Development of Applied Materials in Biomedicine', in Leticia Myriam Torres Martínez, Oxana Vasilievna Kharissova, and Boris Ildusovich Kharisov (eds.), *Handbook of Ecomaterials* (Cham: Springer International Publishing), 3503-22.

Ajalloueian, F., Nikogeorgos, N., Ajalloueian, A.*, et al.* (2018). Compressed collagen constructs with optimized mechanical properties and cell interactions for tissue engineering applications. *International Journal of Biological Macromolecules,* 108, 158-66.

Alarcon, E.I., Vulesevic, B., Argawal, A.*, et al.* (2016). Coloured cornea replacements with anti-infective properties: expanding the safe use of silver nanoparticles in regenerative medicine. *Nanoscale,* 8 (12), 6484-89.

Alarcon, E.I., Udekwu, K., Skog, M.*, et al.* (2012). The biocompatibility and antibacterial properties of collagen-stabilized, photochemically prepared silver nanoparticles. *Biomaterials,* 33 (19), 4947-56.

Alarcon, E.I., Udekwu, K.I., Noel, C.W.*, et al.* (2015). Safety and efficacy of composite collagen–silver nanoparticle hydrogels as tissue engineering scaffolds. *Nanoscale,* 7 (44), 18789-98.

Anshu, A., Lim, L.S., Htoon, H.M., *et al.* (2011). Postoperative Risk Factors Influencing Corneal Graft Survival in the Singapore Corneal Transplant Study. *American Journal of Ophthalmology,* 151 (3), 442-48.e1.

Ashkarran, A.A., Estakhri, S., Nezhad, M.R.H., *et al.* (2013). Controlling the Geometry of Silver Nanostructures for Biological Applications. *Physics Procedia,* 40, 76-83.

Auffan, M., Rose, J., Bottero, J.Y., *et al.* (2009). Towards a definition of inorganic nanoparticles from an environmental, health and safety perspective. *Nature Nanotechnology,* 4 (10), 634-41.

Bauer, A.W. (1966). Antibiotic susceptibility testing by a standardized single disc method. *Am J clin pathol,* 45, 149-58.

Beaton, G.C., Bottomley, A.J., Prezgot, D., *et al.* (2020). Shape control of silver nanoparticles and their stability on Al2O3. *Journal of Materials Chemistry C,* 8 (31), 10755-60.

Bélteky, P., Rónavári, A., Igaz, N., *et al.* (2019). Silver nanoparticles: aggregation behavior in biorelevant conditions and its impact on biological activity. *International journal of nanomedicine,* 14, 667-87.

Bocheux, R., Pernot, P., Borderie, V., *et al.* (2019). Quantitative measures of corneal transparency, derived from objective analysis of depth-resolved corneal images, demonstrated with full-field optical coherence tomographic microscopy. *PLOS ONE,* 14 (8), e0221707.

Brown, R. A, Wiseman, M., Chuo, C. B., *et al.* (2005). Ultrarapid Engineering of Biomimetic Materials and Tissues: Fabrication of Nano- and Microstructures by Plastic Compression. *Advanced Functional Materials,* 15 (11), 1762-70.

Camci-Unal, G., Cuttica, D., Annabi, N., *et al.* (2013). Synthesis and Characterization of Hybrid Hyaluronic Acid-Gelatin Hydrogels. *Biomacromolecules,* 14 (4), 1085-92.

Cheng, Y., Wang, F., Fang, C., *et al.* (2016). Preparation and characterization of size and morphology controllable silver nanoparticles by citrate and tannic acid combined reduction at a low temperature. *Journal of Alloys and Compounds,* 658, 684-88.

Choi, J.R., Yong, K.W., Choi, J.Y., *et al.* (2019). Recent advances in photo-crosslinkable hydrogels for biomedical applications. *BioTechniques,* 66 (1), 40-53.

Desireddy, A., Conn, B.E., Guo, J., *et al.* (2013). Ultrastable silver nanoparticles. *Nature,* 501 (7467), 399-402.

dos Santos, V., Brandalise, R.N., and Savaris, M. (2017), 'Biomaterials: Characteristics and Properties', in Venina dos Santos, Rosmary Nichele Brandalise, and Michele Savaris (eds.), *Engineering of Biomaterials* (Cham: Springer International Publishing), 5-15.

Elsahn, A., Cendra, M.M., Humbert, M.V., *et al.* (2020). Pseudomonas aeruginosa host-pathogen interactions in human corneal infection models. *Journal of EuCornea,* 7, 8-16.

Ferdous, Z. and Nemmar, A. (2020). Health Impact of Silver Nanoparticles: A Review of the Biodistribution and Toxicity Following Various Routes of Exposure. *International Journal of Molecular Sciences,* 21 (7).

Gain, P., Jullienne, R., He, Z.*, et al.* (2016). Global Survey of Corneal Transplantation and Eye Banking. *JAMA Ophthalmology,* 134 (2), 167-73.

Garmany, A., Yamada, S., and Terzic, A. (2021). Longevity leap: mind the healthspan gap. *npj Regenerative Medicine,* 6 (1), 57.

Gonzalez, C.M., Liu, Y., and Scaiano, J.C. (2009). Photochemical Strategies for the Facile Synthesis of Gold–Silver Alloy and Core–Shell Bimetallic Nanoparticles. *The Journal of Physical Chemistry C,* 113 (27), 11861-67.

Gough, J.E., Scotchford, C.A., and Downes, S. (2002). Cytotoxicity of glutaraldehyde crosslinked collagen/poly(vinyl alcohol) films is by the mechanism of apoptosis. *Journal of Biomedical Materials Research,* 61 (1), 121-30.

Guzmán-Soto, I., McTiernan, C.D., Gonzalez-Gomez, M.*, et al.* (2021). Mimicking biofilm formation and development: Recent progress in in vitro and in vivo biofilm models. *iScience,* 24 (5), 102443.

Hancox, Z., Heidari Keshel, S., Yousaf, S.*, et al.* (2020). The progress in corneal translational medicine. *Biomaterials Science,* 8 (23), 6469-504.

Haq, A., Kumar, S., Mao, Y.*, et al.* (2020). Thymoquinone-Loaded Polymeric Films and Hydrogels for Bacterial Disinfection and Wound Healing. *Biomedicines,* 8 (10).

Helling, A.L., Tsekoura, E.K., Biggs, M.*, et al.* (2017). In Vitro Enzymatic Degradation of Tissue Grafts and Collagen Biomaterials by Matrix Metalloproteinases:

Improving the Collagenase Assay. *ACS Biomaterials Science & Engineering,* 3 (9), 1922-32.

Husanu, E., Chiappe, C., Bernardini, A.*, et al.* (2018). Synthesis of colloidal Ag nanoparticles with citrate based ionic liquids as reducing and capping agents. *Colloids and Surfaces A: Physicochemical and Engineering Aspects,* 538, 506-12.

Islam, M.M., Ravichandran, R., Olsen, D.*, et al.* (2016). Self-assembled collagen-like-peptide implants as alternatives to human donor corneal transplantation. *RSC Advances,* 6 (61), 55745-49.

Islam, M.M., AbuSamra, D.B., Chivu, A.*, et al.* (2021). Optimization of Collagen Chemical Crosslinking to Restore Biocompatibility of Tissue-Engineered Scaffolds. *Pharmaceutics,* 13 (6).

Javed, R., Zia, M., Naz, S.*, et al.* (2020). Role of capping agents in the application of nanoparticles in biomedicine and environmental remediation: recent trends and future prospects. *Journal of Nanobiotechnology,* 18 (1), 172.

Jeevanandam, J., Barhoum, A., Chan, Y.S.*, et al.* (2018). Review on nanoparticles and nanostructured materials: history, sources, toxicity and regulations. *Beilstein Journal of Nanotechnology,* 9, 1050-74.

Jeng, B.H. and Ahmad, S. (2021). In Pursuit of the Elimination of Corneal Blindness: Is Establishing Eye Banks and Training Surgeons Enough? *Ophthalmology,* 128 (6), 813-15.

Jhanji, V., Billig, I., and Yam, G.H.F. (2021). Cell-Free Biological Approach for Corneal Stromal Wound Healing. *Frontiers in Pharmacology,* 12 (1339).

Jiang, Z., Wen, G., Luo, Y.*, et al.* (2014). A new silver nanorod SPR probe for detection of trace benzoyl peroxide. *Scientific Reports,* 4 (1), 5323.

Jockusch, S., Landis, M.S., Freiermuth, B.*, et al.* (2001). Photochemistry and Photophysics of α-Hydroxy Ketones. *Macromolecules,* 34 (6), 1619-26.

Jolivet, J.P., Froidefond, C., Pottier, A.*, et al.* (2004). Size tailoring of oxide nanoparticles by precipitation in aqueous medium. A semi-quantitative modelling. *Journal of Materials Chemistry,* 14 (21), 3281-88.

Kalakonda, P. and Banne, S. (2018). Synthesis and Optical Properties of Highly Stabilized Peptide-Coated Silver Nanoparticles. *Plasmonics,* 13 (4), 1265-69.

Khatoon, Z., McTiernan, C.D., Suuronen, E.J.*, et al.* (2018). Bacterial biofilm formation on implantable devices and approaches to its treatment and prevention. *Heliyon,* 4 (12), e01067.

Khatoon, Z., Guzmán-Soto, I., McTiernan, C.D.*, et al.* (2020). Nanoengineering the surface of corneal implants: towards functional anti-microbial and biofilm materials. *RSC Advances,* 10 (40), 23675-81.

Khodashenas, B. and Ghorbani, H.R. (2019). Synthesis of silver nanoparticles with different shapes. *Arabian Journal of Chemistry,* 12 (8), 1823-38.

Koh, L.B., Islam, M.M., Mitra, D.*, et al.* (2013). Epoxy Cross-Linked Collagen and Collagen-Laminin Peptide Hydrogels as Corneal Substitutes. *Journal of Functional Biomaterials,* 4 (3).

Krishnaprabha, M. and Manjunatha, P. (2017). Biogenic synthesis of fluorescent silver nanoparticles using Melastoma Malabathricum flower extract. *AIP Conference Proceedings,* 1832 (1), 050016.

Lazurko, C., Khatoon, Z., Goel, K.*, et al.* (2020). Multifunctional Nano and Collagen-Based Therapeutic Materials for Skin Repair. *ACS Biomaterials Science & Engineering,* 6 (2), 1124-34.

Lee, S.H. and Jun, B.H. (2019). Silver Nanoparticles: Synthesis and Application for Nanomedicine. *International Journal of Molecular Sciences,* 20 (4).

Levard, C., Hotze, E.M., Lowry, G.V.*, et al.* (2012). Environmental Transformations of Silver Nanoparticles: Impact on Stability and Toxicity. *Environmental Science & Technology,* 46 (13), 6900-14.

Liu, Y., Gan, L., Carlsson, D.J.*, et al.* (2006). A Simple, Cross-linked Collagen Tissue Substitute for Corneal Implantation. *Investigative Ophthalmology & Visual Science,* 47 (5), 1869-75.

Lu, X., Rycenga, M., Skrabalak, S.E.*, et al.* (2009). Chemical Synthesis of Novel Plasmonic Nanoparticles. *Annual Review of Physical Chemistry,* 60 (1), 167-92.

Maretti, L., Billone, P.S., Liu, Y.*, et al.* (2009). Facile Photochemical Synthesis and Characterization of Highly Fluorescent Silver Nanoparticles. *Journal of the American Chemical Society,* 131 (39), 13972-80.

Matthyssen, S., Van den Bogerd, B., Dhubhghaill, S.N.*, et al.* (2018). Corneal regeneration: A review of stromal replacements. *Acta Biomaterialia,* 69, 31-41.

McGilvray, K.L., Decan, M.R., Wang, D.*, et al.* (2006). Facile Photochemical Synthesis of Unprotected Aqueous Gold Nanoparticles. *Journal of the American Chemical Society,* 128 (50), 15980-81.

McLaughlin, S., Ahumada, M., Franco, W.*, et al.* (2016). Sprayable peptide-modified silver nanoparticles as a barrier against bacterial colonization. *Nanoscale,* 8 (46), 19200-03.

McTiernan, C.D., Simpson, F.C., Haagdorens, M.*, et al.* (2020). LiQD Cornea: Pro-regeneration collagen mimetics as patches and alternatives to corneal transplantation. *Sci Adv,* 6 (25).

Meek, K.M. and Knupp, C. (2015). Corneal structure and transparency. *Progress in Retinal and Eye Research,* 49, 1-16.

Miernicki, M., Hofmann, T., Eisenberger, I.*, et al.* (2019). Legal and practical challenges in classifying nanomaterials according to regulatory definitions. *Nature Nanotechnology,* 14 (3), 208-16.

Mlalila, N.G., Swai, H.S., Hilonga, A.*, et al.* (2016). Antimicrobial dependence of silver nanoparticles on surface plasmon resonance bands against Escherichia coli. *Nanotechnology, science and applications,* 10, 1-9.

Mobaraki, M., Abbasi, R., Omidian Vandchali, S.*, et al.* (2019). Corneal Repair and Regeneration: Current Concepts and Future Directions. *Frontiers in Bioengineering and Biotechnology,* 7 (135).

Mody, V., Siwale, R., Singh, A.*, et al.* (2010). Introduction to metallic nanoparticles. *Journal of Pharmacy And Bioallied Sciences,* 2 (4), 282-89.

Mukherji, S., Bharti, S., Shukla, G*., et al.* (2019). Synthesis and characterization of size- and shape-controlled silver nanoparticles. *Physical Sciences Reviews,* 4 (1).

Ng, H.W., Zhang, Y., Naffa, R*., et al.* (2020). Monitoring the Degradation of Collagen Hydrogels by Collagenase Clostridium histolyticum. *Gels,* 6 (4).

Oliva, M.S., Schottman, T., and Gulati, M. (2012). Turning the tide of corneal blindness. *Indian Journal of Ophthalmology,* 60 (5).

Pacioni, N.L., Borsarelli, C.D., Rey, V*., et al.* (2015), 'Synthetic Routes for the Preparation of Silver Nanoparticles', in Emilio I. Alarcon, May Griffith, and Klas I. Udekwu (eds.), *Silver Nanoparticle Applications: In the Fabrication and Design of Medical and Biosensing Devices* (Cham: Springer International Publishing), 13-46.

Pal, I., Bhattacharyya, D., Kar, R.K*., et al.* (2019). A Peptide-Nanoparticle System with Improved Efficacy against Multidrug Resistant Bacteria. *Scientific Reports,* 9 (1), 4485.

Pal, S., Tak Yu, K., and Song Joon, M. (2007). Does the Antibacterial Activity of Silver Nanoparticles Depend on the Shape of the Nanoparticle? A Study of the Gram-Negative Bacterium Escherichia coli. *Applied and Environmental Microbiology,* 73 (6), 1712-20.

Palchesko, R.N., Carrasquilla, S.D., and Feinberg, A.W. (2018). Natural Biomaterials for Corneal Tissue Engineering, Repair, and Regeneration. *Advanced Healthcare Materials,* 7 (16), 1701434.

Perez, V.L., Foulsham, W., Peterson, K*., et al.* (2020), 'Pathophysiology of Corneal Graft Rejection', in Kathryn Colby and Reza Dana (eds.), *Foundations of Corneal*

Disease: Past, Present and Future (Cham: Springer International Publishing), 87-96.

Phan, H.T. and Haes, A.J. (2019). What Does Nanoparticle Stability Mean? *The Journal of Physical Chemistry C,* 123 (27), 16495-507.

Pinto, V.V., Ferreira, M.J., Silva, R.*, et al.* (2010). Long time effect on the stability of silver nanoparticles in aqueous medium: Effect of the synthesis and storage conditions. *Colloids and Surfaces A: Physicochemical and Engineering Aspects,* 364 (1), 19-25.

Poblete, H., Agarwal, A., Thomas, S.S.*, et al.* (2016). New Insights into Peptide–Silver Nanoparticle Interaction: Deciphering the Role of Cysteine and Lysine in the Peptide Sequence. *Langmuir,* 32 (1), 265-73.

Rahmati, M., Pennisi, C.P., Budd, E.*, et al.* (2018), 'Biomaterials for Regenerative Medicine: Historical Perspectives and Current Trends', in Kursad Turksen (ed.), *Cell Biology and Translational Medicine, Volume 4: Stem Cells and Cell Based Strategies in Regeneration* (Cham: Springer International Publishing), 1-19.

Ravve, A. (2006), 'Photosensitizers and Photoinitiators', in A. Ravve (ed.), *Light-Associated Reactions of Synthetic Polymers* (New York, NY: Springer New York), 23-122.

Regini, J.W., Elliott, G.F., and Hodson, S.A. (2004). The Ordering of Corneal Collagen Fibrils with Increasing Ionic Strength. *Journal of Molecular Biology,* 336 (1), 179-86.

Restrepo, C.V. and Villa, C.C. (2021). Synthesis of silver nanoparticles, influence of capping agents, and dependence on size and shape: A review. *Environmental Nanotechnology, Monitoring & Management,* 15, 100428.

Rossi, L.M., Fiorio, J.L., Garcia, M.A.S.*, et al.* (2018). The role and fate of capping ligands in colloidally prepared metal nanoparticle catalysts. *Dalton Transactions,* 47 (17), 5889-915.

Rycenga, M., Cobley, C.M., Zeng, J.*, et al.* (2011). Controlling the Synthesis and Assembly of Silver Nanostructures for Plasmonic Applications. *Chemical Reviews,* 111 (6), 3669-712.

Sadtler, K., Singh, A., Wolf, M.T.*, et al.* (2016). Design, clinical translation and immunological response of biomaterials in regenerative medicine. *Nature Reviews Materials,* 1 (7), 16040.

Sarrigiannidis, S.O., Rey, J.M., Dobre, O.*, et al.* (2021). A tough act to follow: collagen hydrogel modifications to improve mechanical and growth factor loading capabilities. *Materials Today Bio,* 10, 100098.

Scaiano, J.C., Stamplecoskie, K.G., and Hallett-Tapley, G.L. (2012). Photochemical Norrish type I reaction as a tool for metal nanoparticle synthesis: importance of proton coupled electron transfer. *Chemical Communications,* 48 (40), 4798-808.

Scaiano, J.C., Billone, P., Gonzalez, C.M.*, et al.* (2009). Photochemical routes to silver and gold nanoparticles. *Pure and Applied Chemistry,* 81 (4), 635-47.

Sharif, Z. and Sharif, W. (2019). Corneal neovascularization: updates on pathophysiology, investigations & management. *Romanian journal of ophthalmology,* 63 (1), 15-22.

Shnoudeh, A.J., Hamad, I., Abdo, R.W.*, et al.* (2019), 'Chapter 15 - Synthesis, Characterization, and Applications of Metal Nanoparticles', in Rakesh K. Tekade (ed.), *Biomaterials and Bionanotechnology* (Academic Press), 527-612.

Sivakala, S., Rishad Baig, E., Molji, C.*, et al.* (2021). Nipping the Shape of the Nanosilver through Bio-Based Capping Strategy and Studies on Their Electrocatalytic Performance Using Electrospectrometry. *Journal of The Electrochemical Society,* 168 (7), 077504.

Smitha, S.L., Nissamudeen, K.M., Philip, D.*, et al.* (2008). Studies on surface plasmon resonance and photoluminescence of silver nanoparticles. *Spectrochimica Acta Part A: Molecular and Biomolecular Spectroscopy,* 71 (1), 186-90.

Sökmen, M., Alomar, S.Y., Albay, C.*, et al.* (2017). Microwave assisted production of silver nanoparticles using green tea extracts. *Journal of Alloys and Compounds,* 725, 190-98.

Sridhar, M.S. (2018). Anatomy of cornea and ocular surface. *Indian journal of ophthalmology,* 66 (2), 190-94.

Stamplecoskie, K.G. and Scaiano, J.C. (2010). Light Emitting Diode Irradiation Can Control the Morphology and Optical Properties of Silver Nanoparticles. *Journal of the American Chemical Society,* 132 (6), 1825-27.

--- (2012). Silver as an Example of the Applications of Photochemistry to the Synthesis and Uses of Nanomaterials†,‡. *Photochemistry and Photobiology,* 88 (4), 762-68.

StatCan (2021), 'Reductions in life expectancy directly associated with COVID-19, 2020', (updated June 1st, 2021) <https://www150.statcan.gc.ca/n1/daily-quotidien/210601/dq210601e-eng.htm>, accessed October 29th, 2021.

Suvarnapathaki, S., Nguyen, M.A., Wu, X.*, et al.* (2019). Synthesis and characterization of photocrosslinkable hydrogels from bovine skin gelatin. *RSC Advances,* 9 (23), 13016-25.

Tam, V.H., Kabbara, S., Vo, G.*, et al.* (2006). Comparative pharmacodynamics of gentamicin against Staphylococcus aureus and Pseudomonas aeruginosa. *Antimicrobial agents and chemotherapy,* 50 (8), 2626-31.

Tanner, E.E.L., Tschulik, K., Tahany, R.*, et al.* (2015). Nanoparticle Capping Agent Dynamics and Electron Transfer: Polymer-Gated Oxidation of Silver Nanoparticles. *The Journal of Physical Chemistry C,* 119 (32), 18808-15.

Tao, A., Sinsermsuksakul, P., and Yang, P. (2006). Polyhedral Silver Nanocrystals with Distinct Scattering Signatures. *Angewandte Chemie International Edition,* 45 (28), 4597-601.

Tejamaya, M., Römer, I., Merrifield, R.C.*, et al.* (2012). Stability of Citrate, PVP, and PEG Coated Silver Nanoparticles in Ecotoxicology Media. *Environmental Science & Technology,* 46 (13), 7011-17.

Thapa, R., Bhagat, C., Shrestha, P.*, et al.* (2017). Enzyme-mediated formulation of stable elliptical silver nanoparticles tested against clinical pathogens and MDR

bacteria and development of antimicrobial surgical thread. *Annals of Clinical Microbiology and Antimicrobials,* 16 (1), 39.

Tsai, I.L., Hsu, C.C., Hung, K.H.*, et al.* (2015). Applications of biomaterials in corneal wound healing. *Journal of the Chinese Medical Association,* 78 (4), 212-17.

Tsintou, M., Dalamagkas, K., and Seifalian, A. (2018). Injectable Hydrogel versus Plastically Compressed Collagen Scaffold for Central Nervous System Applications. *International Journal of Biomaterials,* 2018, 3514019.

Varier, K.M., Gudeppu, M., Chinnasamy, A.*, et al.* (2019), 'Nanoparticles: Antimicrobial Applications and Its Prospects', in Mu Naushad, Saravanan Rajendran, and Francisco Gracia (eds.), *Advanced Nanostructured Materials for Environmental Remediation* (Cham: Springer International Publishing), 321-55.

Vaughan, J., Benson, R., and Vaughan, K. (2011), '10 - Assessing the effectiveness of antimicrobial wound dressings in vitro', in David Farrar (ed.), *Advanced Wound Repair Therapies* (Woodhead Publishing), 227-46.

Vignoni, M., de Alwis Weerasekera, H., Simpson, M.J.*, et al.* (2014). LL37 peptide@silver nanoparticles: combining the best of the two worlds for skin infection control. *Nanoscale,* 6 (11), 5725-28.

Wagoner, M.D., Ba-Abbad, R., Al-Mohaimeed, M.*, et al.* (2009). Postoperative Complications After Primary Adult Optical Penetrating Keratoplasty: Prevalence and Impact on Graft Survival. *Cornea,* 28 (4).

Weng, Y., Liu, J., Jin, S.*, et al.* (2017). Nanotechnology-based strategies for treatment of ocular disease. *Acta pharmaceutica Sinica. B,* 7 (3), 281-91.

Whitcher, J.P., Srinivasan, M., and Upadhyay, M.P. (2001). Corneal blindness: a global perspective. *Bulletin of the World Health Organization,* 79 (3), 214-21.

Wiley, B.J., Im, S.H., Li, Z.Y.*, et al.* (2006). Maneuvering the Surface Plasmon Resonance of Silver Nanostructures through Shape-Controlled Synthesis. *The Journal of Physical Chemistry B,* 110 (32), 15666-75.

Wyatt, Tech. Corp. (2010) *DYNAMICS User's Guide* [online text],

Xeroudaki, M., Thangavelu, M., Lennikov, A.*, et al.* (2020). A porous collagen-based hydrogel and implantation method for corneal stromal regeneration and sustained local drug delivery. *Scientific Reports,* 10 (1), 16936.

Xu, J., Murphy, S.L., Kochanek, K.D.*, et al.* (2021), 'Deaths: Final Data for 2019', *National Vital Statistics Report* (updated July 26, 2021) <https://www.cdc.gov/nchs/data/nvsr/nvsr70/nvsr70-08-508.pdf>, accessed October 29th, 2021.

Yoshioka, S.A. and Goissis, G. (2008). Thermal and spectrophotometric studies of new crosslinking method for collagen matrix with glutaraldehyde acetals. *Journal of Materials Science: Materials in Medicine,* 19 (3), 1215-23.

Zhang, Z., Shen, W., Xue, J.*, et al.* (2018). Recent advances in synthetic methods and applications of silver nanostructures. *Nanoscale Research Letters,* 13 (1), 54.

Zhao, X., Song, W., Liu, S.*, et al.* (2016). Corneal regeneration by utilizing collagen based materials. *Science China Chemistry,* 59 (12), 1548-53.

6. SUPPLEMENTARY MATERIALS

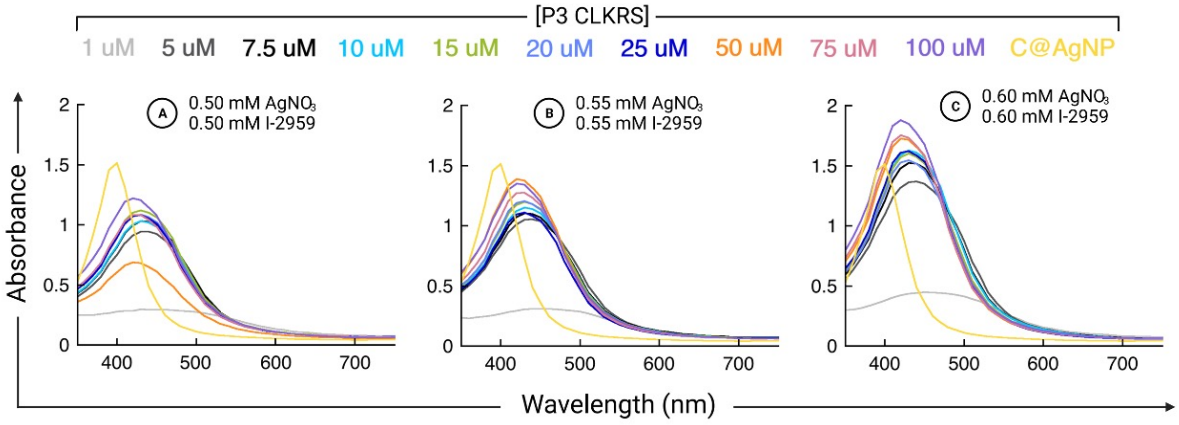

Supplementary Figure 1. Preliminary concentrations of initiators evaluated for P3 peptide from 1 to 100 µM.

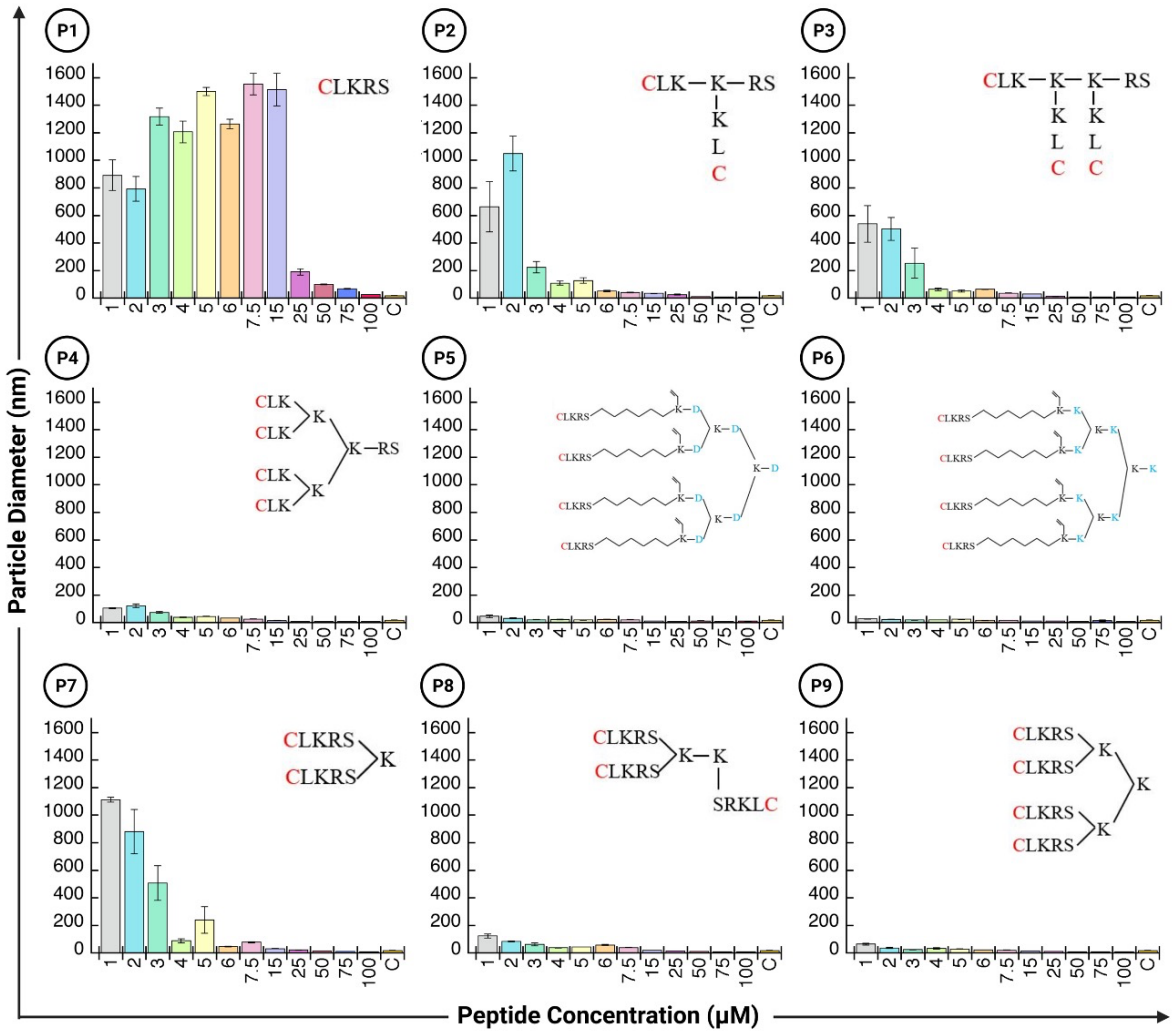

Supplementary Figure 2. Particle size of AgNPs capped with 9 CLKRS peptides at 12 different concentrations.

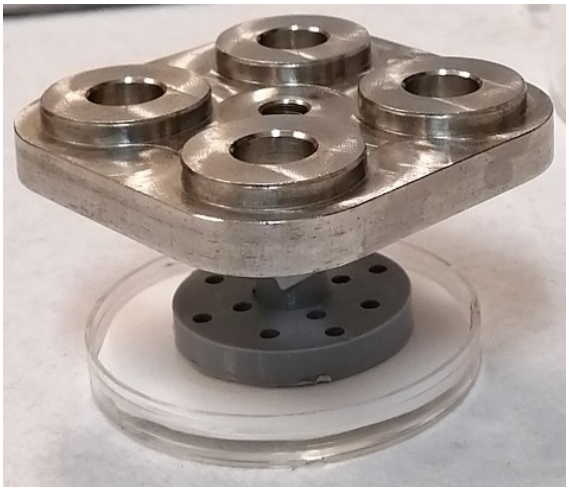

Supplementary Figure 3. Set up used for compression of collagen hydrogels.

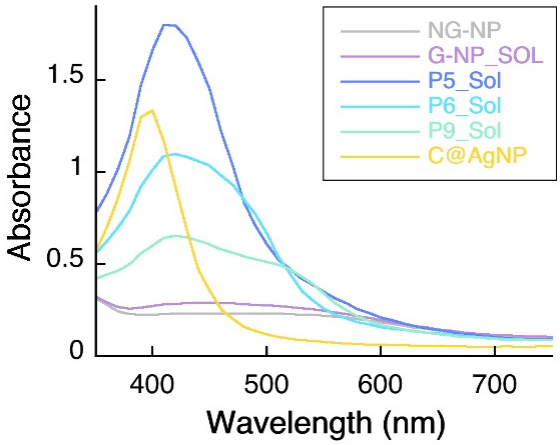

Supplementary Figure 4. SPB of control groups for in situ formation of AgNPs.

- No gel-No peptide (NG-NP): Mix with all components, except peptide and no gel added.
- Gel-No peptide (G-NP): Mix with all components, including hydrogel, and missing peptide.
    - Gel-No peptide Solution (G-NP_Sol): Sample solution from the photoirradiated mix and gel.
- Peptide X_Sol (PX_Sol): Sample solution from the photoirradiated mix and gel for peptide X (either P5, P6, or P9).
- C@AgNPs: Citrate capped AgNPs.

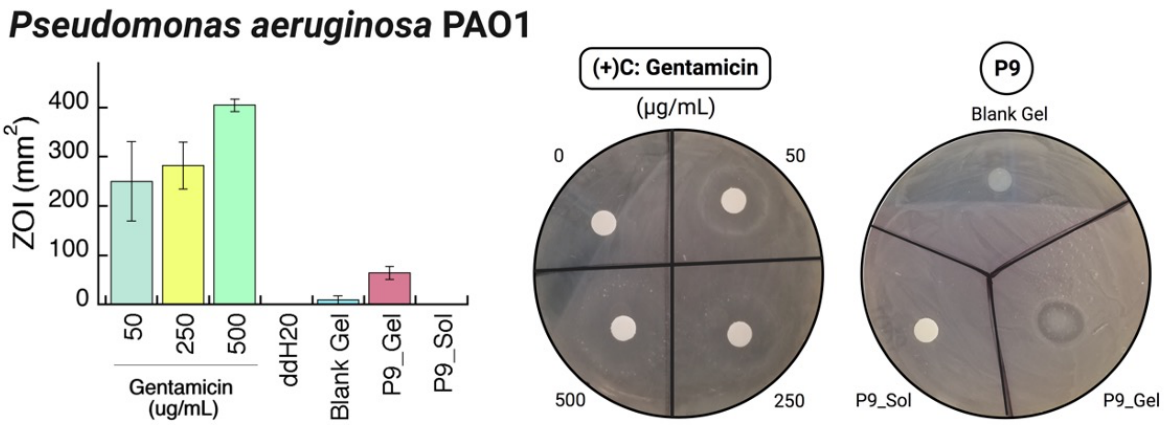

Supplementary Figure 5. ZOI test results for functionalized compressed collagen hydrogels in the bacterial strain *Pseudomonas aeruginosa* PAO1. (+)C: Positive control (gentamicin).

Supplementary Table 1. Previous formulations evaluated for CLKRS peptide (Khatoon *et al.*, 2020).

Formulation	[$AgNO_3$], mM	[I-2959], mM	[P3 CLKRS], mM
A	0.50	0.50	0.10
B	0.55	0.55	0.015
C	0.60	0.60	0.02

Supplementary Table 2.

A) Mean values of NP diameters for P5, P6, and P9 at concentrations ranging from 3 to 7.5 μM.

	P5		P6		P9	
[Peptide]	Mean	Std Deviation	Mean	Std Deviation	Mean	Std Deviation
3	21.2	2.696294	18.93333	0.665833	24.93333	2.672701
4	22.16667	3.444318	19.33333	0.378594	33.46667	9.481737
5	19.5	1.777639	24.43333	2.685765	28.86667	1.404754
6	23.53333	3.655589	16.66667	0.981495	22.63333	0.763763
7.5	21.2	1.126943	17.5	0.655744	21	0.6245
C@AgNP	18.48605	6.593922	***Control:*** *AgNPs synthesized by traditional photochemical method*			

B) p Values from statistical comparisons of NP diameter between C@AgNPs and peptide(P5/P6/P9)-capped AgNPs at concentrations of 3 μM, 4 μM, 5 μM, 6 μM, and 7.5 μM.

	[Peptide], μM	P5	P6	P9
C@AgNP vs	3	0.2172	0.6801	0.0246
	4	0.1930	0.4147	0.1070
	5	0.5021	0.0323	<0.0001
	6	0.1196	0.1284	0.000618
	7.5	0.0360	0.3645	0.0237